12-2018

Development of Thermoplastic Composite Reinforced Ultra-High Performance Concrete Panels for Impact Resistance

Reagan M. Smith Gillis
University of Maine, reagan.smith@maine.edu

DEVELOPMENT OF THERMOPLASTIC COMPOSITE REINFORCED

ULTRA-HIGH PERFORMANCE CONCRETE PANELS

FOR IMPACT RESISTANCE

By

Reagan M. Smith Gillis

B.S. University of Maine, 2017

A THESIS

Submitted in Partial Fulfillment of the

Requirements for the Degree of

Master of Science

(in Civil Engineering)

The Graduate School

The University of Maine

December 2018

Advisory Committee:

Eric N. Landis, Professor of Civil and Environmental Engineering, Advisor

Roberto A. Lopez-Anido, Professor of Civil and Environmental Engineering

Todd S. Rushing, External Graduate Faculty in Forest Resources

DEVELOPMENT OF THERMOPLASTIC COMPOSITE REINFORCED

ULTRA-HIGH PERFORMANCE CONCRETE PANELS

FOR IMPACT RESISTANCE

By Reagan M. Smith Gillis

Thesis Advisor: Dr. Eric N. Landis

An Abstract of the Thesis Presented
in Partial Fulfillment of the Requirements for the
Degree of Master of Science
(in Civil Engineering)
December 2018

Recent studies investigating the impact performance of ultra-high performance concrete (UHPC) reported a quasi-brittle flexural failure that transitioned to a brittle punching-shear failure as the size of the impact head was reduced. A potential technology to increase the flexural strength and impact resistance of concrete is applying fiber reinforced polymer (FRP) composites to the exterior faces of the beam or slab. In this work, E-glass fiber reinforced thermoplastics were utilized in two different systems to apply reinforcement to UHPC. Thermoplastic materials were chosen over traditional thermoset materials for their unique advantages, such as rapid fabrication, automated manufacturing and the ability to weld to the material. These advantages could create an ideal system for large scale production of UHPC panels with thermoplastic reinforcement for use in protective systems. The two systems investigated were stamped thermoforming and vacuum infusion. For stamped thermoforming, the UHPC, fiber reinforced prepreg tapes and an additional layer of thermoplastic resin were heated then consolidated. Upon cooling the multiple prepreg layers of thermoplastic tapes were formed into a complete laminate, which was completely bonded to the UHPC core. The second system to reinforce the UHPC was vacuum infusion using a two-part liquid thermoplastic resin-system and a woven roving fabric. The impact performance of the thermoplastic composite reinforced UHPC panels was

characterized using a combination of drop-weight impact testing and quasi-static testing. After testing it was confirmed that the application of thermoplastic composite skins to UHPC panels improved the impact resistance of the UHPC. Preliminary results showed little or no performance differences between the thermoplastic tapes and the vacuum infused panels. Thermoplastic tape reinforcement may have a fabrication method well suited for automated production, which is an advantage over the labor intensive vacuum infusion procedure. More work must be performed in order to optimize the thermoplastic composite reinforced UHPC panel design for impact resistance.

ACKNOWLEDGEMENTS

This work was supported by the U.S. Army Engineer Research and Development Center (ERDC) through a contract with the Advanced Structures and Composites Center (ASCC) at the University of Maine. Beyond financially support, I would like to thank everyone at ERDC for their hospitability during my visits to the facility and for their assistance with many aspects of this project. Most importantly I would like to thank them for the development of the UHPC mix and their help during the fabrication of the UHPC panels. I owe a special thank you to Todd Rushing, not only for serving on my committee, but for his continued support and guidance throughout the entirety of this project.

A special thank you to the many students and staff at the Advanced Structures and Composites Center who played important roles in making this project a success. The development and fabrication of the thermoplastic composite reinforcement would not have been possible without the expertise of Roberto Lopez-Anido, Nicholas Fitzpatrick and Stephen Berry.

Without the continued guidance of my advisor and mentor, Eric Landis, this project would not have been possible. His support throughout not only my graduate career, but also my undergraduate career is greatly appreciated.

I would like to thank my undergraduate assistant, Stephanie Ayotte, for taking on any task I asked of her, while also making the long hours spent in the lab more enjoyable. Thank you to my fellow graduate students and office mates for offering advice and support when things got stressful. A special thank you to Yi Peng, for helping me navigate the ins-and-outs of graduate school and for making multiple trips down to ERDC with me.

Last, but not least, I would like to thank my family and friends for their support and encouragement.

TABLE OF CONTENTS

LIST OF TABLES

LIST OF FIGURES

CHAPTER 1: INTRODUCTION

Ultra-high performance concrete (UHPC) is a relatively new material. It did not become commercially available in the United States until 2000. The use of UHPC is gaining popularity in the construction industry, but has been used more for the construction of protective structures. UHPC is defined by distinct characteristics such as high mechanical strength, both compressive and flexural, superior durability and self-consolidating properties. The superior durability can be partially attributed to low permeability, which is caused by the low water to cement ratios used in UHPC mix design. Typically mix designs for UHPC also produce a high packing density, which contributes to the high compressive strength and superior durability.

Since, UHPC is a common material used to construct ballistic and blast-proof structures its impact resistance is an important characteristic. The impact performance of a structural element made with concrete, such as UHPC, is often defined by the ability of the material to resist penetration or total perforation and prevent rear face scabbing (Dancygier et al. 2007). UHPC specimens without steel fiber reinforcement have a brittle failure mechanism with large craters forming on the front face of the specimen and large fragments of material separating from the rear face of the specimen (Dancygier et al. 2007; Verma et al. 2016). Due to this brittle failure mechanism some form of steel fiber is typically included in UHPC mixes. The steel fibers decrease the brittleness of the UHPC and provide resistance against punching-shear through a phenomenon known as the bridging effect (Dancygier et al. 2007; Verma et al. 2016; Yoo and Banthia 2017a; Zhang et al. 2007). Even with the added benefits of steel fibers the results of a recent study showed that when subjected to impact loading Cor-tuf, a UHPC mix developed by the U.S. Army Corps of Engineers Research and Development Center (ERDC), had a quasi-brittle flexural failure. But, as the size of the impact head was reduced the failure mode of the panel

transitioned to brittle punching-shear (Ranade et al. 2017). Due to these concerns a UHPC panel with external reinforcement was developed.

There are two types of external reinforcement commonly used to improve the impact resistance of UHPC. Steel reinforcement is shown to significantly increase the impact resistance of concrete, but steel skins add significant weight to the structure (Abdel-Kader and Fouda 2014). The other alternative is FRP skins, creating a sandwich panel configuration. FRP sandwich panels have been extensively studied in the literature with different materials acting as the core of the panel. In these studies, the FRP skins increased the impact resistance of the core material without the significant weight increase of steel (Sarva et al. 2007; Schubel et al. 2005, 2007; Zhou et al. 2012). The FRP skins provide another advantage. The stacking sequence of FRP skins can be adjusted to create an ideal FRP laminate for impact resistance (Cantwell and Morton 1991; Hongkarnjanakul et al. 2013; Strait et al. 1992). These advantages supported the selection of FRP skins to improve the impact resistance of UHPC.

The main goal of this research was to improve the impact performance of UHPC. In order to do so two different variables were introduced. The first variable was the introduction of cellulose nanofibrils (CNFs) to the UHPC mix. The addition of CNFs to cementitious materials, such as UHPC, has been shown to improve the flexural strength of the material. (Peng et al. 2017) Impact loading induces bending stresses throughout UHPC panels, therefore improving the flexural strength of the UHPC through the addition of CNFs has the potential to improve the impact performance of the UHPC. The second variable used to improve the impact performance of the UHPC was the addition of FRP skins. Using steel plate lining or FRP lining has developed as a method to increase the impact resistance of different materials. FRP skins were explored to determine if they improve the impact performance of UHPC.

This thesis describes the materials and fabrication processes used in the development of the UHPC and FRP sandwich panels, as well as the proposed panel performance testing. A control UHPC panel and a

CNF-modified UHPC panel were investigated to determine the effect of the CNFs on the panel performance. Other variables investigated were the FRP skin type and the amount and direction of the FRP reinforcement. The two FRP skin systems selected were a thermoplastic tape applied through stamped thermoforming and a woven fabric applied through infusion with a thermoplastic resin. Once the fabrication of the panels was complete the performance testing started. Quasi-Static and low velocity impact testing was performed as well as three-point bend tests. The quasi-static and bending tests served as preliminary tests for the impact tests that determined if the FRP skins increased the resistance of the UHPC panels against low velocity impact loadings.

1.1 Experimental Program

This section gives an overview of the mechanical testing performed during the evaluation of the thermoplastic composite UHPC panels. More detail into the procedures of the three-point bending, quasi-static, and low velocity impact tests is available in Chapters 4 and 5.

1.1.1 Beam Testing

In the literature there are many experimental procedures to classify the bond of FRP reinforcements to concrete. These procedures are often complex and require specialized specimen configurations that could not be produced using the thermoplastic composite reinforced panels. The specimen availability was limited to a panel with thermoplastic composite reinforcement applied to either one or both sides of the UHPC. Therefore, a bending test was selected since it could be performed on beams cut from the single-sided panels. Although literature is available on beams reinforced with FRP reinforcement and the testing procedures of these beams, the results typically provide a more qualitative description of the bond between the FRP reinforcement and the concrete.

A three-point bending test method was selected to study the bond between the thermoplastic composites and the UHPC because three-point bend tests allow for easy calculation of the dissipated energy at the midspan of the beam. Four possible failure mechanisms were possible when performing either three-point bending or four-point bending on a simply supported beam reinforced with a FRP. The failure mode of interest for the thermoplastic composite reinforced beams was brittle delamination due to intermediate crack-induced interfacial debonding.

1.1.2 Quasi Static and Impact Testing

Classifying the impact resistance of a new prototype depends on the impact level of interest. Low velocity impact versus high velocity impact can cause different failure mechanisms and influence the performance of materials, such as UHPC. Low velocity impact is characterized as an object of high mass impacting a structure with a low velocity, while high velocity impact involves the impact of an object of low mass at a high velocity. To characterize the impact resistance of the thermoplastic composite reinforced panels low velocity impact testing was selected for the preliminary characterization.

An estimate of the energy absorption capacity of the thermoplastic composite reinforced UHPC panels was obtained through quasi-static testing, before the low velocity impact testing was performed. The support and loading geometry for the quasi-static testing was identical to the low velocity impact testing. A goal for the thermoplastic composite reinforced panels was to eventually perform high velocity impact testing, therefore the low velocity impact parameters were selected to have loading characteristics similar to a projectile test. The high velocities of a projectile test could not be obtained through a drop-weight setup, but the low velocity impact testing served as a good preliminary estimate for the impact resistance of the thermoplastic composite reinforced panels. When performing low velocity impact tests the potential for inertial effects must be considered, but there are specific situations where inertial effects can be neglected. Since the thermoplastic composite reinforced panel

specimens were of relatively low mass two studies were used to justify that the inertial effects could be neglected during the low velocity impact testing (Leissa 1969; Verma et al. 2016).

1.2 Organization

The organization of this thesis follows the development process of the thermoplastic composite reinforced UHPC panels. The first step in the process was performing an extensive literature review on the different design factors. The factors considered were the impact resistance of UHPC, the response of different sandwich panel configurations to impact loading, the impact resistance of FRPs, and the performance of FRP reinforced concrete beams under bending loads. The details of this literature review are in Chapter 2. Next, the material selection and fabrication of the thermoplastic composite reinforced UHPC panels is discussed in Chapter 3. This describes the UHPC mix, as well as the two different thermoplastic composites selected as external reinforcement. The mechanical testing begins in Chapter 4, where three-point bend tests were used to gain an understanding of the UHPC-thermoplastic bond. The testing continues in Chapter 5, where the quasi-static and low velocity impact panel testing is discussed. In this section the quasi-static testing is discussed in conjunction with the low velocity impact testing, since its results were used to select the initial impact energy. Chapter 6 provides a summary of the thermoplastic composite reinforced UHPC panel testing, as well as detailing the suggestions for future work.

CHAPTER 2: BACKGROUND

In order to develop the thermoplastic composite reinforced UHPC panels described in this thesis, extensive literature review was required to determine the ideal materials and structure for impact resistance. This section discusses the important aspects of the development process, such as the impact resistance of ultra-high performance concrete. The impact response of sandwich panel structures will be discussed, as well as the impact resistance of composite laminates. These three topics made up the primary concerns involved in the design process. Finally, FRP reinforced beam testing will be discussed.

2.1 Impact Resistance of Ultra-High Performance Concrete

The goal for developing the thermoplastic composite reinforced UHPC panels was to increase the impact resistance of the UHPC, therefore a thorough understanding of the impact resistance of plain UHPC and fiber-reinforced UHPC was required. When discussing the impact resistance of UHPC it is important to make the distinction between low velocity impact and high velocity impact. Low velocity impact of a heavy object can have a different effect on UHPC then a light projectile with a high impact velocity. An example of low velocity impact becoming a concern is flying debris caused by extreme weather events, such as a hurricane. The most common concern in regards to high velocity or projectile impact is protective structures. The low velocity and high velocity impact resistance of UHPC has been extensively studied and is well represented in the literature.

Low velocity impact testing of UHPC had been performed with beams, thin slabs and thick blocks. The simplest way to think about the low velocity impact resistance of UHPC was looking at flexural testing of beams (Bindiganavile et al. 2002; Yoo et al. 2016, 2017; Yoo and Banthia 2017a). As expected UHPC beams had a flexural failure mode even under impact loading. It is typical for UHPC mixes to contain some form of steel reinforcement, such as steel fibers. Therefore, a majority of the UHPC mixes

considered contain some form of steel fiber reinforcement. The first thing the literature established was the superior performance of UHPC with fiber reinforcement (UHPFRC) over traditional concrete with fiber reinforcement (FRC). It had been concluded that under low velocity impact loading, UHPFRC dissipated more energy than conventional FRC. This superior performance was assumed to be the effects of the higher strength matrix and the high fraction of steel fibers typically included in UHPFRC mixes (Bindiganavile et al. 2002). An interesting aspect to evaluate was the effect of steel fibers on the impact resistance of UHPC beams. The addition of steel fibers was shown to increase the initial stiffness of the UHPC, as well as the residual capacity after impact (Yoo et al. 2017). There was even more benefit when the alignment of the steel fibers was optimized. Having a better fiber alignment in UHPC beams increased the flexural strength, normalized deflection capacity, and increased the toughness, but it did not have an effect on the first-cracking properties (Yoo et al. 2016). There were limited resources available on high velocity impact testing of UHPC beams.

The trends set forth in the low velocity impact testing of UHPC beams were also seen when thin slabs were tested. The superior performance of UHPFRC over FRC was confirmed for thin panels in a study by Farnam et al. (Farnam et al. 2010). The failure of thin UHPFRC panels was characterized by localized cracking and excessive spalling around the impact zone (Farnam et al. 2010; Habel and Gauvreau 2008; Ong et al. 1999; Ranade et al. 2017; Verma et al. 2016). A study by Ranade et al. produced an interesting concern regarding the low velocity impact of thin UHPFRC slabs. When a large (75 mm) diameter impact head was used the UHPFRC failed through quasi-brittle flexural and shear failure, but when the diameter of the impact head was reduced to 50 mm a premature punching-shear failure was induced (Ranade et al. 2017). Since impacts by objects smaller than 50 mm are not uncommon, this punching-shear failure must be addressed, which was one of the goals of the thermoplastic composite reinforced UHPC panels. The effect of panel thickness on low velocity impact resistance was investigated in a study by Verma et

al. This study established that when the panel thickness was increased the peak impact force from the low velocity impact was increased. The increase in peak impact force was attributed to the stiffness of the panel being proportional to the cube of the panel thickness (Verma et al. 2016). Similar to UHPFRC beams, the steel fibers had a significant effect on the performance of UHPFRC thin panels. With steel fibers included there is significant research supporting the occurrence of strain-hardening in UHPFRC beams and thin panels at higher strain rates (Habel and Gauvreau 2008; Yoo et al. 2017; Yoo and Banthia 2017a; b). In addition to causing strain-hardening, the steel fibers also increased the ductility of the UHPC. Increasing the ductility increased the energy dissipation capacity, which is an important element of impact resistance (Verma et al. 2016). Yoo et al. established that a better fiber alignment had little effect on the first-cracking properties of UHPFRC beams. Verma et al. confirmed this same phenomenon for the effect of fiber volume on peak impact load because the fibers only become active after the first crack was established (Verma et al. 2016). The low velocity impact of UHPFRC blocks had also been investigated (Yu et al. 2014).

It was important to compare the low velocity impact resistance of UHPC to the high velocity impact resistance. The difference in impact velocity did not appear to have a significant effect on the performance of UHPC. Instead, the literature on high velocity impact testing of UHPC confirmed many of the low velocity impact conclusions, especially when discussing the effect of steel fiber addition. Similar to low velocity impact, UHPFRC was superior to FRC under high velocity impact loading with the same failure mechanism of localized cracking and spalling (Almansa and Cánovas 1999; Dancygier et al. 2007; Máca et al. 2014; Tai 2009; Wu et al. 2015; Zhang et al. 2005, 2007). Multiple studies concluded that the addition of steel fibers reduced the size of the damaged area, meaning the crater diameter and crack propagation in the impact zone, but the steel fibers had little effect on the penetration depth. Reducing the penetration depth of the projectile required increasing the compressive strength of the UHPC

through adjustments to the mix design (Almansa and Cánovas 1999; Dancygier et al. 2007; Máca et al. 2014; Zhang et al. 2005, 2007).

The conclusions discussed above had a significant effect on the development of the thermoplastic composite reinforced UHPC panels, because it provided not only a starting point for the improvement of the UHPC impact resistance, but also helped with the selection of the steel fiber content. As previously stated the addition of steel fibers reduced the size of the damaged area after impact. This reduction in damage was caused by a phenomenon known as the bridging effect. The bridging effect represents a steel fiber's ability to bridge cracks at high loading rates. This reduces fragmentation and absorbs energy through fiber pullout (Bindiganavile and Banthia 2005; Dancygier et al. 2007; Verma et al. 2016; Yoo and Banthia 2017a; Zhang et al. 2007). Since, steel fibers had a significant effect on the impact resistance of UHPC it was decided that steel fibers would be included in the newly developed mix for the thermoplastic composite reinforced UHPC panels. Straight steel fibers were selected based on a conclusion by Yoo and Banthia, that straight steel fibers increased the fiber pullout bond strength, which increased the energy dissipation capacity of the UHPFRC (Yoo and Banthia 2017a). Once the type of steel fiber was selected the fiber content was considered. In the literature it was repeatedly reported that a fiber volume greater than 2% had no significant effect on the impact resistance of the UHPFRC (Máca et al. 2014; Wu et al. 2015; Yoo et al. 2017; Yoo and Banthia 2017a; Zhang et al. 2007). Therefore, the steel fiber content was selected as 1.5%.

There were also consequences associated with the addition of steel fibers. When steel fibers were added to a higher strength matrix, such as UHPC, the fiber-matrix bond became more brittle under quasi-static and impact loading (Bindiganavile and Banthia 2005). This was evident in the study by Ranade et al. discussed above, where the punching-shear failure developed in the UHPFRC panels. Also, after an impact the ultimate deflection capacity of UHPFRC was reduced due to crack localization and

the high bond strength between the fibers and the UHPC (Yoo and Banthia 2017a). Therefore, an external reinforcement mechanism should be introduced to further improve the impact resistance of the UHPFRC. The reinforcement on the front face should reduce the penetration depth of the projectile, while the rear face reinforcement catches any spalling or fragmentation.

2.2 Impact Response of Sandwich Panels

There are presently many forms of external reinforcement being utilized in different industries, but two of the most common forms are metals, such as thin steel plate, and fiber reinforced polymers (FRP). In order to properly design the thermoplastic composite reinforced UHPC panels both forms of external reinforcement were considered with a specific interest in their impact response. The effect of metallic skins on the impact resistance of concrete had been thoroughly investigated, while it was more common to see the impact resistance of FRP skins applied to a foam or honeycomb material investigated, since these are common materials used in the aerospace industry.

The effect of different thin steel plate and concrete structures were tested for impact resistance by Abdel-Kadar and Fouda. A single steel plate on the front face versus the rear face of the concrete plate was tested, as well as a sandwich panel structure with steel plate on the front and rear face of the concrete. It was observed that the single steel plate on rear face had a significant effect on the perforation resistance of the concrete, while the single steel plate on the front face prevented spalling with little effect on the perforation resistance of the concrete. The main benefit of rear face steel plate lining was prevention of the secondary shrapnel effect, which was caused by the rear-face scabbing of the concrete (Abdel-Kader and Fouda 2014). A sandwich panel structure with steel plate lining increased the impact resistance of concrete, but there were conflicting reports regarding its effectiveness compared to rear-face steel lining (Abdel-Kader and Fouda 2014; Remennikov and Kong 2012; Wright et al. 1991). A study on sandwich panels with corrugated metallic skins and reactive-powder concrete (RPC)

produced an interesting consideration for the design of the thermoplastic composite UHPC panels. The corrugated sandwich structure, where an epoxy-resin was used to fill the voids in the RPC, had the best impact resistance of the different sandwich structures considered (Ni et al. 2015). This indicated that an external reinforcement fabrication method, such as vacuum infusion, could increase the performance of UHPC.

The literature on the use of thin steel plate lining supported the use of some form of external reinforcement on the rear face of the concrete to prevent the secondary shrapnel effect. The secondary shrapnel effect was one of the main issues discussed when considering the impact resistance of UHPC. The benefit of external reinforcement on the front face of concrete was presented in a study by Sarva et al. where the effect of thin membrane restraint on ceramic plates was investigated. In this study different forms of FRP were used to form thin membranes on the front and rear face of different ceramic panels. This thin membrane was found to help confine and restrict the flow of the pulverized ceramic, which acts similarly to an impacted UHPC panel. When the study focused on the effect of the front face membrane, it was observed that this membrane was effective in delaying the back face displacement of the ceramic by eroding and slowing down the projectile (Sarva et al. 2007). When combined with the conclusions from studies using thin steel plate linings, it was decided that the thermoplastic composite reinforced UHPC panels would have a sandwich panel structure to utilize both the delay in back face displacement from the front face reinforcement and the prevention of the secondary shrapnel effect from the rear face reinforcement (Abdel-Kader and Fouda 2014; Sarva et al. 2007). Another conclusion by Sarva et al. added further support for the use of a sandwich panel structure with FRP skins. It was concluded that the restraint effect of the FRP membranes effectively altered the failure modes of the ceramic plates (Sarva et al. 2007). This was an important factor in the decision to use a sandwich structure, since a main goal of the thermoplastic composite reinforced UHPC

panels was to prevent the punching-shear failure in UHPC from a small diameter projectile. The weight difference between steel plate and FRP was an additional factor supporting the use of FRP skins.

Once it was decided that FRP skins would be used with the UHPC in a sandwich panel structure an extensive literature review was done into the behavior of composite laminate sandwich panels with a variety of foam and honeycomb cores under impact loading. There was a wealth of knowledge available on this subject due to the popularity of these materials in the aerospace industry. The literature produced a few different considerations for the sandwich panel design of the thermoplastic composite reinforced UHPC panels, such as the effect of specimen size on failure modes, similarly the different failure modes that need to be considered, and the residual strength of a sandwich panel configuration after impact. A study by Anderson and Madenci used small specimens for impact testing and after the impact it was observed that both the foam and honeycomb core specimens experienced cracking and tearing that originated at the impact site and propagated to the specimen edge (Anderson and Madenci 2000). This could be an initial concern for laboratory-scale testing, but it was hypothesized that this behavior would not have the same effect in larger specimens. In larger specimens, a dent localized in the region of impact would be the expected failure mode (Anderson and Madenci 2000). It had been shown through post-impact mechanical testing that even if there was no visible damage to the structure there could still be negative effects from the impact on the mechanical properties of the sandwich structure (Caprino and Teti 1994; Schubel et al. 2007). The mechanical property that was typically effected was compressive strength due to delamination in the skins, which was not always visibly apparent upon inspection of the structure (Schubel et al. 2007).

The failure mode of composite laminate sandwich panels had been well established over the past few decades (Abrate 1997; Akil Hazizan and Cantwell 2002; Anderson and Madenci 2000; Caprino and Teti 1994; Dear et al. 2005; McGowan and Ambur 1999; Nemes and Simmonds 1992; Reyes Villanueva and

Cantwell 2004; Scarponi et al. 1996; Schubel et al. 2005; Wen et al. 1998; Zhou et al. 2007, 2012). A variety of quasi-static and low velocity impact testing had been performed and produced an interesting conclusion regarding the response of composite laminate sandwich panels. Due to load contact characteristics between the impactor and the composite face sheet, there were localized effects that cause the response of the sandwich panels to quasi-static loading to be similar to their response under low velocity impact loading. This indicated that low velocity impact could be characterized as having a quasi-static nature, but quasi-static loading tended to produce more severe deformation in the face sheet then low velocity impact (Schubel et al. 2005). Therefore, quasi-static testing could be used as a preliminary test method for low velocity impact testing. The impact resistance of composite laminate sandwich panels had been shown to rely on a variety of energy absorbing mechanisms. The composite laminate skins absorbed energy through fiber-matrix delamination, longitudinal splitting, and fiber fracture, while the core, typically either foam or honeycomb, absorbed energy through indentation, progressive collapse, and densification (Reyes Villanueva and Cantwell 2004). Since, one goal of the thermoplastic composite reinforcement on the UHPC panels was to reduce the damage to the UHPC more energy should be absorbed by the thermoplastic composite skins. Therefore, the thermoplastic composite reinforcement was designed to have a high energy absorption capacity. Even with the energy absorption from the composite laminate skins, it was shown that the perforation resistance of sandwich panels follows the shear fracture properties of the core material (Akil Hazizan and Cantwell 2002; Zhou et al. 2012). This was a concern for the design of the thermoplastic composite reinforced UHPC panels because UHPC was shown to have a punching-shear failure (Ranade et al. 2017). Therefore, there was still the potential for the UHPC to fail through punching-shear even after the sandwich panel structure was implemented using the thermoplastic composite skins.

Research on the impact response of composite laminate sandwich structures with varying foam core densities showed the failure mode of the structure varies with the core density (Akil Hazizan and Cantwell 2002; Caprino and Teti 1994). Since UHPC is a high density material it was important to consider this research. When the density of the core was low the failure mode was typically shear cracking in the brittle foam core. But, as the density of the foam core increased to a high density the failure mode of the structure transitioned into the composite laminates. With an intermediate core density and a high core density the failure modes were fiber-buckling close to the point of impact and delamination in the top surface skins, respectively (Akil Hazizan and Cantwell 2002). This indicated that when UHPC was the core material in the sandwich structure the failure of the structure could occur in the front face skin through delamination. This failure mode could help prevent the punching-shear in the UHPC, therefore the delamination behavior of the thermoplastic composites was an important consideration in the thermoplastic composite reinforced UHPC panel design.

2.3 Impact Resistance of Composite Laminates

Designing the thermoplastic composite reinforcement for low velocity impact resistance was an important aspect of this work, therefore it was important to determine what affects this resistance. Many studies had been performed to develop the impact response of composite laminates (Curson et al. 1990; Hong and Liu 1989; Takeda et al. 1981, 1982). There had also been multiple comprehensive reviews written on the impact resistance of composite laminates (Agrawal et al. 2014; Cantwell and Morton 1991; Richardson and Wisheart 1996). These reviews provided six major factors that affect the impact resistance of composite laminates. The first three factors were all material properties of the composite. They were the strain energy absorbing capacity of the fibers, the forward shear properties of the matrix, and the strength of the fiber-matrix interphase region. The first two properties should be maximized to increase the impact resistance of a composite laminate (Cantwell and Morton 1991;

Chamis et al. 1972; Dan-Jumbo et al. 1989; Elber 1983). The selection of the fiber-matrix interphase strength depended on the application of the composite laminate. If the purpose of the composite laminate was to completely stop a projectile, then a weaker interphase should be selected. The weak interphase region would develop splitting and delamination, which are energy absorption mechanisms. If residual strength was the goal of the composite laminate, then a stronger interphase should be selected (Cantwell and Morton 1991). The material selection of the thermoplastic composite skins is discussed in Chapter 3 of this thesis.

The remaining three factors affecting the impact resistance of composite laminates were not material properties, instead they were design decisions that can be changed to fit the purpose of the laminate. The impact velocity or strain rate acting on the laminate was an import factor affecting the failure mode (Cantwell and Morton 1991; Harding 2011; Husman et al. 1975; Ross and Sierakowski 1973; ROTEM 1988). Low velocity impact loading with a heavy object caused a full target response over the entire laminate, while high velocity impact by a light projectile had a localized effect. This localized effect resulted in energy being dissipated over a small region surrounding the point of impact. On the other hand, low velocity impact typically resulted in large areas of delamination, which reduced the residual strength of the laminate (Cantwell and Morton 1991). Therefore, the composite laminate should be designed to resist either low velocity impact or high velocity impact. The thermoplastic composite reinforced specimens were initially tested with low velocity impact, but high velocity impact testing should be planned for the future. Ultimately, the goal of the thermoplastic composite reinforcement was energy absorption, which was achieved through delamination in the laminate.

The literature showed a strong correlation between the fiber stacking sequence or reinforcement type in a laminate and the impact resistance (Agrawal et al. 2014; Cantwell and Morton 1991; Chamis et al. 1972; Evci and Gülgeç 2012; Hong and Liu 1989; Hongkarnjanakul et al. 2013; Liu 1988; Lopes et al.

2009; Richardson and Wisheart 1996; Stevanović et al. 1987; Strait et al. 1992; Su 1989). This was a design decision that can be specifically tailored by the designer to produce an ideal laminate for the FRP reinforcement's specific purpose. There were many different forms of FRP typically compared for impact resistance. The first and most basic form was unidirectional laminates, which had fiber reinforcement in one direction only. Unidirectional composites failed through splitting at very low impact energies, which made them unsuitable for impact resistance (Cantwell and Morton 1991; Chamis et al. 1972). This did not mean unidirectional FRPs can never be used for impact resistance. Stacking unidirectional laminates with the fiber direction at different angles can be used to produce composite laminates with high resistance to impact. The stacking sequence of the thermoplastic composite tapes was an important design decision. Many different studies were considered to settle upon a stacking sequence that would provide the high energy absorption capacity desired.

Cantwell and Morton provided initial guidance in their review, when they reported that delamination in multi-angle composites was more likely to occur at ply-interfaces where there was a large mismatch in bending stiffness. The largest change in ply bending stiffness was reported to occur at angle changes of 90° (Cantwell and Morton 1991; Liu 1988). This was confirmed in a study by Hongkarnjanakul et al. where seven different stacking sequences were tested for low velocity impact resistance. This study confirmed that a stacking sequence of [0,90,±45]s had a greater delaminated area than a stacking sequence of [0,45,90,-45]s. Since, delamination was an energy absorption mechanism the [0,90,±45]s laminate had more dissipated energy (Hongkarnjanakul et al. 2013). This was again confirmed by another study that found the use of quasi-isotropic laminates increased dissipated energy significantly over cross-ply and [0,±45] laminates (Strait et al. 1992). These two studies significantly influenced the decision to use a stacking sequence of [0,90,±45]s with the thermoplastic composite tapes in order to increase the energy dissipated by the laminate on the front face of the UHPC.

If residual compressive strength became a concern for the thermoplastic composite reinforced UHPC panels then a different stacking sequence would need to be considered. Residual strength could become a concern if the thermoplastic composite reinforced UHPC panels were utilized in a load bearing protective structure. Using a ±45 surface ply on the outside of a composite laminate had been shown to significantly benefit the residual strength of the laminate, as well as increase the impact resistance (Cantwell and Morton 1991; Hongkarnjanakul et al. 2013). Using ±45 surface plies was not considered for the thermoplastic composite tapes due to fabrication concerns and the preliminary nature of the design. In the future it is recommended that a stacking sequence utilizing ±45 surface plies be considered and studied.

Woven and stitched fabrics were other possible forms of fiber reinforcement commonly studied for composite laminate impact resistance (Cantwell and Morton 1991; Evci and Gülgeç 2012; Strait et al. 1992; Su 1989). These reinforcement forms were typically suggested for use when the designer wanted to minimize the damaged area after impact in the laminate (Cantwell and Morton 1991). A study by Evci and Gülgeç showed that under low velocity impact woven fabrics increased the perforation resistance of a composite laminate, while reducing the damaged area (Evci and Gülgeç 2012). Stitched fabric had been shown to be even more effective in reducing the size of the delaminated area (Su 1989). Woven and stitched reinforcements are typically used in vacuum infusion because they can be simpler to layup than unidirectional fabrics. Since, vacuum infusion was one of the fabrication methods selected for the thermoplastic composite reinforcement a woven fabric was utilized to try and achieve as much delamination as possible.

The final factor influencing the impact resistance of composite laminates was the geometry of the specimen. This was a special consideration throughout the development of the thermoplastic composite reinforced UHPC panels because it had been proven that there was a difference between the impact

resistance of lab specimens and the impact resistance in a full scale composite laminate (Cantwell 2007; Cantwell and Morton 1989, 1991; Mall et al. 1987). Due to geometric effects small-scale lab specimens typically had a greater energy absorption capacity over full-scale structures. It was unrealistic to perform the initial testing of a preliminary design, such as the thermoplastic composite reinforced UHPC panels, with full-scale specimens due to the high cost associated with the production of large specimens. Therefore, if successful the initial lab testing on the thermoplastic composite reinforced UHPC panels should be followed up with testing on full-scale specimens in order to accurately determine the impact resistance.

2.4 Fiber-Reinforced Polymer (FRP) Reinforced Beam Testing

One of the biggest questions regarding the impact performance of the thermoplastic composite reinforced UHPC panels was how the thermoplastic composite reinforcement would bond to the UHPC. On way to answer this question was to review the existing literature on FRP reinforced beams. Stiffening and strengthening older concrete structures, especially bridges, with FRP plates had been thoroughly discussed in the literature because it is becoming a popular retro-fit option. In order to validate this retro-fit option extensive testing had been done to quantify the FRP to concrete bond and the possible failure modes. Test methods to quantify the bond were typically complex and required a specific specimen type. Gunes et al. described a fracture mechanics based model to calculate the interface fracture energy for quantifying a debonding failure in FRP reinforced concrete beams bend tests (Gunes et al. 2009). The use of this model and others required the debonding failure to occur in a controlled manner that way it can be recorded in the resulting load-deflection relationship (Au and Büyüköztürk 2006; Gunes et al. 2009; Leung Christopher K. Y. 2001; Qiao and Chen 2008; Wang 2006).

Since, the test methods mentioned above required specific specimen types and a controlled test environment that could not easily be provided with the thermoplastic composite reinforced UHPC

panels a more qualitative method was adopted. In these tests a specific bond strength was not provided, instead the FRP reinforced-to-unreinforced strengths and deflections were compared (Arduini and Nanni 1997; Attari et al. 2012; Chajes et al. 1994; Saadatmanesh Hamid and Ehsani Mohammad R. 1991). These test methods allowed for the failure mechanisms of the FRP reinforced beams to be evaluated. The common failure mechanisms associated with flexural loading of FRP reinforced beams were FRP tensile rupture, concrete crushing, debonding and shear-tension failure (Aram et al. 2008; Arduini et al. 1997; Arduini and Nanni 1997; Buyukozturk et al. 2004; Buyukozturk Oral and Hearing Brian 1998; Leung Christopher K. Y. 2001; Liu I. S. T. et al. 2007; Nguyen Dai Minh et al. 2001; Oehlers 2006; Pan and Wu 2014; Teng et al. 2006). Arduini and Nanni provided simple definitions for each of the four failure mechanisms. When the tensile strain in the FRP exceeds the ultimate tensile strain of the fibers FRP tensile rupture occurs. Concrete crushing is similar to FRP tensile rupture, the difference is concrete crushing occurs when the compressive strain in the concrete exceeds its ultimate value. These two fail modes were not common since they typically occurred at large deflections. Debonding between the concrete and the FRP reinforcement is caused by failure of the adhesive interface. It is common for this failure mechanism to initiate at a crack and propagate to the nearest end of the FRP plate. The final failure mechanism was only applicable to concrete reinforced with longitudinal steel bars, therefore it was not applicable to the thermoplastic composite reinforced UHPC specimens.

For this work the debonding failure mode was of interest. There were two forms of debonding failure that occurred when a FRP reinforced beam was loaded in bending (Aram et al. 2008). The first was plate-end debonding, which starts near the FRP plate end and propagates into the concrete. The other was midspan debonding where a shear or flexural crack forms and propagates through the concrete-FRP interface. These debonding failures were caused by high tensile and bond shear stresses, which were also defined as a combined pulling and peeling force (Aram et al. 2008; Pan and Wu 2014). In order to

further understand the debonding phenomenon researchers had extensively studied the different stages that occur when the bending load was increased on a FRP reinforced beam (Liu I. S. T. et al. 2007; Teng et al. 2006). Teng et al. described five stages of debonding where each stage involved a combination of three phenomena, either linear elasticity, softening, or debonding, in the concrete adhesive interface. The first stage, or the elastic stage, occurred at low loads when the entire bond length was linear elastic. Then as the load was slowly increased the elastic-softening stage began. In the elastic-softening stage the concrete adhesive interface at either one or both ends of the FRP plate entered the softening state, while the remainder of the bond length remained linear elastic. Debonding began in the third stage, or the elastic-softening-debonding stage. Here debonding occurred at one end of the FRP plate. Once debonding progresses to a certain point there was no longer any part of the concrete adhesive bond still linear elastic. This was the softening-debonding stage. The final stage, the softening stage, described failure of the FRP reinforced beam. At this point the bond length along the concrete adhesive interface was very small, and this short bond length was experiencing only softening.

Debonding failures were likely to occur in large beams, beams with low adhesive thickness, beams where the FRP reinforcement had a low stiffness and beams with a small area of contact between the concrete and the FRP reinforcement (Leung Christopher K. Y. 2001). Since, the concrete was the weakest part of the bond it was extremely important that proper surface preparation was performed prior to the addition of the FRP reinforcement (Aram et al. 2008). This surface preparation could also be used to increase the contact area between the concrete and the adhesive or the FRP reinforcement. Different studies had been performed to determine an ideal surface preparation method for concrete that will be reinforced with an FRP plate (Davood and Ehsan 2010; Galecki et al. 2001; Toutanji and Ortiz 2001). Two common methods of surface preparation were sand blasting and water jetting. The use of a water jet for surface preparation was shown to produce a better bonding strength over sandblasting (Galecki et al.

2001; Toutanji and Ortiz 2001). Davood and Ehsan had proposed a new method for concrete surface preparation that appeared to cause a significant increase in the bond strength between the concrete and the FRP. This surface preparation method was grooving, where small grooves were etched or cut into the concrete surface. The use of transverse and diagonal grooves were both effective in increasing the ultimate failure load of the FRP reinforced beams. But, longitudinal grooving provided the largest improvement over traditional methods of surface preparation (Davood and Ehsan 2010). This confirmed that the surface preparation method used on the UHPC panels prior to the application of the thermoplastic composite skins will be an important step affecting the overall performance of the panels. A traditional method of surface preparation was used for the preliminary design of the thermoplastic composite panels because the grooving method could put the structural integrity of the thin UHPC panels at risk.

2.5 Summary

The literature described above was important throughout the design of the thermoplastic composite reinforced UHPC panels. The research surrounding the impact performance of UHPC helped establish a base line for the design process. One of the biggest concerns presented was the prevalence of rear face scabbing in UHPC panels under all forms of impact loading. The addition of steel fibers increases the impact resistance of UHPC, but it also increases the brittleness. This was apparent in the development of a brittle punching-shear failure when a UHPC panel was impacted with a small diameter loading head. The literature on the impact response of sandwich panels provided a potential fix for these issues. The addition of FRP skins to UHPC in a sandwich structure is shown to have the potential to increase the impact resistance of the UHPC. The FRP on the rear face could catch any potential debris from the scabbing and the front face FRP has the potential to slow the projectile and spread the load preventing the brittle punching-shear failure. Once the decision was made to use FRP skins as external

reinforcement to increase the impact performance of UHPC literature review was performed to properly design the skins. The literature on the impact resistance of composite laminates was important for material and stacking sequence selection. Different stacking sequences were analyzed under impact loading to determine which sequence had the greatest energy dissipation, since that was one of the goals of the front face FRP skin. Through different studies a layup was selected for the thermoplastic composite tapes. This layup was replicated in the design of the vacuum infused skins with a woven fabric. In summary, the first three sections of this chapter describe the essential details required to design the thermoplastic composite reinforced UHPC panels. The literature on testing of FRP reinforced beams was used to select the three-point bending method used for the analysis of the thermoplastic composite to UHPC bond.

CHAPTER 3: DESIGN OF THERMOPLASTIC REINFORCED UHPC PANELS

Literature review showed UHPC is a common material used to construct ballistic and blast-proof structures. In a recent study by Ranade et al. the low-velocity impact resistance of a high strength – high ductility concrete and an ultra-high performance concrete was investigated. When subjected to impact loading the UHPC had a quasi-brittle flexural failure. But, as the size of the impact head was reduced the failure transitioned to a brittle punching-shear (Ranade et al. 2017). Due to these concerns a CNF-modified UHPC and fiber reinforced polymer (FRP) sandwich panel prototype was developed. This chapter describes the design and manufacturing of the prototype. Material selection is discussed for the UHPC and the FRP reinforcement, as well as the manufacturing processes. Two different FRP systems were considered. By implementing both the flexural performance improvements of the CNFs and the additional reinforcement from the FRPs, the impact resistance of UHPC has the potential to be improved.

3.1 Material Selection

Cellulose based materials have emerged as a potential sustainable modifier for cement based composites, such as UHPC. Cellulose nanofibrils (CNFs) have a high aspect ratio, both amorphous and crystalline phases and a high axial elastic modulus. These properties give CNFs the potential to increase the strength of the UHPC system and prevent micro-cracking by creating a smaller inter-fibre spacing and improving the interaction between the cellulose and cement (Bhalerao et al. 2015). It had been reported that a small addition of CNFs can increase the flexural and compressive strengths of cement pastes (Jiao et al. 2016). Therefore, a CNF modified UHPC mix was explored, as well as a traditional UHPC mix with no modifications.

Thermoplastic materials were selected as the FRP reinforcement. Thermoplastics are plastic materials that melt and become pliable at a specific temperature. Then, upon cooling the materials become solid again. Thermoplastic materials were chosen over traditional thermoset materials for their unique advantages, such as rapid fabrication, automated manufacturing, the ability to weld to the material and recyclability. These advantages could create an ideal system for large scale production of UHPC panels with thermoplastic skins for use in modular protection systems. Fiber reinforced thermoplastics were utilized in two different systems to apply reinforcing skins to the UHPC. E-glass fiber reinforcement was used due to its cost-effectiveness. The two systems investigated were thermoplastic composite tapes and an in-situ polymerized thermoplastic composite.

3.1.1 Ultra-High Performance Concrete

A new simplified UHPC mix was developed at the US Army Engineer Research & Development Center (ERDC) in Vicksburg, MS for use in this project. The materials included in this mix were: type I/II cement, silica fume, silica sand, superplasticizer (SP) – a high-range water-reducing admixture and 12 mm long, 0.20 mm diameter straight brass-coated steel fibers. Table 3.1 below summarizes the mix constituents of the UHPC mix. The selected CNF content for the CNF-modified UHPC mix is discussed in the next section. A steel fiber content of 1.5% by weight was used.

Table 3.1. UHPC Mix Constituents

Material	Proportion By Weight
Type I/II Cement	0.3837
Silica Fume	0.0674
Silica Sand	0.4745
Water	0.0679
Superplasticizer	0.0065
Steel Fibers	0.0482

Dispersion of the CNFs was performed by hand until the CNFs appeared to spread out evenly throughout the water. The dry constituents were mixed for 5 minutes, then the wet mixture was gradually added, which included water with or without CNF and ADVA 198. Then, the mixing resumed until kick over. Once all the ingredients were homogeneously mixed the steel fibers were slowly added.

Fabrication of the UHPC panels was performed at ERDC in Vicksburg, MS. The fabrication was a collaboration between graduate students from the University of Maine and researchers at ERDC. Four seventy-pound batches with a 0.05% CNF content and two 70-pound reference batches were produced. Each batch made eight panels and six 2-inch compression cubes.

A panel size of 12-inch by 12-inch with a ½-inch thickness was chosen. ERDC provided 16 12-inch by 12-inch panel molds with a 1-inch thickness. In order to achieve the desired thickness of ½-inch, plastic inserts with a thickness of ½-inch were placed in the molds. Figure 3.1 shows one of the molds with the ½-inch thick insert used to fabricate the UHPC panels.

Figure 3.1. Panel mold with ½ thick insert (front and rear view)

In order to ensure an even thickness of ½-inch the density of the steel fiber reinforced UHPC mix was calculated to find the exact weight required to fill the mold. Each mold was filled with 6.625 pounds of UHPC mix. A vibration table was used to consolidate and level the panels. Next the molds were moved to the wet room for 24 hours. After 24 hours the panels were demolded and placed back in the wet room for approximately 5 days. To accelerate the curing process, the panels were steam cured for 2-4 days. Sixteen of the UHPC panels with CNFs were steam cured for 4 days, while the remaining panels with and without CNFs were steam cured for two days. Figure 3.2 shows panels prior to placement in the wet room and Figure 3.3 shows panels and cubes after demolding. The panels were shipped to the University of Maine after steam curing.

Figure 3.2. Panels prior to placement in the wet room

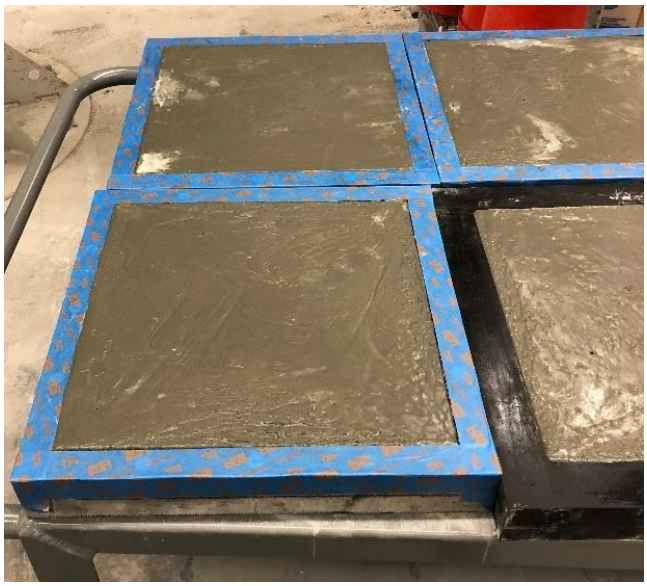

Figure 3.3. Panels and cubes after demolding

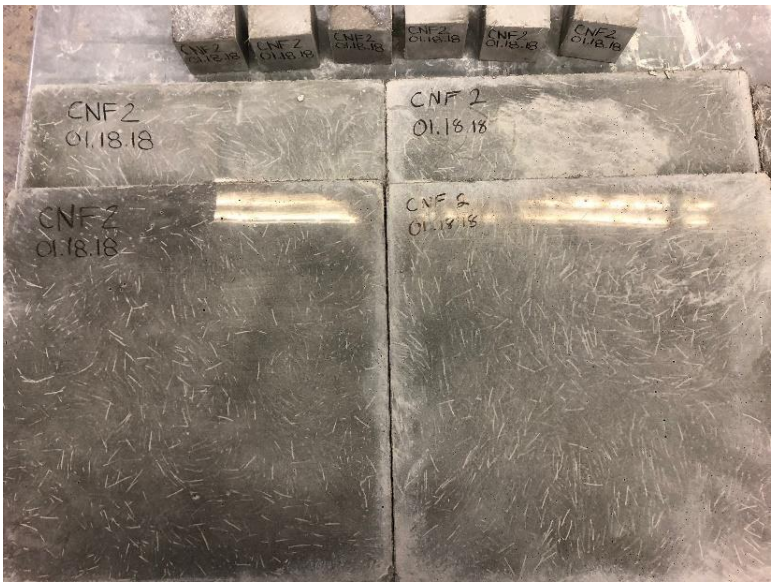

3.1.1.1 CNF Content

The changes to the rheological properties of UHPC from CNFs have an effect on the dispersion of the steel fibers. For use as the core of the sandwich panels, it was important that the fibers were

homogeneously distributed throughout the UHPC for ballistic and blast resistance. Previous research using Cor-tuf, another ultra-high performance concrete developed by ERDC, investigated the effect of CNFs on rheology. In Figure 3.4 the rheological properties from the study are plotted (Peng et al. 2017). The reference batch, with 0% CNF content, was assumed to have optimized rheological properties for fiber dispersion. Figure 3.5 is the result of a study by Wang et al. showing the fiber distribution coefficient as a function of the rheological performance. This figure was for a steel fiber content of 3%, which is similar to the fiber content of Cor-tuf, 3.26% (Wang et al. 2017). The values for yield stress and viscosity cannot be universally compared. Rheological property values vary depending on the instrument, therefore the values in Figure 3.5 are only applicable when the same instrument is used (Ferraris and Martys 2003). The red zone in Figure 3.5 represents the rheological properties providing the best fiber dispersion. By assuming the reference batch was equivalent to the red zone the fiber dispersion properties of CNF-modified UHPC could be evaluated. Based on this comparison there will be a negative effect on fiber dispersion when CNFs are added to UHPC. The most applicable mix to preserve a high fiber distribution coefficient had a CNF content of 0.05% with 50% of the CNF suspension water included as additional water. All other batches decreased the distribution coefficient by an approximate value of at least 10%.

Figure 3.4. Viscosity* versus yield stress (Peng et al. 2017)

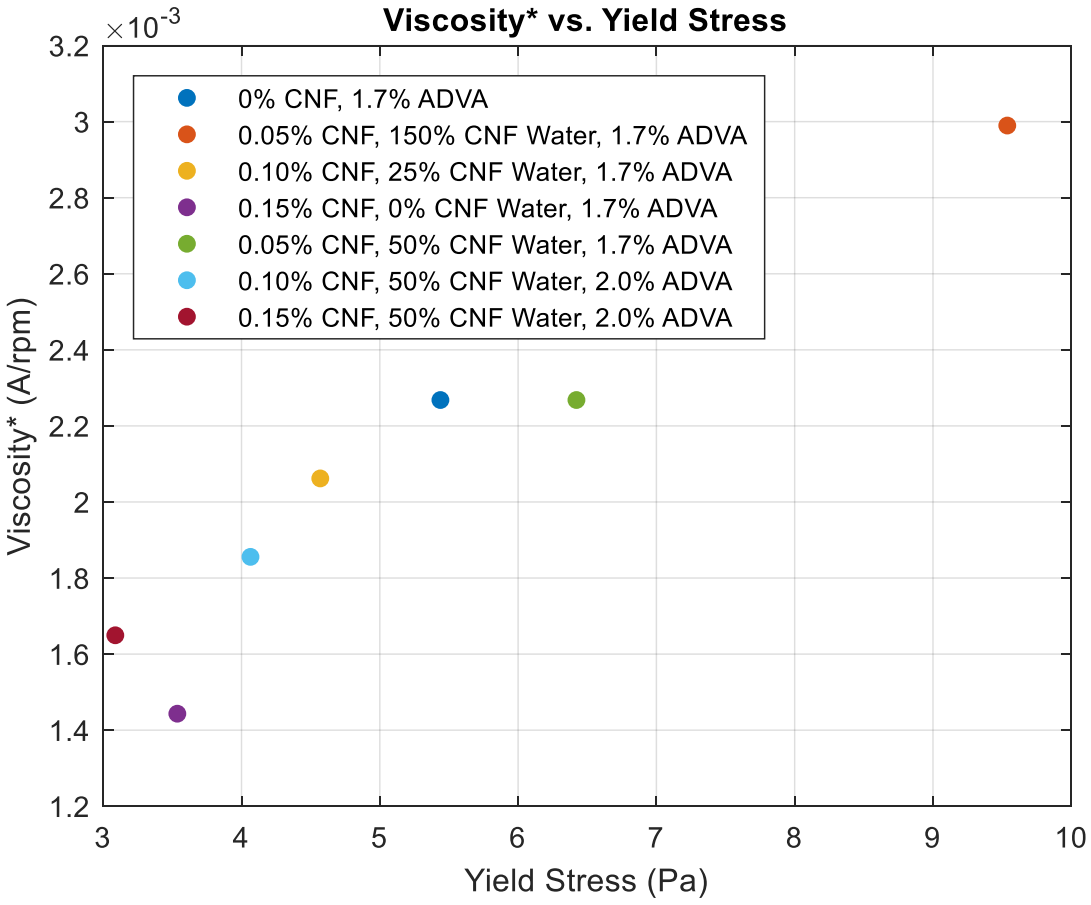

Figure 3.5. Fiber dispersion versus rheological performance (Wang et al. 2017)

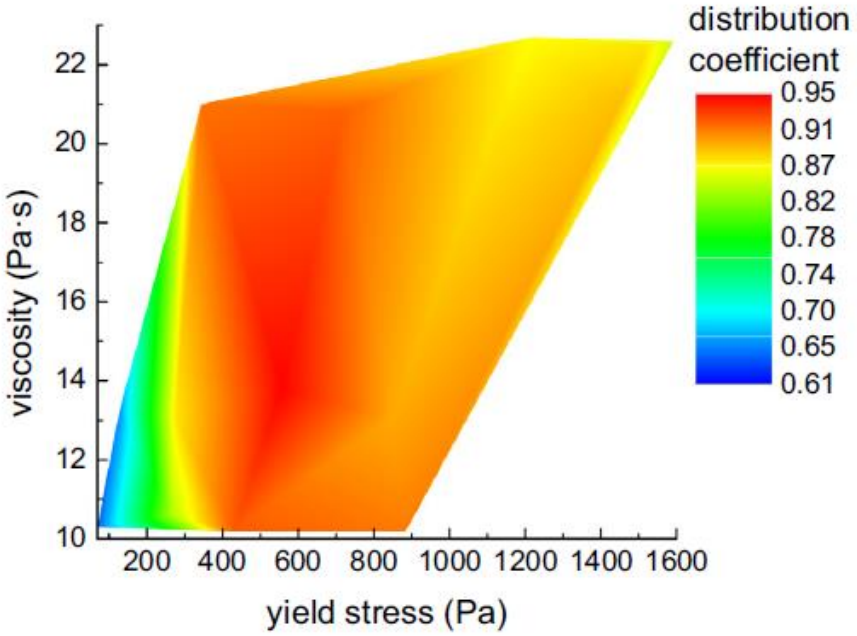

(c) Fiber content=3%

CNFs were obtained from the Process Development Center at the University of Maine. As received CNFs were a suspension designed to have a 3% solid content. But, after drying samples the solid content was determined to be 2.64%. Figure 3.6 shows a high CNF content suspension in water (on the left) and a low CNF content suspension in water (on the right). A low dose, 0.05%, of CNFs was incorporated into the UHPC mix as described above. All CNF percentages were calculated based on solid CNF weight to cement weight.

Figure 3.6. High and low CNF content suspension in water

3.1.1.2 Compressive Strength

Six cubes from each of the six batches fabricated at ERDC were tested per ASTM C109. The preliminary strength testing was performed by technicians at ERDC when the cubes were 36 to 42 days old. The remaining cubes from each batch were shipped to the University of Maine. The final strength testing was done in conjunction with the panel testing when the cubes were 184 to 190 days old.

All of the batches fabricated at ERDC had a preliminary compressive strength greater than 28 kips per square inch. The additional two days of steam curing for batches CNF3 and CNF4 caused an increase in compressive strength of approximately 5%. This strength increase counteracted the negative effects of CNFs on compressive strength. Therefore, batches CNF3 and CNF4 were of comparable strength to the reference (base) batches, while CNF1 and CNF2 had slightly lower strengths. The preliminary strength results for all six batches are located in Table 3.2.

The final strength results from the University of Maine were not consistent with the preliminary strength results. Some batches gained compressive strength while others had a decrease in compressive strength. UHPC is expected to gain strength over time, therefore, this inconsistency could be a result of specimen damage during shipping, mechanical error or human error. The final strength results for all six batches are located in Table 3.3.

Table 3.2 Preliminary Strength Results

Batch No.	Age (days)	Duration of Steam Curing (days)	Average Compressive Strength (ksi)
CNF1	42	2	28.3
CNF2	42	2	28.7
CNF3	41	4	30.3
CNF4	41	4	29.8
BASE1	36	2	29.5
BASE2	36	2	29.9

Table 3.3 Final Strength Results

Batch No.	Age (days)	Duration of Steam Curing (days)	Average Compressive Strength (ksi)
CNF1	190	2	27.5
CNF2	190	2	29.4
CNF3	189	4	27.1
CNF4	189	4	29.8
BASE1	184	2	28.7
BASE2	184	2	30.1

3.1.2 Thermoplastic Composite Unidirectional Tapes

Polyethylene terephthalate glycol (PETg) was selected for use as the polymer in the thermoplastic composite tapes. PETg has a balance between an amorphous and crystalline solid structure making it an ideal material for use with stamp thermoforming or heated consolidation. One of the most important advantages of PETg is its low processing temperature of 215°C. In order to consolidate PETg to UHPC both materials were placed in the same oven. To reduce the amount of expansion experienced by the UHPC a low processing temperature was ideal. Tapes with continuous E-glass reinforcement and PETg polymer manufactured by Polystrand were chosen for use with the stamp thermoforming process. This product was chosen based on its availability and cost-effectiveness, as well as its competitive engineering mechanical properties. The tape IE 5842 was selected for use. IE 5842 has a dye added to the resin, which turns the tapes solid black. Instead of the typical 25-inch wide rolls, IE 5842 comes in 2-inch rolls which can be used in the automated tape layout placement machine at the Advanced Structures and Composites Center (ASCC). The unidirectional tape has a 58% fiber weight fraction. Layers of IE 5842 can be seen below in Figure 3.7.

Figure 3.7. Layers of IE 5842

3.1.3 In-Situ Polymerized Thermoplastic Composite

Elium is a two-part liquid thermoplastic resin-system produced by Arkema. The composition of Elium is between 50 to 85% methyl methacrylate and 10 to 50% acrylic copolymers. Since, Elium is a liquid resin-system it can be vacuum infused. The Elium system is similar to thermoset resin systems, but with unique advantages. Like thermoset resin systems Elium requires an activation agent called Luperox. Elium can be used to infuse very large parts, minimal equipment is required to execute infusion, and the manufacturing process is already commonly accepted in the composites industry. These advantages and the unique properties of an infusible thermoplastic made Elium a potential system for the fabrication of UHPC panels with thermoplastic skins. Another potential application of Elium for the thermoplastic composite reinforced UHPC panels would be to manufacture E-glass reinforced Elium plates, which could be thermoformed onto the UHPC panels. The vacuum infusion process was selected to manufactured the Elium-reinforced UHPC panels.

3.2 Manufacturing

The UHPC cores were all uniformly prepped prior to the application of the thermoplastic composite skins. 20 CNF-modified UHPC panels and 12 reference UHPC panels were prepped. The first step in the preparation process was to remove the white residue from the UHPC surface. The residue would prevent bonding between the thermoplastic and the UHPC, therefore it was removed using a wire brush. Figure 3.8 shows a UHPC panel with white residue on the surface. After the white residue was removed the UHPC surface was roughened with a 4-inch diamond wheel. Literature review showed that surface preparation is an important factor in the bond between concrete and FRP. Figure 3.9 shows the UHPC surface after roughening.

Figure 3.8. White residue on UHPC surface

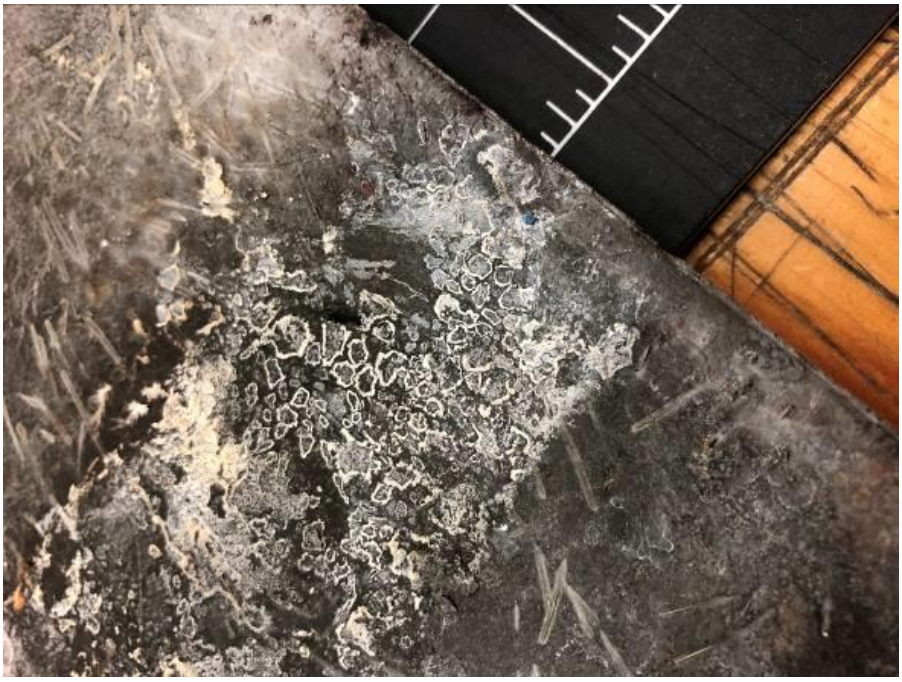

Figure 3.9. Roughened UHPC surface

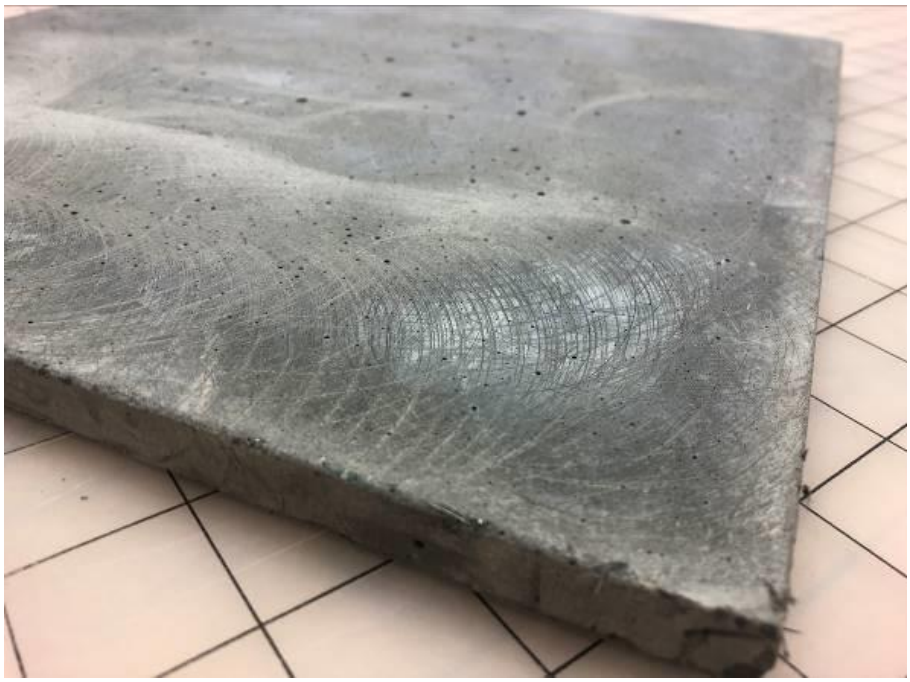

3.2.1 Stamp Thermoforming of Thermoplastic Composite Tapes

Literature review was performed to determine the ideal fiber architecture for use with impact loading. The literature showed a strong dependence on the orientation of unidirectional plies, such as the thermoplastic composite tapes. A review on the impact resistance of composite materials by Cantwell and Morton provided the most insight. It was recommended to avoid using unidirectional laminates because they split apart and fail at low energies. Ply orientation changes of 90° were also not recommended due to an increased amount of damage at the interface from mismatched ply bending stiffness (Cantwell and Morton 1991). The recommendation to avoid ply orientation changes of 90° applied when a composite laminate was the only reinforcement against impact and minimal internal damage was required. But, in the case of the thermoplastic composite reinforced UHPC panels the laminate's purpose was to prevent damage to the UHPC. One way to do this was by minimizing the amount of energy the UHPC needed to absorb, in other terms increasing the energy absorbed by the

laminate. An energy absorption mechanism of composite laminates is layer delamination, which can be induced through 90° ply changes. Therefore, an eight-layer thermoplastic composite tape layup with the following orientation was selected. For the fiber layup, 0° was in the direction of the fibers, shown in Figure 3.10. The selected layup was [0, 90, -45, +45]s . A study by Hongkarnjanakul et al. examined the effect of stacking sequence on CFRP laminates under low velocity impact loading. A stacking sequence of [0, 90, 45, -45]s dissipated more energy during impact than a stacking sequence of [0, 45, 90, -45]s, which had no 90° ply orientation changes (Hongkarnjanakul et al. 2013).

Figure 3.10. Fiber orientations

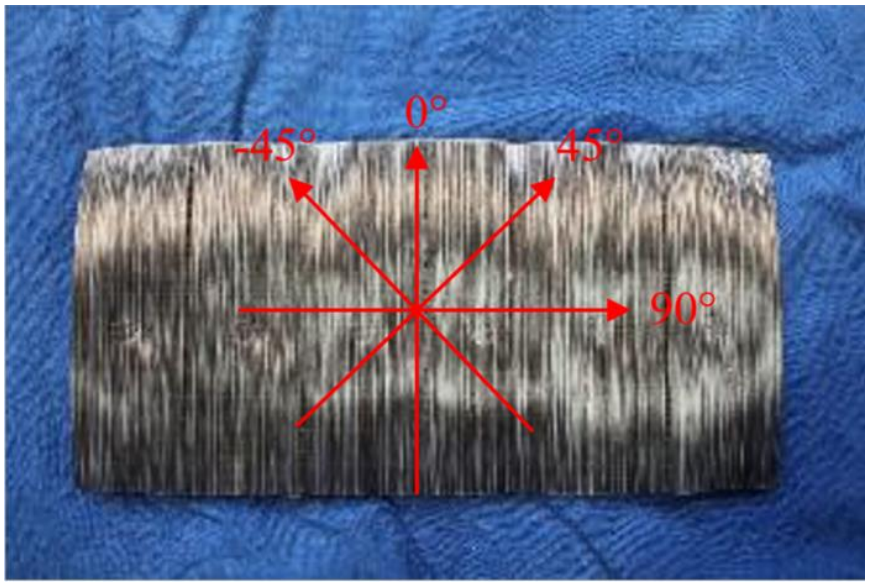

Fabricating the double-sided panels was a two-step process where the PETg tape layup was applied one side at a time. Therefore, only one procedure for a single-sided panel was needed. The layup for a single-sided panel was a UHPC panel, followed by a PETg neat resin sheet and topped with a PETg tape multi-directional tailored blank. The additional layer of PETg resin was used to create a better bond between the UHPC and the reinforcement by flowing into the small pores of the concrete. The panel was then placed on an aluminum sheet and a silicone mat. The entire panel was placed in a 210°C oven

for 14 minutes. The panel was rotated 180° halfway through heating to ensure even heating. Before the panel was placed in the 50-ton press another silicone mat and aluminum plate were placed on top of the multi-directional tailored blank. An effective pressure of approximately 100 psi was used to consolidate the panel for 5 minutes. At the 5-minute mark the pressure was released and the silicone mat was replaced to help cool the PETg resin. This process was repeated until the panel had been consolidated for a total of 15 minutes. To fabricate a double-sided panel this process was repeated on the other side once the panel was completely cooled. Figure 3.11 shows a double-sided panel in the 50-ton press.

Figure 3.11. Double-sided PETg panel during fabrication

3.2.2 Vacuum Infusion of In-Situ Polymerized Thermoplastic Composite

Cantwell and Morton recommended the use of woven fabrics to reduce the interface damage in composite laminates subject to impact loads (Cantwell and Morton 1991). Therefore, the fabric selected

as the E-glass fiber reinforcement of the in-situ polymerized thermoplastic composite was an 18 ounce woven roving purchased from Fibre Glast. The product data sheet provided by Fibre Glast indicated the fabric had 4.5 to 5.5 ends per inch and 3 to 4 picks per inch. Eight layers of fabric were used for each double-sided panel, or four layers per side. The orientation of the eight layers of fabric was [0, -45, +45, 0, 0, +45, -45, 0]. The UHPC panel was placed between the two middle 0 layers, therefore the +45 layer was always placed closest to the UHPC panel in the layup. This layup created a balanced and symmetric laminate. A single-sided panel followed the same orientation, but with only four layers of fabric on the top face of the UHPC.

The vacuum infusions were performed on an aluminum table. Before an infusion could be performed the aluminum table was cleaned with acetone. Once the table had been cleaned the size of the infusion was determined. The area of the infusion needed to be large enough to accommodate the layup, vacuum line and resin line. The following guidelines were established to determine the size of the infusion area:

- Infusion must be at least 4 inches from the edge of the table.
- There must be 6 inches from the vacuum line to the nearest panel.
- Add 11 inches per 12-inch by 12-inch panel.
- There must be 4 inches between each panel.

Figure 3.12 represents the infusion setup for twelve Elium infused UHPC panels. Chemlease 41-90 EZ and flash tape were used to prevent the panels from sticking to the table. Next, the fabric and UHPC panels were placed on the table in the appropriate orientation. For the single-sided and double-sided panels the excess fabric was trimmed to the edge of the UHPC to avoid having glass adhered to the sides of the UHPC. The infusion was set up with a helio-coil feed line running between two rows of panels and

the helio-coil vacuum line around the perimeter. Peel o' ply was cut wide enough to extend about 1 inch past either side of the part and long enough to span the entire infusion, including the vacuum line. Once the peel o' ply was in place on top of the infusion, the flow media was cut to a width 2 inches shorter than the size of the panels being covered. This prevented the infusion from ending prematurely. The peel o' ply and flow media carried the vacuum and Elium throughout the infusion. In order to calculate the size of the vacuum bag needed 2 inches were added to the infusion length and width at every geometry change. Geometry changes included the resin line, vacuum line and mold surface. A 1-inch tall pleat was created using tacky tape at every change in geometry when the bag was sealed. Next, the vacuum line was connected to the paint pot after the pump pressure reached 30 inHg. A drop test was performed while vacuum bag leaks from the steel fibers were sealed with tacky tape. A respirator was used and was required to infuse with Elium. The Elium resin was mixed following the proper proportions for the infusion size and the resin bucket was placed in a bucket of water. Someone needed to be present throughout the infusion until the resin had kicked to make sure the resin level didn't run low and the resin bucket didn't get too hot. The panels were left to sit overnight before being debagged in the morning. Figure 3.13 shows the different stages of the vacuum infusion process.

Figure 3.12. Infusion layup for twelve Elium-reinforced UHPC panels

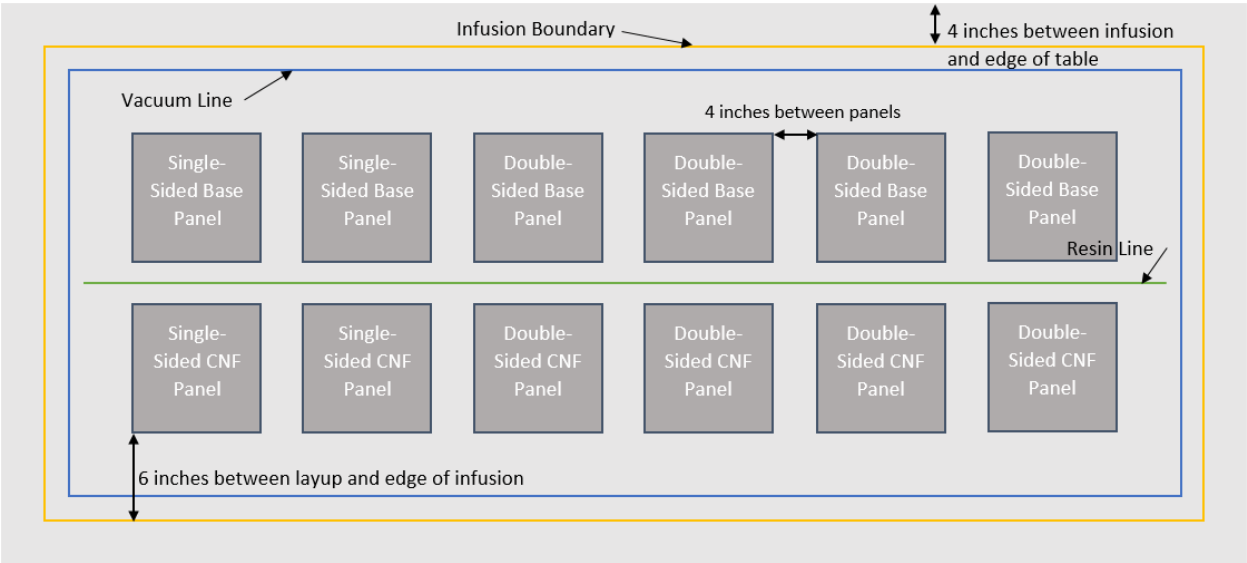

Figure 3.13. Different stages of the vacuum infusion process

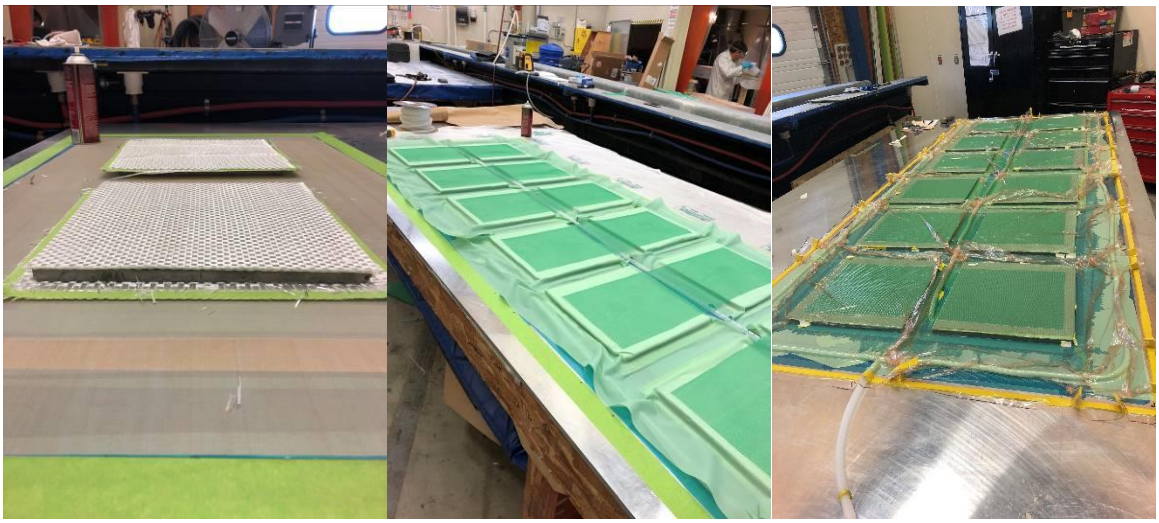

Once the panels were infused with Elium, two problems presented themselves upon debagging. The first problem was caused by vacuum leaks in the bag. Since the UHPC panels had multiple steel fibers protruding out of the UHPC it was difficult to find every location where a fiber caused a leak in the bag. The leaks caused dry spots in the fabric on the bottom of the double-sided panels. Figure 3.14 shows

examples of the dry spots. The image on the left shows a small dry spot. These were simply fixed by using a paint brush to brush on more Elium. The large dry spots shown in the figure on the right were reinfused. Figure 3.15 shows a panel during reinfusion. Once the dry spots were repaired the panels were post cured at 80°C for 24 hours. The second problem was encountered during the removal of the single-sided panels. The release agent, Chemlease 41-90 EZ, used on the table was not compatible with the concrete-Elium interface, therefore large chunks of concrete were left on the table. One single-sided panel with a CNF modified core was cracked during removal due to this incompatibility. Figure 3.16 shows the concrete left on the aluminum table. In order to fix this issue in future infusions a different release agent should be used or peel o' ply should be placed below the single-sided panels.

Figure 3.14. Dry spots on the bottom of the double-sided panels

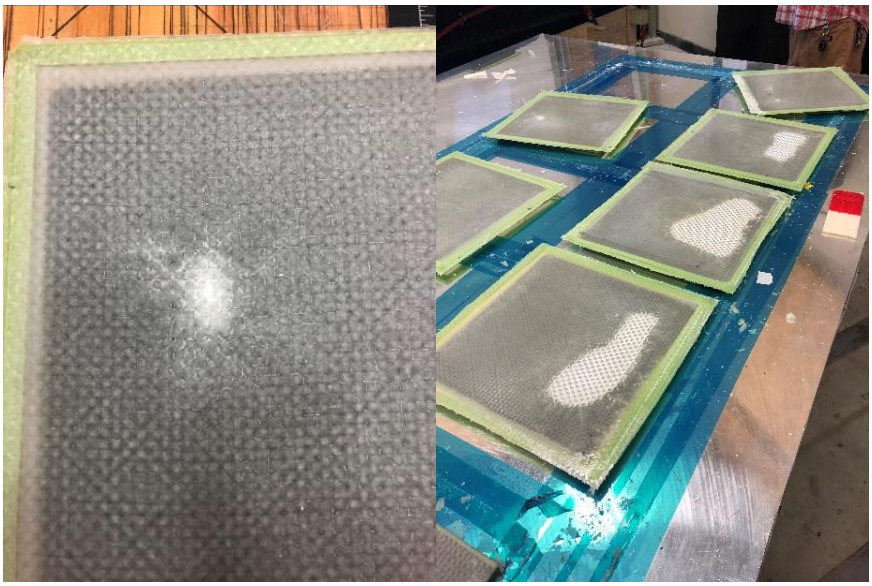

Figure 3.15. Reinfusion of a large dry spot

Figure 3.16. Concrete damage from removal of single-sided panels

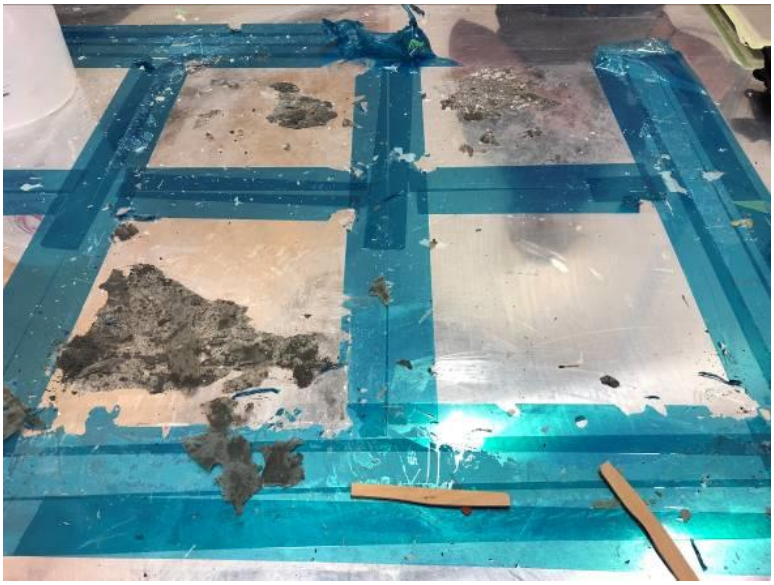

CHAPTER 4: BOND ANALYSIS

An important characteristic involved in classifying the performance of the thermoplastic composite reinforced UHPC panels was the bond of the thermoplastic composite to the surface of the UHPC. This chapter describes the experiments performed to quantify this bond and the results.

4.1 Introduction

Literature review provided many experimental procedures for classifying the bond of FRP reinforcement to concrete. Unfortunately, many of these procedures could not be used due to the complex nature of the tests and the limited specimen configuration provided by the thermoplastic composite UHPC panels. Since the specimen availability was limited to a panel with thermoplastic composite reinforcement applied in either a single-sided or double-sided configuration, a bending test on beams cut from the panels was determined to be the best option. There was ample literature available on beams reinforced with FRP and the testing procedures associated with these beams, but it provided a more qualitative description of the bond between the FRP reinforcement and the concrete.

Throughout the literature either three-point bending or four-point bending methods were utilized to study the effect of FRP reinforcement on concrete beams, which typically contain some form of steel reinforcement. To classify the bond between the thermoplastic composites and the UHPC a three-point bending method was selected for easy calculation of the energy dissipation at the midspan of the beam. Four failure mechanisms are possible when performing either three-point bending or four-point bending on a simply supported beam reinforced with a FRP. The first is FRP tensile rupture, which occurs when the tensile stress in the FRP becomes too large and the fiber reinforcement fails. Concrete crushing is the second possible mechanism. Concrete crushing is similar to FRP tensile rupture because it occurs when the compressive stress in the concrete overcomes its ultimate value and the concrete begins to

crush. The third failure mechanism is FRP debonding. This was the failure mechanism of interest for the experiments described in the following sections. The final failure mechanism is shear failure at the ends of the beams (Arduini and Nanni 1997). A review on the bond strength of FRP laminates to concrete provided more insight into the different failure mechanisms of FRP reinforced concrete beams under bending. This review explored the different forms of debonding and their causes. The most critical case of brittle delamination occurs due to intermediate crack-induced interfacial debonding. This form of failure typically occurs when a flexural crack is formed in the concrete causing debonding of the FRP reinforcement to start. Once this debonding begins it will propagate along the length of the beam until eventually a brittle failure of the beam occurs (Sayed-Ahmed et al. 2009). Typically, experiments utilizing either three-point bending or four-point bending were quantified by comparing the performance of equivalent concrete beams with and without FRP reinforcement. Gunes et al. described a fracture mechanics based model for quantifying debonding failure of FRP reinforced concrete beams under bending. This model calculated the interface fracture energy involved in the FRP debonding (Gunes et al. 2009). The use of this model required the debonding failure to occur in a controlled manner that could be observed through a three-point bend test and the resulting load-deflection relationship.

4.2 Experimental Procedure

The beam specimens were produced using the single-sided thermoplastic composite reinforced UHPC panels. The UHPC panels reinforced on a single side through vacuum infusion were from batch CNF1 and batch BASE2 and the UHPC panels reinforced on a single side through stamp thermoforming were from batch CNF4 and batch BASE1. Starting with a 12-inch by 12-inch panel a wet saw was used to quarter the panel into 6-inch by 6-inch specimens. Each 6-inch square specimen produced five beam specimens with a nominal width of 1-inch. The UHPC panels were fabricated to be ½-inch thick, therefore including the depth of the thermoplastic composites the depth to width ratio of the Elium-reinforced and PETg tape

reinforced beams was 0.563 and 0.625, respectively. A model of a typical Elium-reinforced beam is shown in Figure 4.1, the only difference for a beam reinforced with PETg tapes is the reinforcement thickness of ⅛-inch. Figure 4.2 shows the three types of beam specimens. The top photo is an Elium-reinforced beam, the middle photo is a PETg tape reinforced beam and the bottom photo is an unreinforced beam.

Figure 4.1. Model of a reinforced beam specimen

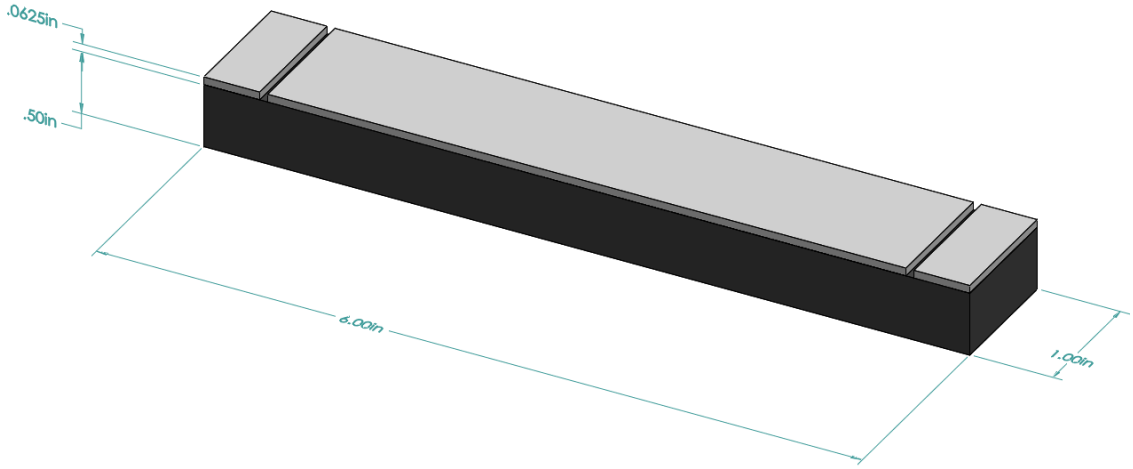

Figure 4.2. Elium-reinforced (top), PETg-reinforced (middle) and unreinforced (bottom) beam specimens

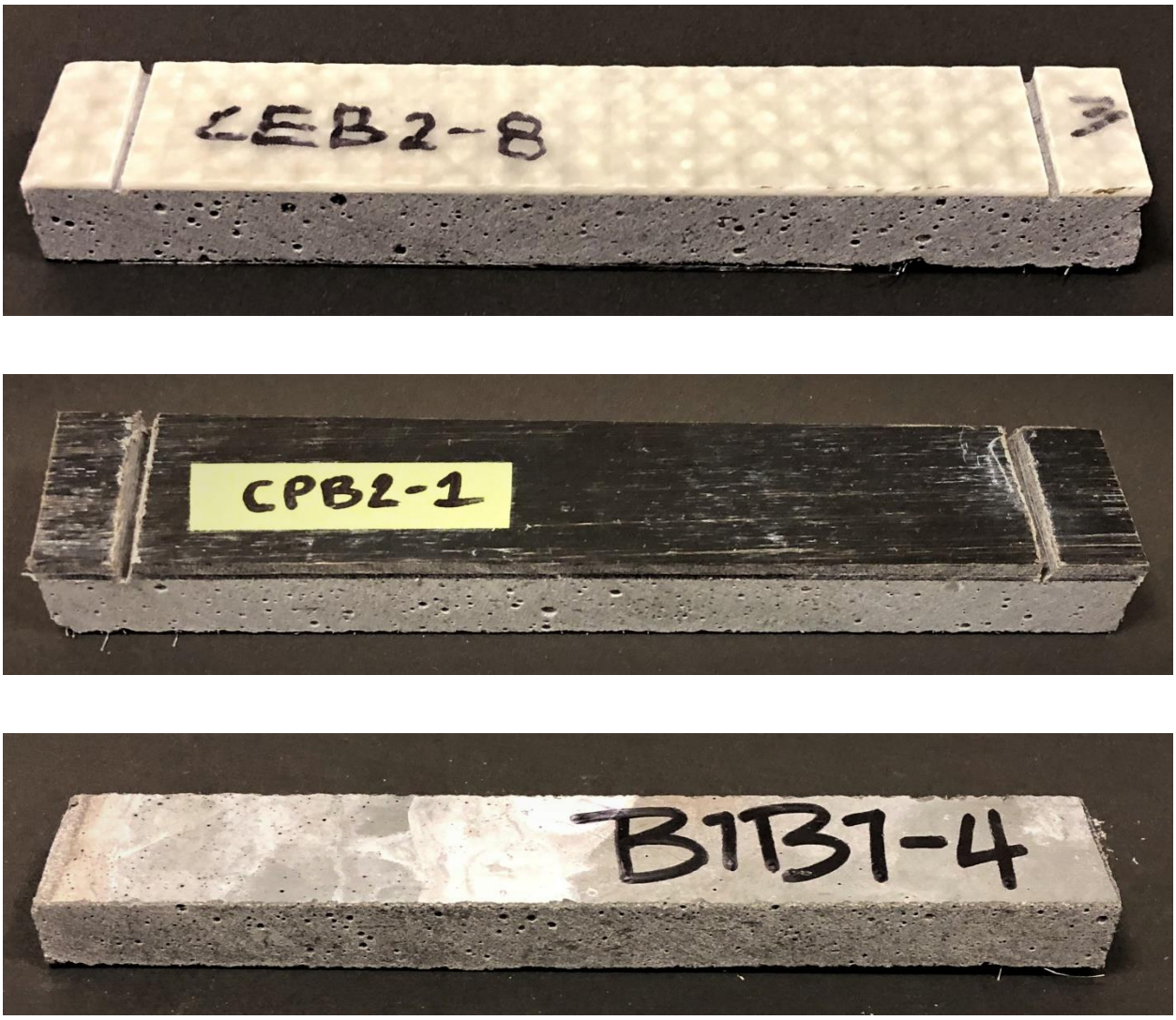

Since the goal of the beam testing was to evaluate the bond between the UHPC and thermoplastic composite reinforcement, the reinforcement was notched ½-inch from each end of the beam. This terminated the composite action between the UHPC and the thermoplastic composite at that point, which prevented any increase in bond performance from the reaction at the support. The notches were initially cut using a wet saw, but multiple challenges occurred during the process. In order to avoid a shear failure in the beam it was important to avoid coming in contact with the UHPC during notching.

Unfortunately, in some cases the UHPC surface was not perfectly level and the notches were cut slightly into the UHPC panel. Figure 4.3 shows a beam where a notch was cut into the concrete. The wet saw was set to cut just above the surface of the concrete to try and prevent the occurrence of deep notches, then each notch was individually examined under a microscope to check for any remaining connection of the thermoplastic composite reinforcement. If a connection was found the notch would be extended using hack saws and an exacto knife under the microscope until there was no remaining connection.

Figure 4.3. Beam specimen with a deep notch extending into the concrete

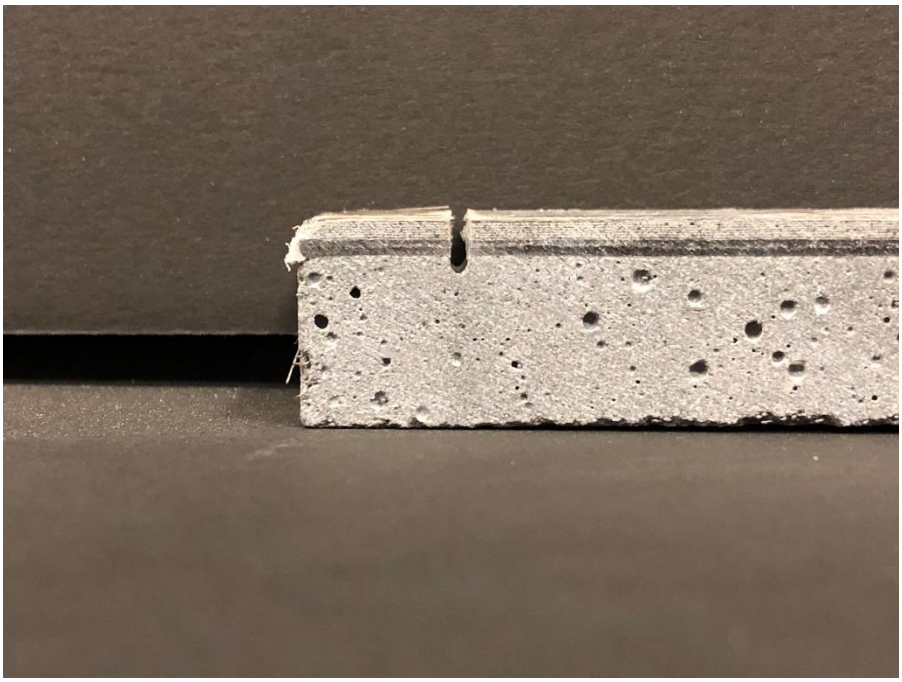

Once the beam specimens were all prepared and notched they were measured to record any potential geometric flaws in the specimen. Each specimen was weighed and measured using a caliper for the following measurements: length, width, depth, UHPC depth and notch depth. The width, depth, and UHPC depth were taken at the center and each end of the beam, then averaged. All measurements were recorded in millimeters.

A total of 98 beam specimens were tested in static three-point bend tests on a 5kN Instron. 38 of the 98 specimens were reinforced with Elium through vacuum infusion, 40 were reinforced with PETg tapes through stamp thermoforming and 20 were unreinforced. For the PETg tape reinforced and unreinforced beams 50 percent of the specimens contained CNF. The Elium-reinforced beams had 18 specimens containing CNF and 12 without due to a fabrication error. The thermoplastic composite reinforcement was placed facing down on the fixture, therefore the reinforcement was on the tension face of the beam during bending. Two linear variable differential transformers (LVDTs) were used to measure midspan displacement. The test setup held the LVDTs independently from the beam to ensure deflection was measured relative to the specimen instead of a fixed point. Figure 4.4 show the test setup on the 5kN Instron machine.

Figure 4.4. Beam test setup on a 5kN Instron machine

The thermoplastic composite reinforced beam specimens were tested using displacement control at a rate of 0.5 mm/min. The Instron unloaded when the load on the specimen dropped more than 500 N below the peak load. This indicated failure through shear or delamination. Figure 4.5 shows a beam in the test setup after delamination failure from a flexural crack. After each test the delaminated specimens were placed under a microscope to determine the approximate delaminated area. To determine the delaminated area, the length of delamination was measured on each side and averaged before being multiplied by the average beam width. The unreinforced beams were also tested using displacement control at a rate of 0.5 mm/min, but the Instron was instructed to unload manually by the operator after approximately 1 millimeter of deflection. The end value was determined through post

processing of the thermoplastic composite reinforced beams since most specimens failed in delamination at approximately 1 millimeter of deflection.

Figure 4.5. Beam specimen after delamination failure

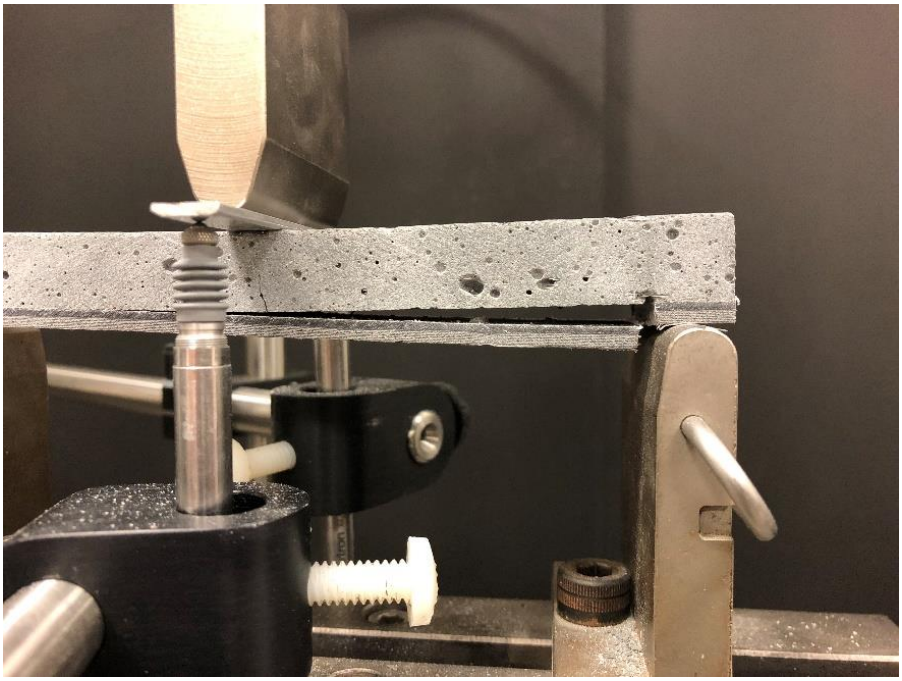

4.3 Results and Discussions

The first major result obtained through the three-point bending tests of the thermoplastic composite reinforced beams was the failure mechanism of each beam. The two failure mechanisms that presented themselves during the testing was debonding of the thermoplastic composite and shear failure near the supports. The depth of the notches cut into the thermoplastic composite, and in some cases the concrete, was recorded for all specimens. There was a concern that the deeper notches would cause shear failure, but there did not appear to be a correlation between the notch depth and the occurrence of shear failures. The Elium-reinforced beams had a total of 8 beams fail in shear, 6 of those shear failures occurred on beams with CNF-modified UHPC. The high occurrence of shear failures in these

beams could be related to the issue discussed in section 3.2.2, where the release agent used during the vacuum infusions was not compatible with the Elium resin to UHPC interface. This incompatibility made removing the single-sided Elium-reinforced panels from the aluminum table difficult and in some cases the panels were damaged in the removal process. When selecting which beam specimens to test this damage was considered and specimens were selected with hopes of avoiding any negative effects from the damage. Unfortunately, the concrete within the beam could not be examined. Therefore, the relatively high occurrence of shear failures in the Elium-reinforced CNF-modified beams could be a consequence of this damage. Even though the damage occurred during the manufacturing of the Elium single-sided panels, there was a similar occurrence of shear failures with the PETg tape reinforced beams. There were 10 beams out of the 40 PETg tape reinforced beams that failed in shear. Unlike with the Elium beams, there was no clear explanation for all the shear failures. One possible explanation was the PETg tape reinforcement is twice as thick as the Elium reinforcement. It had been reported that the peeling of FRP reinforcement as a result of shear cracks occurred in beams with thicker laminates (Sayed-Ahmed et al. 2009). Therefore, the high occurrence of shear failures in PETg tape reinforced beams could be caused by the increased laminate thickness.

The results discussed in the rest of this section will only consider the 30 Elium-reinforced beams and the 30 PETg tape reinforced beams that failed through thermoplastic composite debonding, along with the 40 unreinforced beams that were tested. This distinction was made since the debonding and shear failures were both brittle mechanisms, that resulted in similar load versus displacement plots for all of the thermoplastic composite reinforced beams. Figure 4.6 is an example of a load versus displacement plot for a thermoplastic composite reinforced beam failing through debonding and Figure 4.7 represents thermoplastic composite reinforced beam failing through shear. Both Figure 4.6 and Figure 4.7 are

comparative plots showing an unreinforced, PETg tape reinforced, and Elium-reinforced specimen. The results from the three-point bending tests for each individual specimen is included in Appendix A.

Figure 4.6. Comparative load-displacement curves for beam specimens failing through debonding

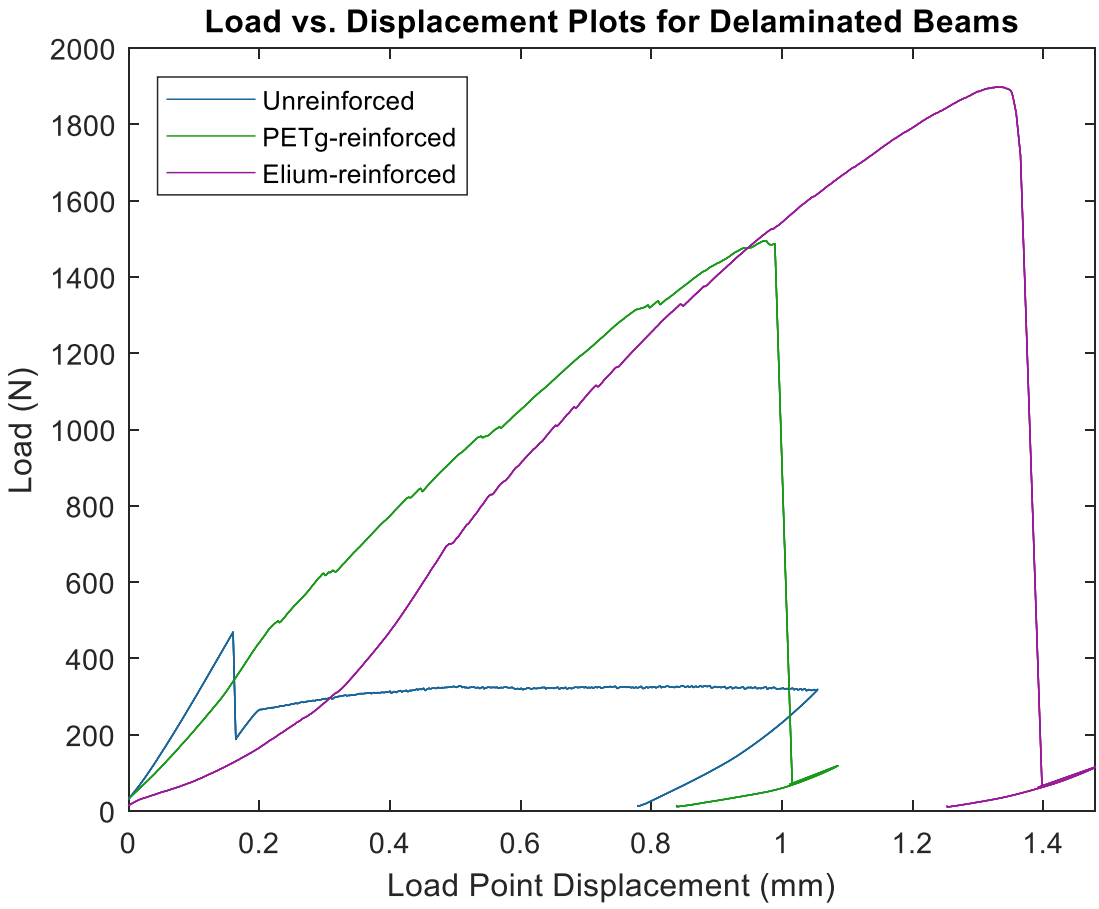

Figure 4.7. Comparative load-displacement curves for beam specimens failing through shear

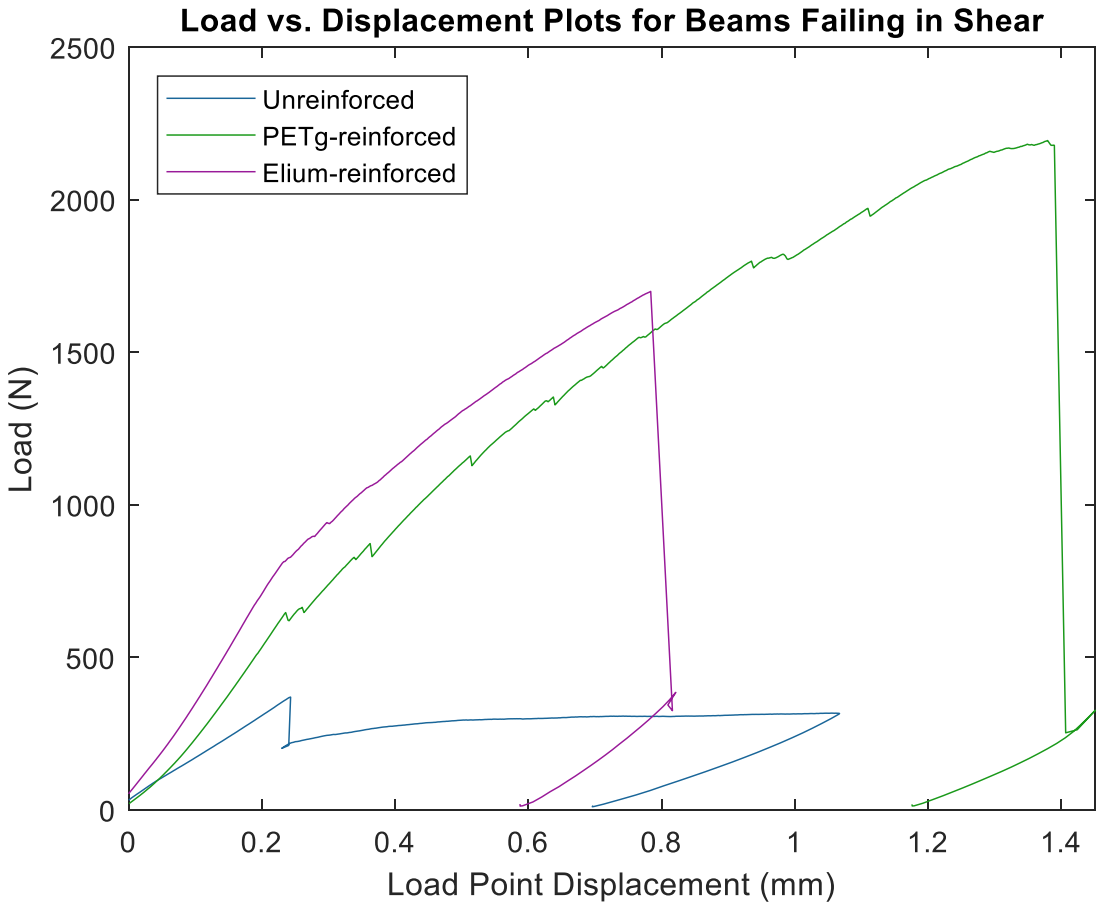

Due to the unstable failure of specimens during testing, fracture mechanics could not be used to characterize the bond between the concrete and the thermoplastic interface. Instead the results of the thermoplastic composite reinforced panels were compared to the unreinforced panels. The unreinforced panels all developed flexural cracks at the midspan, while the majority of thermoplastic composite reinforced specimens failed due to flexural cracks that induced delamination of the thermoplastic skin. The peak load, energy dissipation at the midspan, and peak displacement were analyzed for each specimen.

The peak load results are shown in Figure 4.8 separated by UHPC type and thermoplastic composite reinforcement. The error bars represent one standard deviation above and below the mean value for peak load. As expected there was minimal variation in the peak load values for the unreinforced panels. The base UHPC specimens slightly outperformed the CNF-modified UHPC specimens with a mean peak load of 570 N. The mean peak load of the CNF-modified specimens was 444 N, which is a 20% reduction compared to the base specimens. When thermoplastic skins were applied the difference between the base specimens and the CNF-modified specimens was minimal. The Elium-reinforced base specimens had a mean peak load of 1740 N, while the mean peak load for the CNF-modified specimens with the same skins was slightly higher at 1940 N. This was only an 11% increase in peak load over the Elium-reinforced base panels, but the standard deviation of the CNF-modified Elium-reinforced specimens was higher at 283 N. The Elium-reinforced CNF-modified specimens had two distinct data groups that corresponded to which 12-inch by 12-inch panel the specimens originated from. The lower group corresponded to the panel that suffered the most damage upon separation from the aluminum table after the vacuum infusion. This correlation indicated that despite efforts there was likely damage to these specimens prior to testing. All the specimens reinforced with PETg tapes produced significant scatter in the results. The mean peak load in the PETg tape reinforced base and CNF-modified specimens was 1560 N and 1670 N, respectively. This was less than a 10% difference between the two UHPC types.

Due to the insignificant difference between the base UHPC and the CNF-modified UHPC the groups were combined to compare the thermoplastic composite type to the unreinforced specimens. The mean peak load of the unreinforced specimens was 507 N, which was significantly lower than the mean peak load of both thermoplastic composite reinforced specimen groups. The Elium reinforcement provided a 259% increase in the mean peak load, while the PETg tape reinforcement provided a slightly smaller increase of 222%. The mean peak load of the Elium-reinforced group was 1820 N and the mean peak load of the

PETg tape reinforced group was 1630 N. These values showed the Elium-reinforced group was 11% greater than the PETg tape reinforced group, which was only a slight increase.

Figure 4.8. Peak load results separated by panel type

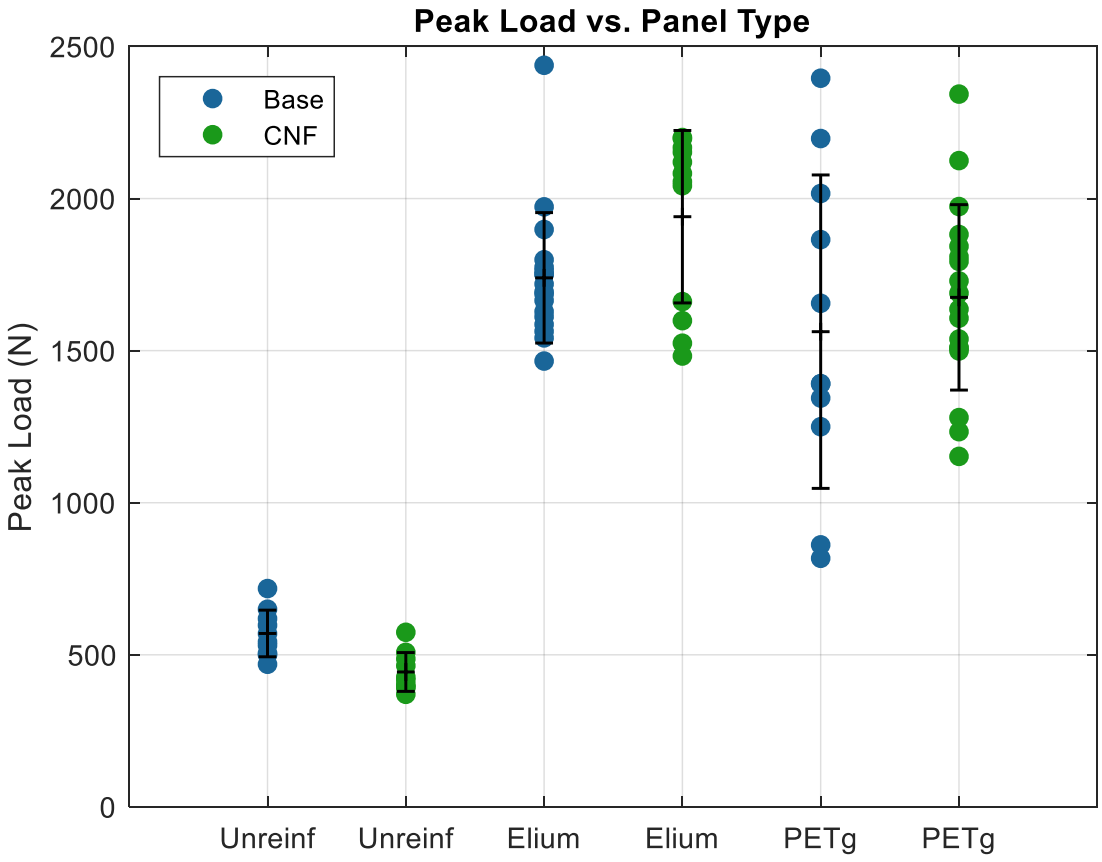

The results for the energy dissipated at the midspan are shown in Figure 4.9 separated by UHPC type and thermoplastic composite reinforcement. Similar to Figure 4.8, the error bars represent one standard deviation above and below the mean value for energy dissipation. Again there was minimal variation in the energy dissipation values for the unreinforced panels. The base UHPC specimens had a mean energy dissipation value of 337 N·mm. The CNF-modified UHPC specimens had a mean energy dissipation 33% smaller at 266 N·mm. The Elium-reinforced base specimens had a mean energy dissipation of 1050

N·mm. Similar to the peak load results the CNF-modified specimens with Elium reinforcement had the larger mean energy dissipation of 1250 N·mm. This was a 20% increase in dissipated energy over the Elium-reinforced base panels. In the case of the dissipated energy results the base and CNF-modified thermoplastic composite reinforced specimens had similar scatter among the data points. The mean energy dissipation value for the PETg tape reinforced base and CNF-modified specimens was 818 N·mm and 942 N·mm, respectively. This was a 15% difference between the two specimen types.

Again, there was little difference between the base UHPC and the CNF-modified UHPC. Therefore, the groups were combined once again. The mean energy dissipation value of the unreinforced specimens was 301 N·mm. In comparison the mean energy dissipation value of the Elium-reinforced specimens was 1130 N·mm, which was an increase in dissipated energy of 274%. The PETg tape reinforcement increased the mean energy dissipation by 197% with a value of 895 N·mm. When the two thermoplastic composite reinforcement groups were compared against one another the Elium-reinforced specimens dissipated approximately 25% more energy than the PETg tape reinforced specimens.

Figure 4.9. Work results separated by panel type

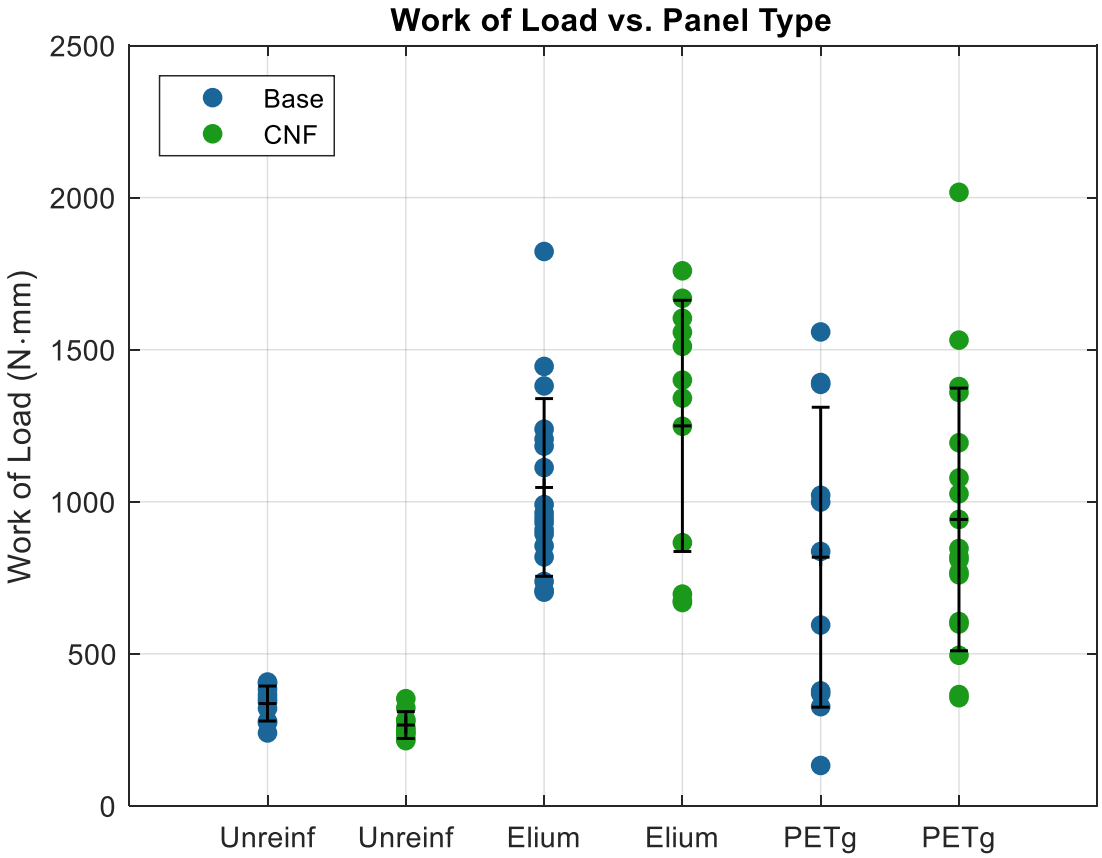

The peak displacement results shown in Figure 4.10 show significant scatter in all of the specimens, but especially the base and CNF-modified unreinforced specimens. This was a result of how the peak displacement was calculated. Simply taking the maximum displacement measured by the LVDT would not have provided an accurate measurement of the displacement at the peak load, which is where debonding occurred for the thermoplastic composite reinforced specimens. Therefore, the peak displacement was calculated as the displacement when the peak load occurred. The scatter in the unreinforced panels corresponds to the differing location of the peak load when unreinforced panels are

loaded in bending. Due to this discrepancy the comparison of the thermoplastic composite reinforced specimens to the unreinforced specimens would be inconclusive.

There was little difference between the mean peak displacement of the Elium-reinforced base specimens, 1.03 mm, and the Elium-reinforced CNF-modified specimens, 1.06 mm. The PETg tape reinforced base specimens had a mean peak displacement of 0.76 mm. The CNF-modified specimens had a mean peak displacement that was 10% greater, a value of 0.84 mm. Since the difference between the base and CNF-modified groups appear to be insignificant the two different thermoplastic composite groups were combined and compared. The Elium-reinforced specimens deflected 28% more than the PETg tape reinforced specimens before debonding.

Figure 4.10. Peak displacement separated by panel type

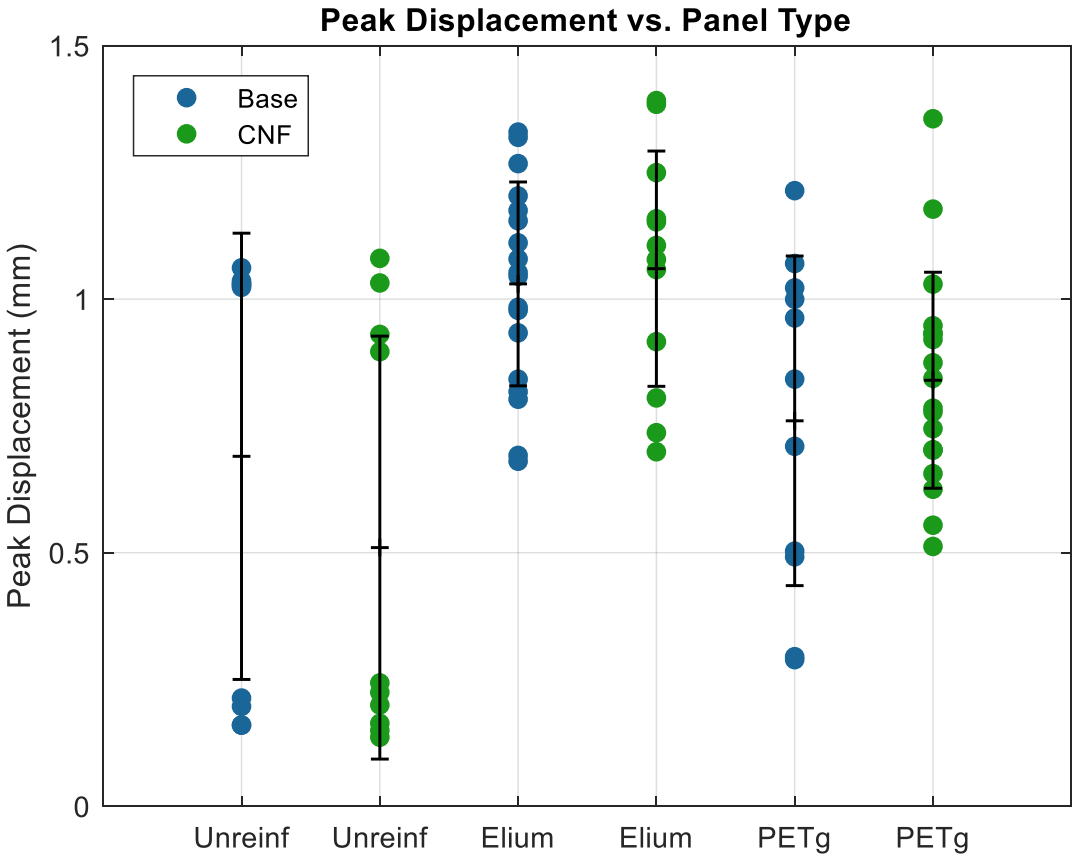

The size of the debonded surface area of each specimen was analyzed for each specimen that failed through debonding. Unfortunately, the debonded area varied significantly from specimen to specimen with no apparent correlation to the type of UHPC or thermoplastic composite reinforcement. In order to calculate the debonded area each specimen was examined under a microscope. These examinations show a correlation between the location of the first crack and the start of the thermoplastic composite debonding. This type of debonding was known as intermediate crack-induced interfacial debonding (Sayed-Ahmed et al. 2009). Therefore, a correlation between the debonded area and energy dissipation could exist. Depending on the direction of crack propagation after the flexural crack formed the crack

may have propagated a distance greater than half the thermoplastic composite length. Delamination of longer lengths would dissipate more energy propagating to the end of the thermoplastic composite causing the brittle failure. The Elium-reinforced specimens had a mean debonded area of 2120 mm^2 and a mean energy dissipation value of 1130 N·mm. In comparison the PETg tape reinforced specimens had a smaller mean debonded area of 1730 mm^2, as well as a smaller mean energy dissipation value of 895 N·mm. The Elium-reinforced values were both approximately 25% larger than the PETg tape reinforced values, which confirmed the potential for a correlation between debonded area and dissipated energy.

4.4 Conclusions and Recommendations

In terms of the three-point bend tests there did not appear to be a significant benefit from the addition of CNF to the UHPC. Therefore, the three-point bend testing was treated solely as a method for comparing the thermoplastic composite types to each other and the unreinforced beam specimens. The Elium thermoplastic composites had the highest mean beam performance in terms of peak load, energy dissipation, and peak displacement. The mean debonded area of the Elium-reinforced specimens was also higher than that of the PETg tape reinforced specimens. Therefore, the Elium-reinforced specimens' high beam performance could be a function of where the first flexural crack developed, which was not necessarily correlated to the bond between the UHPC and the Elium thermoplastic composite. But, the higher mean peak displacement value of the Elium-reinforced specimens showed that Elium was a more ductile composite than the PETg tape reinforcement, which allowed it to undergo higher rates of deflection before brittle failure. The increased thickness of the PETg tape reinforcement could have induced the brittle delamination failure faster in the PETg tape reinforced specimens because thicker materials tend to be stiffer and thus less ductile. In the future adjusting the layup of the PETg tapes, applied to the UHPC panels, to control the stiffness of the laminate could increase its overall performance and utilize the glass fibers' tensile reinforcement to a greater extent.

The three-point bending tests provided an initial classification of the thermoplastic composite to UHPC bond, but in order to fully understand and quantify these bond values a standardized test method must be developed. There were many test methods to quantify the FRP reinforcement to concrete bond in the literature. But, many of these test methods required specialized specimens and test fixtures. It will be important to select a test method with a specimen type that can be easily fabricated using stamp thermoforming and vacuum infusion. A standard peel test appears to be the most applicable test method for classifying the bond strength of the thermoplastic composite reinforced panels. The specimens for a peel test could be fabricated with the same methods as the beam specimens, except a material would need to be selected to prevent the bonding of the thermoplastics along the outer edge of the single-sided panels. Then, after fabrication a wet saw could be used to cut the panels into the appropriate specimen size. Using these specimens, a standard peel test could be performed to quantify the fracture energy required to peel the thermoplastic composite from the UHPC substrate.

Once a standardized test method has been developed the major factors effecting the thermoplastic composite to UHPC bond can be evaluated. These factors are the difference between the thermoplastic composite types (PETg vs. Elium) and the UHPC surface preparation procedures used. Literature showed a rougher surface will produce a better bond between concrete and FRP, therefore different methods to roughen the surface of the UHPC should be experimented with. By observation, the UHPC-thermoplastic bond of the existing panels appeared to perform better when small voids were present on the surface. The voids were filled with either the PETg from the neat resin layer during stamp thermoforming or Elium during the vacuum infusion. Once the thermoplastic cured it acted as an anchor for the thermoplastic composite. Finding a method to distribute these surface voids across the UHPC surface could potentially increase the UHPC-thermoplastic bond performance. One method discussed in the literature that could be applicable to the production of the thermoplastic composite reinforced panels is

grooving. Cutting longitudinal grooves into concrete beams increased the amount of dissipated energy required to cause debonding of the FRP reinforcement (Davood and Ehsan 2010). One concern with the method of grooving is the depth of the groves and the effect it will have on the thin UHPC panels. If grooves were going to be introduced into the UHPC panels it would need to be done during the fabrication of the panels. It was discovered while notching the thermoplastic composites that even when the wet saw was set to cut a constant depth the UHPC surface was not level resulting in uneven notches. Therefore, uniform grooves would not be possible unless they were introduced during the fabrication process of the panel. Developing a panel mold with either groves or a roughened surface would help increase the bond between the thermoplastic composites and the UHPC.

CHAPTER 5: LOW VELOCITY IMPACT TESTING

As discussed previously there is an important distinction that needs to be made when discussing the impact resistance of UHPC. This distinction is the difference between low velocity impact and high velocity impact. Low velocity impact is characterized as an object of high mass with a slow impact velocity, while high velocity impact typically involves the impact of an object with a low mass at a high velocity. When it is time to characterize the impact resistance of a new prototype, such as the thermoplastic composite reinforced panels, low velocity impact testing is often selected for the preliminary characterization. The low velocity impact testing of the thermoplastic composite panels was a two-step process including quasi-static testing and low velocity impact testing. This chapter will discuss the procedures for the quasi-static and low velocity impact testing, as well as the results.

5.1 Introduction

Since the thermoplastic composite reinforced panels were newly developed an estimate of their energy absorption capacity was required. This estimate was obtained through quasi-static testing at a support and loading geometry identical to the low velocity impact testing. The quasi-static testing was essentially a penetration test at a low strain rate, which allowed for the calculation of the energy required to penetrate the specimen. The quasi-static testing also allowed for the failure mechanism of the specimens to be observed in a controlled manner. One of the main goals involved in the development of the thermoplastic composite panels was to prevent the punching-shear failure of the UHPC, it was essential that the failure mechanisms of the UHPC and thermoplastic composite reinforced panels were observed and compared. These quasi-static energy values and failure mechanisms provided a baseline for the impact resistance of the panels.

The most common form of low velocity impact testing is drop-weight testing. The study by Ranade et al. where the punching-shear failure of the UHPC panels was discussed used a drop-weight test setup (Ranade et al. 2017). The goal of the thermoplastic composite reinforced panels was to address the punching-shear failure observed by Ranade et al., therefore a drop-weight test setup was selected to investigate the impact resistance of the panels. Another goal for the panels was to eventually perform high velocity impact testing, therefore the drop-weight parameters were selected to have loading characteristics similar to a projectile test. A small diameter striker was selected and used with a low mass. The impact energy of a drop-weight system is calculated as a function of the system mass and the drop-height. If a low mass is used then the drop-height must be increased, which causes an increase in the impact velocity of the striker. Though the high velocities of a projectile test cannot be obtained through a drop-weight setup, the low velocity impact testing was able to serve as a good preliminary estimate for the impact resistance of the thermoplastic composite reinforced panels.

An important factor that was considered when performing the low velocity impact testing was the potential for inertial effects. Inertial effects are defined as the portion of the load placed upon the tup resulting from specimen acceleration (Saxton et al. 1974). The inertial loading is often identified as the first point of discontinuity in the recorded load time traces, since the inertial load will cause the tup to read a higher load than it would only considering the mechanical bending of the specimen. Different studies have been performed to calculate and account for the inertial effects when performing impact testing on concrete using a drop-weight impact machine (Banthia et al. 1989; Ong et al. 1999). These methods utilized an accelerometer and the virtual work principle to calculate a generalized inertial load. Then the true bending load was calculated using dynamic equilibrium as the difference between the load measured by the tup and the generalized inertial load. There are specific situations where inertial effects can be neglected during low velocity impact testing. One of these situations was described in a

study by Verma et al. where the mass of the impactor was greater than 3.5 times the mass of the panel. It was stated that due to this significant difference in mass the inertial effects of the panel could be neglected (Verma et al. 2016). Further investigation into this phenomenon lead to a technical report on the vibration of plates. This report stated that if the mass of a plate plus some mass, in this case the mass of the impactor, was greater than 2 times the mass of the plate then crossover points exist. These crossover points were points where the frequency of the plate plus the mass is equal to the frequency of the plate by itself (Leissa 1969). This assertion allowed for the assumption that if the mass of the impactor was great enough the panel would accelerate to match the velocity of the impactor immediately, therefore the inertial effects could be neglected. Since the 6-inch by 6-inch panel specimens were of relatively low mass the study by Verma et al. and the technical report by Leissa were used to ensure that inertial effects could be neglected during the low velocity impact testing of the thermoplastic composite reinforced panels.

5.2 Experimental Procedure

The specimens for quasi-static and low velocity impact testing were produced using the double-sided thermoplastic composite reinforced panels. The UHPC panels reinforced on both sides through vacuum infusion were from batch CNF2 and batch BASE2 and the UHPC panels reinforced on both sides through stamp thermoforming were from batch CNF4 and batch BASE1. Starting with a 12-inch by 12-inch panel a wet saw was used to quarter the panel into 6-inch by 6-inch squares. A model of a typical Elium-reinforced panel is shown in Figure 5.1, the only difference for a panel reinforced with PETg tapes is the reinforcement thickness of ⅛-inch. Figure 5.2 represents the numbering system used to vary where the different test specimens were cut from the original 12-inch by 12-inch panel. Specimens one and two were used for quasi-static testing and specimens three and four were used for low velocity impact

testing. This numbering system was only used for the thermoplastic composite reinforced panels to account for potential weak points in the thermoplastic to UHPC bond caused by manufacturing issues.

Figure 5.1. Model of a double-sided panel specimen

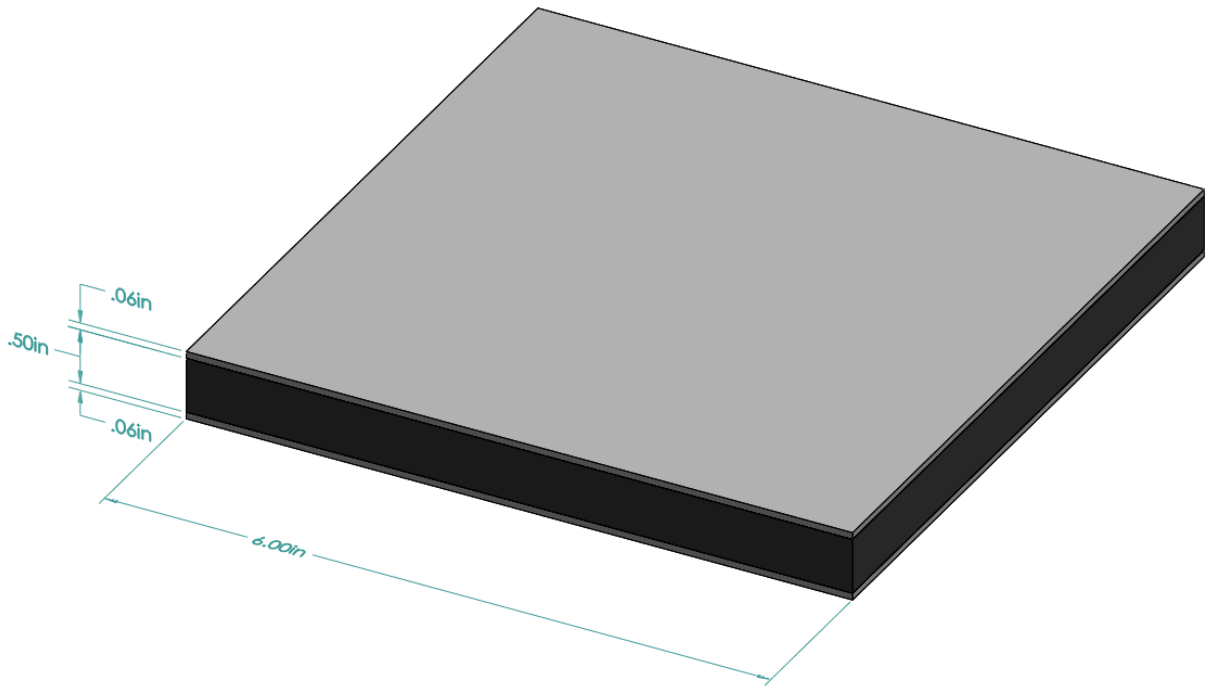

Figure 5.2. Numbering system for the double-sided panel specimens

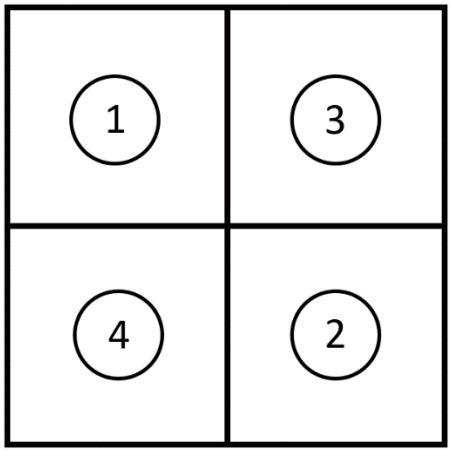

Once the 6-inch panel specimens were all prepared they were measured to record any potential geometric flaws in the specimen. Each specimen was weighed and measured along all four sides using a caliper for the following measurements: length, depth and UHPC depth. The dimensions of the panel were simplified by averaging together the length of sides one and three to get a panel length and the length of sides two and four to get a panel width. The depth and UHPC depth of all four sides were averaged together. All measurements were recorded in millimeters.

5.2.1 Quasi-Static Testing

A total of 42 6-inch panel specimens were tested under quasi-static loading on a 100kN Instron. Of the 42 specimens 16 were reinforced with E-glass and Elium through vacuum infusion, 16 were reinforced with E-glass PETg tapes through stamp thermoforming and 10 were unreinforced. For the Elium-reinforced, PETg tape reinforced, and unreinforced panels 50 percent of the specimens contained CNF. The test fixture used for quasi-static loading was designed to have the same geometry as the Instron 9350 CEAST drop tower used for low velocity impact testing. The panel specimen was supported by a steel base and frame designed to handle a 90kN point load at the center of the panel with the specimen acting as a two-way slab. The load was applied at the center of the panel using a 16 mm ball bearing, which provided the same loading geometry as the 16 mm hemispherical tup insert used for low velocity impact testing. A linear variable differential transformer (LVDT) was used to measure the load point displacement of the panel. Figure 5.3 shows the quasi-static test setup on a 100kN Instron machine.

Figure 5.3. Quasi-Static test setup on a 100kN Instron machine

Initially all the panel specimens were tested under displacement control at a rate of 1 mm/minute until the displacement reached 4 mm. This procedure was used to obtain a starting energy value for the low velocity impact testing. Once the panels were tested the load and load point displacement data was analyzed using MATLAB. The energy absorbed by the specimen during the quasi-static testing was calculated as the area under the load-displacement curve. In order to evaluate the failure mode of the different specimen types, the LVDT was removed from the test fixture and some specimens were again loaded under displacement control at a rate of 1 mm/minute. Failure of the specimen was defined as

reaching a load point deflection of 10 mm or the debonding of the thermoplastic composite reinforcement.

5.2.2 Low Velocity Impact Testing

A total of 42 6-inch panel specimens were tested for low velocity impact resistance. Of the 42 specimens 16 were reinforced with Elium and E-glass through vacuum infusion, 16 were reinforced with PETg tapes through stamp thermoforming and 10 were unreinforced. For the Elium-reinforced, PETg tape reinforced, and unreinforced panels 50 percent of the specimens contained CNF. The low velocity impact testing utilized both an Instron 9350 CEAST drop tower impact system and a 25kN Instron. As previously stated the loading and support geometries were identical for the quasi-static testing and the low velocity impact testing. Therefore, the test setup for the 25kN Instron used for the quasi-static portion of the low velocity impact was identical to the setup shown in Figure 5.3. The LVDT was used to measure the residual deflection from the low velocity impact. The Instron 9350 CEAST drop tower used for the low velocity impact was a drop weight system. A 16mm diameter tup insert was used to strike the panels. This size tup was selected in order to evaluate whether the thermoplastic composite skins benefit the UHPC by preventing the brittle punching-shear failure typically associated with small diameter strikers (Ranade et al. 2017). Figure 5.4 shows the test setup for the low velocity impact testing. As seen in Figure 5.4, the impact machine was controlled through a computer with the Instron VisualIMPACT Software and the specimens were contained in a blast resistant chamber during testing. Inside the chamber the panel specimen was supported by a steel base with the same geometry as the quasi-static testing support frame. For the low velocity impact tests the system was programmed to impact the specimen with a certain energy value input by the user. The system could also take the desired drop height, mass, or impact velocity as an input. The CEAST data acquisition system collected data through a moveable photocell, as well as a load cell and accelerometer within the tup. The

moveable photocell was adjusted to record the impact velocity and to activate the anti-rebound system. The instrumentation in the tup recorded the impact load and acceleration data. Then, the software integrated the acceleration data to provide the tup displacement.

Figure 5.4. Instron 9350 CEAST Drop Tower test setup

The procedure for the low velocity impact testing was a three step process. The first step was performed using the 25kN Instron to get an initial stiffness measurement and baseline for the residual deflection measurement. Once the specimen was placed in the steel frame and preloaded to 500 N the LVDT was balanced to set the initial deflection reading to zero. This allowed the LVDT to measure the residual

deflection after the low velocity impact. Then, the specimen was loaded using load control at a rate of 5000 N per minute for the thermoplastic composite reinforced panels and 2500 N per minute for the unreinforced panels. The unload point for the unreinforced and thermoplastic composite reinforced UHPC panels was 1500 N and 4000 N, respectively. This initial loading provided a measure of the specimen stiffness prior to impact. Once the specimen was unloaded the 25kN Instron data acquisition system called WaveMatrix paused. With the system paused the specimen was removed from the frame and transferred to the Instron 9350 CEAST drop tower.

The second step in the low velocity impact test procedure was a single impact in the CEAST. The panel specimen was moved to the CEAST and secured in the steel base using four bolts and washers. Figure 5.5 shows a specimen prepared for impact, in some cases cardboard was used to secure the specimen when a gap occurred between the top of the specimen and the washers. This prevented the specimen from bouncing after impact. Based on the results of the quasi-static testing the drop tower was initially programmed to impact the specimens with 20 joules of energy. This energy value was used for the unreinforced specimens and some of the thermoplastic composite reinforced specimens. The thermoplastic composite reinforced specimens were also impacted with 30, 40 and 50 joules of energy. In order to achieve a high impact velocity, the mass of the system was set at 2.5 kilograms. This mass was selected to satisfy the criteria for neglecting inertial forces, which states inertial forces can be neglected if the mass of the impactor is greater than 3.5 times the mass of the panel. (Leissa 1969; Verma et al. 2016) This criteria was selected over the assertion set forth by Leissa because it was more conservative. Unfortunately, due to a mechanical error in the weight system of the CEAST the actual mass of the system was only 1.8 kg. When the weight of the tup and striker was taken into account the mass became a total of 2.97 kg. Therefore, the mass of the impactor was only 3 times larger than the mass of the panel. This still satisfied the criteria set by Leissa so the inertial effects were neglected. This

error effected the falling weight parameters of the system and caused the impact energies to be reduced to 16, 24, 32, and 40 J. The falling weight parameters at the different energy levels are listed in Table 5.1. To ensure only a single impact the anti-rebound system was engaged before the impact. After the impact the specimen was removed from the steel base and transferred back to the 25kN Instron.

Figure 5.5. Unreinforced specimen prepared for impact in the CEAST 9350 test fixture

Table 5.1 CEAST 9350 Falling Weight Parameters

Impact Energy	**16 J**	**24 J**	**32 J**	**40 J**
Mass	2.97 kg	2.97 kg	2.97 kg	2.97 kg
Impact Velocity	3.29 m/s	4.03 m/s	4.65 m/s	5.20 m/s
Drop Height	0.552 m	0.827 m	1.103 m	1.379 m

When the specimen was returned to the steel frame of the 25kN Instron the third step of the low velocity impact procedure began. Resuming the test in WaveMatrix recorded the residual deflection from the low velocity impact since the LVDT was balanced prior to the impact. Then, similar to step one, the specimen was loaded through load control at a rate of 5000 N per minute for the thermoplastic composite reinforced specimens and 2500 N per minute for the unreinforced specimens. The unreinforced specimens unloaded at 1500 N, while the thermoplastic composite reinforced specimens unloaded at 4000 N. This step provided the data to calculate the specimen stiffness after the low velocity impact.

The low velocity impact testing provided two sets of data to analyze. The data provided by the 25kN Instron and LVDT was used to get the residual deflection and to quantify the change in compliance after the impact. The residual deflection was simply pulled from the LVDT data at the point where the data acquisition resumed after the low velocity impact. The loading data before and after the impact was analyzed to get the pre- and post-impact structural stiffness values, which were converted into compliance. Compliance was calculated as the inverse of the structural stiffness. In order to get a good measure of the overall compliance the load-displacement plot was analyzed for each individual specimen and the best two points were selected to estimate the true compliance. Once the two compliance values were calculated the difference between the two was used to quantify the damage done to the panel during the low velocity impact. The data from the CEAST 9350 was analyzed to compare the peak impact force and the maximum deflection of the tup during the impact. The area under the load-deflection curve was also calculated to confirm the amount of energy imparted to the specimen during the impact. The data analysis for the low velocity impact testing was performed in MATLAB.

5.3 Results and Discussions

This section will discuss the results from the quasi-static and low velocity impact testing of the thermoplastic composite reinforced panels. The results from the quasi-static testing will include a discussion of the peak load and energy dissipation results, as well as a discussion of the observed failure mechanisms. The low velocity impact testing results consist of the results provided by the Instron 9350 CEAST and the 25kN Instron.

5.3.1 Quasi-Static Testing

The quasi-static testing produced load and load point deflection data for each specimen. With this data the peak load was determined for each specimen. The energy dissipated at the center of the panel was calculated by calculating the area under the load versus load point displacement curve. Figure 5.6 is a representation of load-deflection curves for an unreinforced, PETg tape reinforced, and Elium-reinforced specimen. The quasi-static testing results for all of the unreinforced and thermoplastic composite reinforced specimens is included in Appendix B.

Figure 5.6. Comparative load-displacement plot for panels specimens

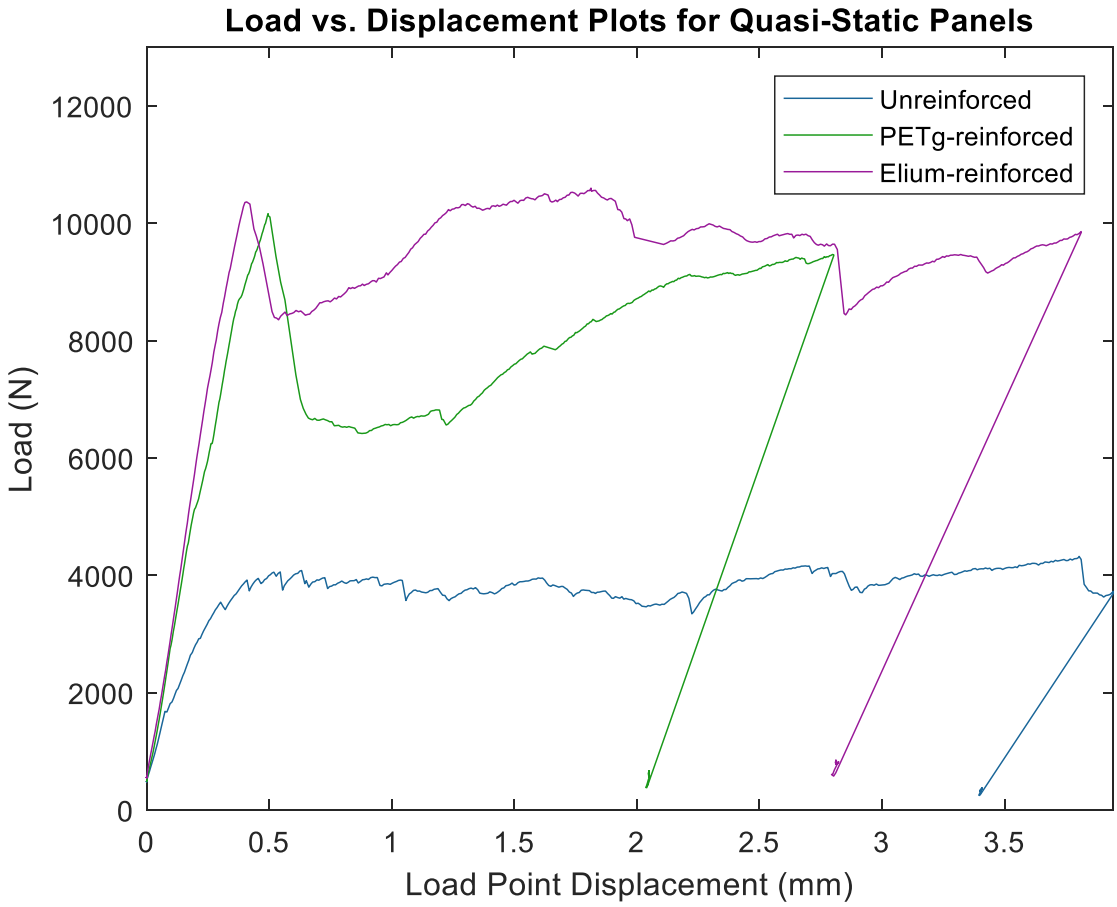

The peak load results shown in Figure 5.7 are separated by UHPC type and thermoplastic composite reinforcement. The error bars represent one standard deviation above and below the mean value for peak load. There was minimal variation in the peak load values for the unreinforced panels since the behavior of UHPC under quasi-static loading was previously well established. The base UHPC specimens performed equivalent to the CNF-modified UHPC specimens with a mean peak load of 4160 N. The mean peak load of the CNF-modified specimens was 4200 N. There was only a 1% difference between the mean peak load of the base panels and the mean peak load of the CNF-modified panels. Due to the insignificant difference between the base UHPC and the CNF-modified UHPC the groups were combined

to compare the thermoplastic composite types to the unreinforced specimens. The mean peak load of the unreinforced specimens was 4180 N. There was a significant increase in the load carried by the specimen when thermoplastic composite reinforcement was included. The Elium reinforcement provided a 155% increase in the mean peak load, while the PETg tape reinforcement provided a larger increase of 178%. The mean peak load of the Elium-reinforced group was 10600 N and the mean peak load of the PETg tape reinforced group was 11600 N. These values showed the PETg tape reinforced group to be approximately 10% greater than the Elium-reinforced group.

Figure 5.7. Quasi-Static peak load separated by panel type

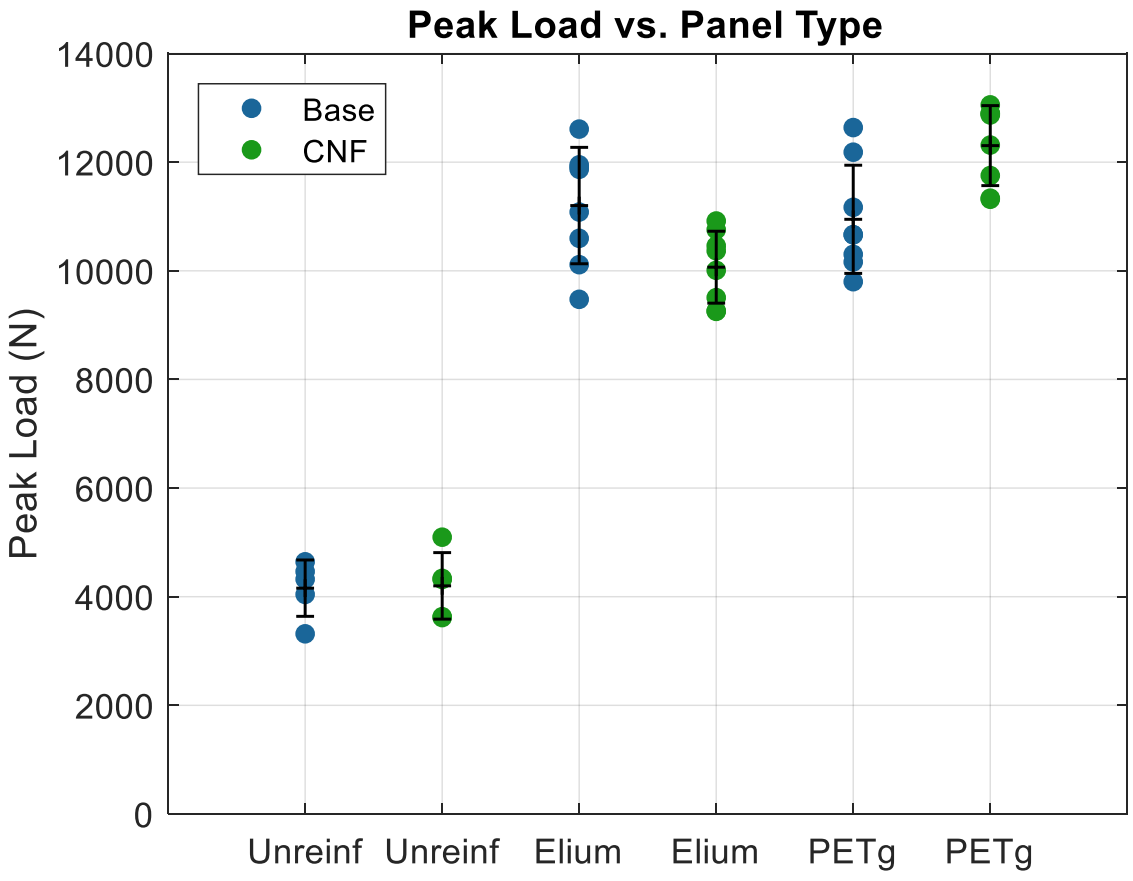

The results shown in Figure 5.8 represent the main goal of the quasi-static testing, to get an initial energy absorption capacity. These initial values determined the starting impact energy value for the low velocity impact testing. The calculated energy dissipation values developed more variation between reference specimens and specimens containing CNF. Therefore, the difference between UHPC types was considered before comparing the thermoplastic reinforcement types. The base UHPC specimens had a mean energy dissipation value of 13400 N·mm. The CNF-modified UHPC specimens had a mean energy dissipation value 12% smaller at 11700 N·mm. When Elium reinforcement was introduced to the base UHPC the mean energy dissipation value was 28100 N·mm. The CNF-modified specimens with Elium reinforcement had a smaller mean energy dissipation value of 24900 N·mm. This was an 11% decrease in dissipated energy over the Elium-reinforced base panels. The mean energy dissipation value for the PETg tape reinforced base and CNF-modified specimens was 17500 N·mm and 18500 N·mm, respectively. This was approximately a 6% reduction when CNF was added to the PETg tape reinforced panels.

The largest difference between the base UHPC and the CNF-modified UHPC was 12% for the unreinforced specimens. Since this was a fairly insignificant difference the groups can be combined to compare the thermoplastic composite reinforcement types. The mean energy dissipation value of the unreinforced specimens was 12500 N·mm. In comparison the mean energy dissipation value of the Elium-reinforced specimens is 26500 N·mm, which was an increase in dissipated energy of 111%. The PETg tape reinforcement increased the mean energy dissipation by 44% with a value of 18000 N·mm. When the two thermoplastic composite reinforcement groups were compared against on another the Elium-reinforced specimens dissipated approximately 47% more energy than the PETg tape reinforced specimens. Based on these mean energy dissipation values an initial impact energy value of 20 J was selected for the low velocity impact testing, but due to the mechanical error of the Instron 9350 CEAST

the initial impact value was only 16 J. This value was expected to cause significant damage to the unreinforced specimens, while initiating the early stages of damage to the thermoplastic composite reinforced panels.

Figure 5.8. Quasi-Static work separated by panel type

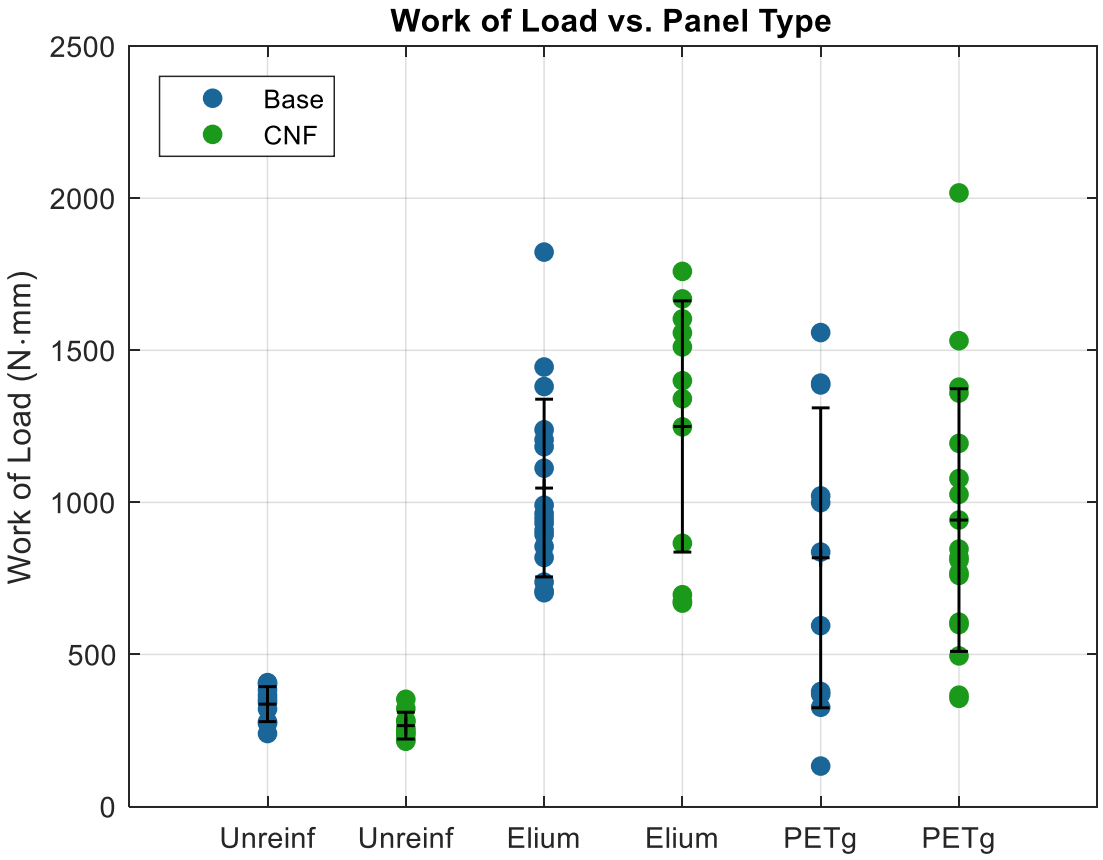

The quasi-static tests demonstrated similar results to those suggested by Ranade et al. where ultra-high-performance concrete was tested for impact resistance. Ranade et al. described a UHPC panel failure due to brittle punching-shear with a small diameter loading head (Ranade et al. 2017). When the unreinforced UHPC panels were subjected to a 16mm ball bearing loading head, a punching shear failure was induced. Figure 5.9 shows the brittle punching shear failure of an unreinforced UHPC panel. This

was the common failure for all of the unreinforced panels. Figure 5.10 shows the typical failure mode of both the Elium-reinforced and the PETg tape reinforced panels. The photo on the left shows the rear face of an Elium-reinforced panel where radial delamination occurred. The radial delamination was assumed to be caused by the concrete displacement from the punching-shear. Sometimes the radial delamination travelled to the edge of the panels causing the skin to separate from the UHPC along that edge. The photo on the right shows the full penetration that eventually occurred on the front face of the Elium-reinforced panel. This failure of the front face thermoplastic composite was due to the large local strains that occurred at the load point due to the small radius of the ball bearing (Schubel et al. 2005). The PETg tape reinforced specimens also developed these permanent indentations in the front face. All of the thermoplastic composite panels had similar failure mechanisms when they were subject to quasi-static loading. A few specimens were pushed past the initial loading threshold to complete failure. The failure mechanism of the unreinforced panels remained constant as brittle punching-shear. The failure mechanism of the thermoplastic composite reinforced panels was still a brittle mechanism. The Elium and PETg tape reinforced panels failed through brittle debonding of the rear face composite skin. The front face composite skin typically failed through composite rupture prior to the debonding of the rear skin. Upon completion of the failure test the rear face skin of the thermoplastic composite reinforced panels were removed to examine the UHPC. This examination showed the UHPC was still failing through punching-shear, which was assumed to be the cause of the radial delamination of the rear face skin. Figure 5.11 shows a PETg tape reinforced specimen with the rear face composite removed after testing.

Figure 5.9. Punching-shear failure of an unreinforced panel from quasi-static loading

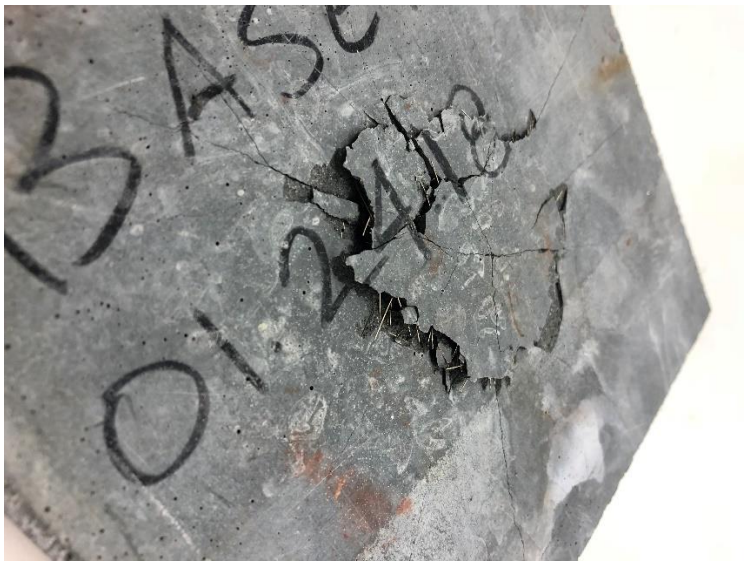

Figure 5.10. Damage to an Elium-reinforced panel from quasi-static loading

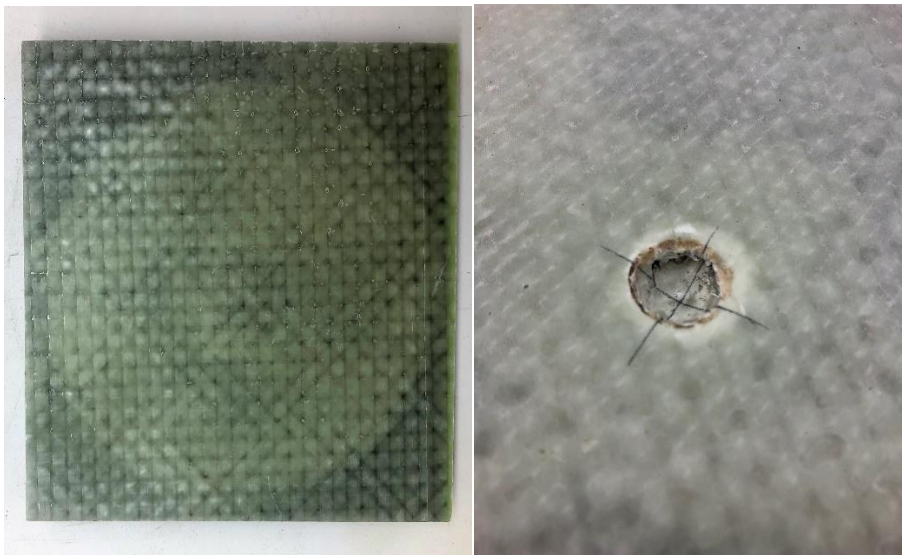

Figure 5.11. PETg-reinforced panel failing through debonding with the rear face skin removed

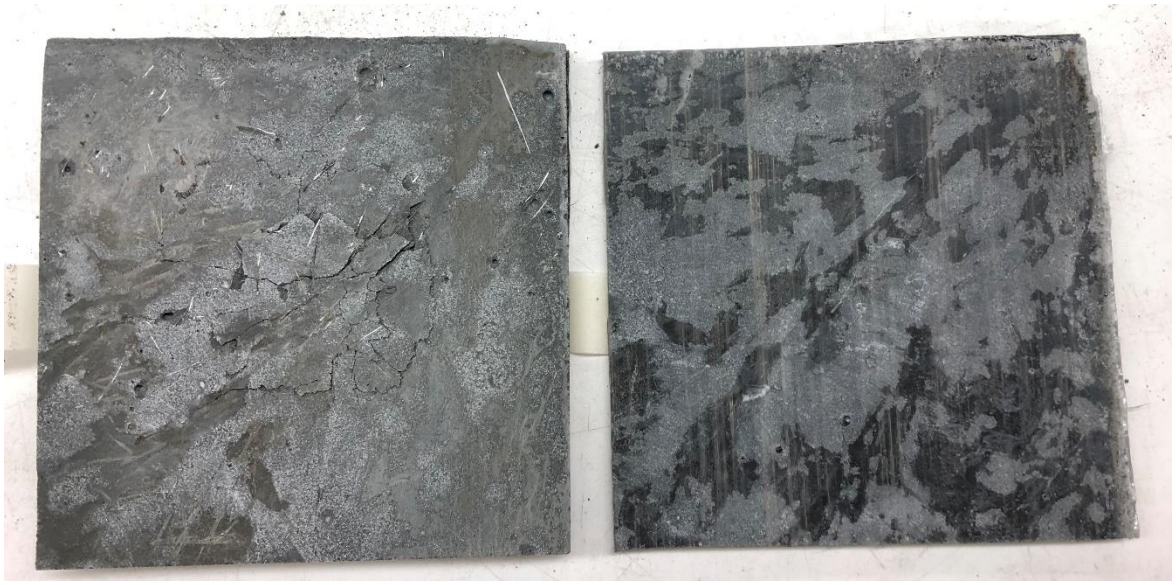

5.3.2 Low Velocity Impact Testing

The results from the impact testing were separated into two categories depending on the testing apparatus. The Instron data when analyzed provided a measure of the impact damage using the change in the specimen's compliance. The LVDT included in the Instron testing apparatus provided a measure of the specimen's residual deflection from the impact. The CEAST impact machine and its data acquisition system provided the following data: force, energy, displacement and velocity throughout the entire impact. Out of these parameters the peak impact force and the maximum impact displacement were of interest. Figure 5.12 represents the impact force as a function of time for all of the PETg tape reinforced base UHPC specimens. The impact force-time plots for the remaining specimen types can be found in Appendix C. The area under the CEAST impact load-deflection plots was analyzed to provide a confirmation of the impact energy. The specimens impacted with 16 J had a mean area under the load-deflection curve of 19 J. This value was higher than expected, which indicated there could be

unaccounted for inertial effects. The specimens impacted with 24 J, 32 J, and 40 J also exhibited this rise in the area under the load-deflection curve with mean areas of 29 J, 38 J, and 44 J, respectively.

Figure 5.12. Force-Time plots for the PETg-reinforced base UHPC panel impacts

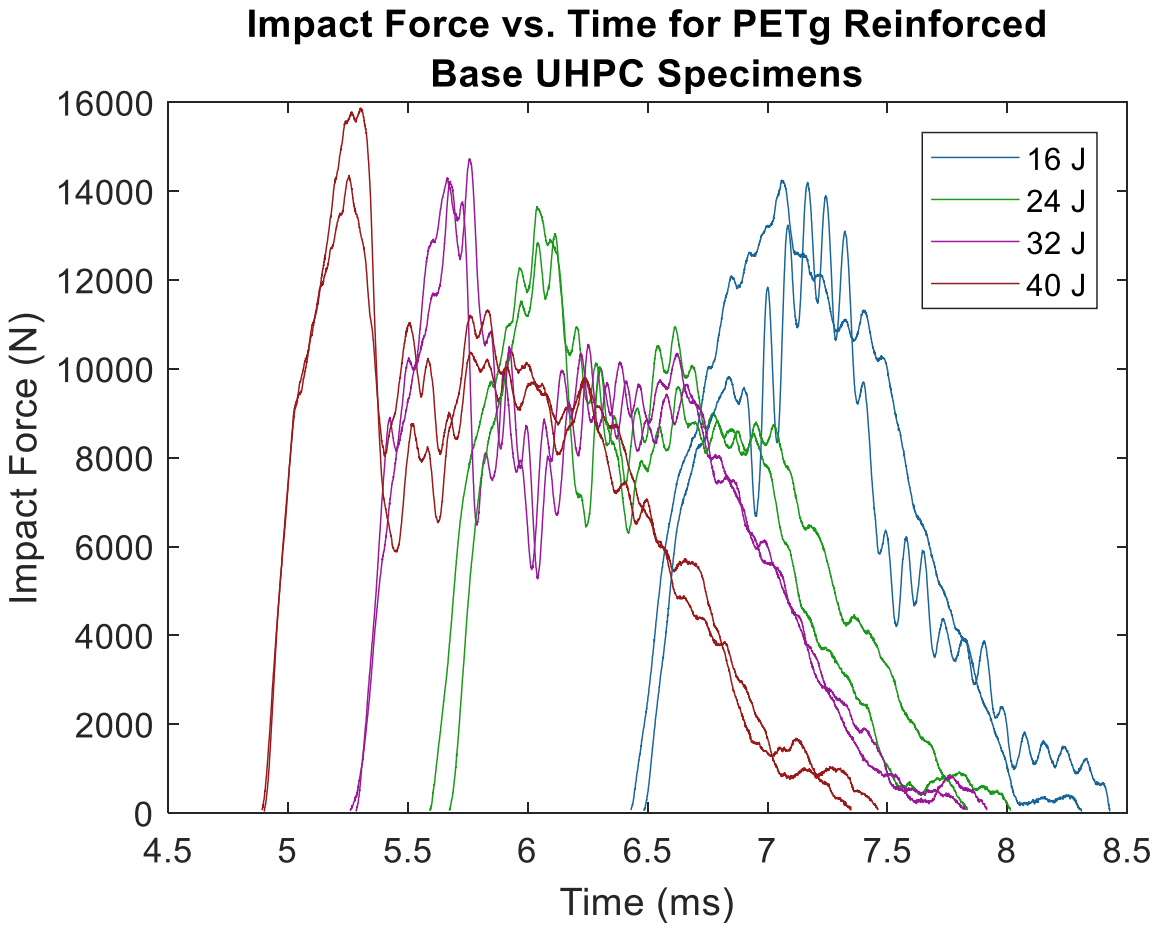

Figure 5.13 shows the peak impact load of all specimen types for an impact energy of 16 J. Since the peak impact load was a result of the specimen's initial compliance there was little scatter associated with the data. There was also minimal change in the peak impact force at different energy levels for the thermoplastic composite reinforced UHPC panels. The thermoplastic composite reinforced UHPC panels had peak impact loads varying between 12000 N and 15000 N at all impact energy levels. The lack of change in peak impact load at different energy levels confirmed that it was a function of the initial panel

compliance. The different specimen types exhibited a constant initial compliance unless a fabrication error occurred. The peak impact load was used as an indicator of impact resistance. The unreinforced UHPC panels, which have the lowest impact resistance, only had a mean peak impact load around 6000 N. Therefore, including a thermoplastic skin increased the peak impact force of the UHPC panels by at least 100%.

Figure 5.13. Peak impact load for all specimen types at an impact energy of 16 J

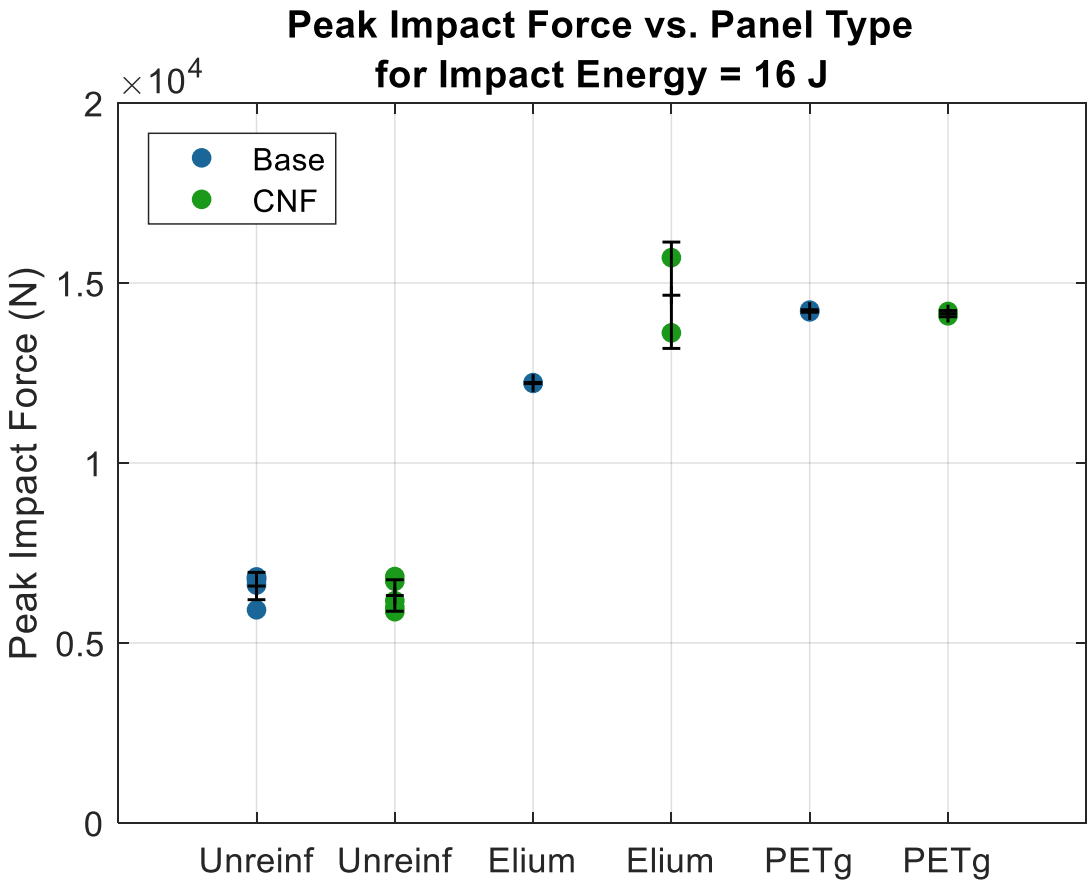

Figure 5.14 shows the maximum panel deflection during a 16 J impact for all specimen types. The maximum deflection during impact was another indicator of the impact resistance. As seen in Figure 5.14 the unreinforced UHPC panels had a significantly larger deflection during impact than the

thermoplastic composite reinforced panels. This was due to the radial cracking that occurred in the unreinforced UHPC panels upon impact. The unreinforced UHPC panels also had far more scatter in the results. This was due to the random orientation of the steel fibers. The steel fibers play an essential role in UHPC impact resistance (Dancygier 1997; Yoo and Banthia 2017a; Zhang et al. 2007). The CNF-modified unreinforced specimens had the largest mean displacement during impact. These specimens deflected 6.25 mm on average during impact while the base UHPC unreinforced specimens deflected 6.00 mm on average. There was less than a 5% difference between these values, which indicated the addition of CNF had an insignificant effect on the UHPC. The Elium reinforcement reduced the mean maximum displacement during impact by 61% with a mean value of 2.39 mm. This value was slightly greater than the mean maximum displacement during impact of the PETg tape reinforced panels, which was 2.22 mm. The PETg tape reinforcement reduced the mean deflection during impact by 64% when compared to the unreinforced panels. Based on these results there was minimal difference between effect of the Elium and PETg tape reinforcement on the deflection of a UHPC panel during impact. They both caused a significant reduction in the maximum impact deflection.

Figure 5.14. Max impact deflection from a 16 J impact for all specimen types

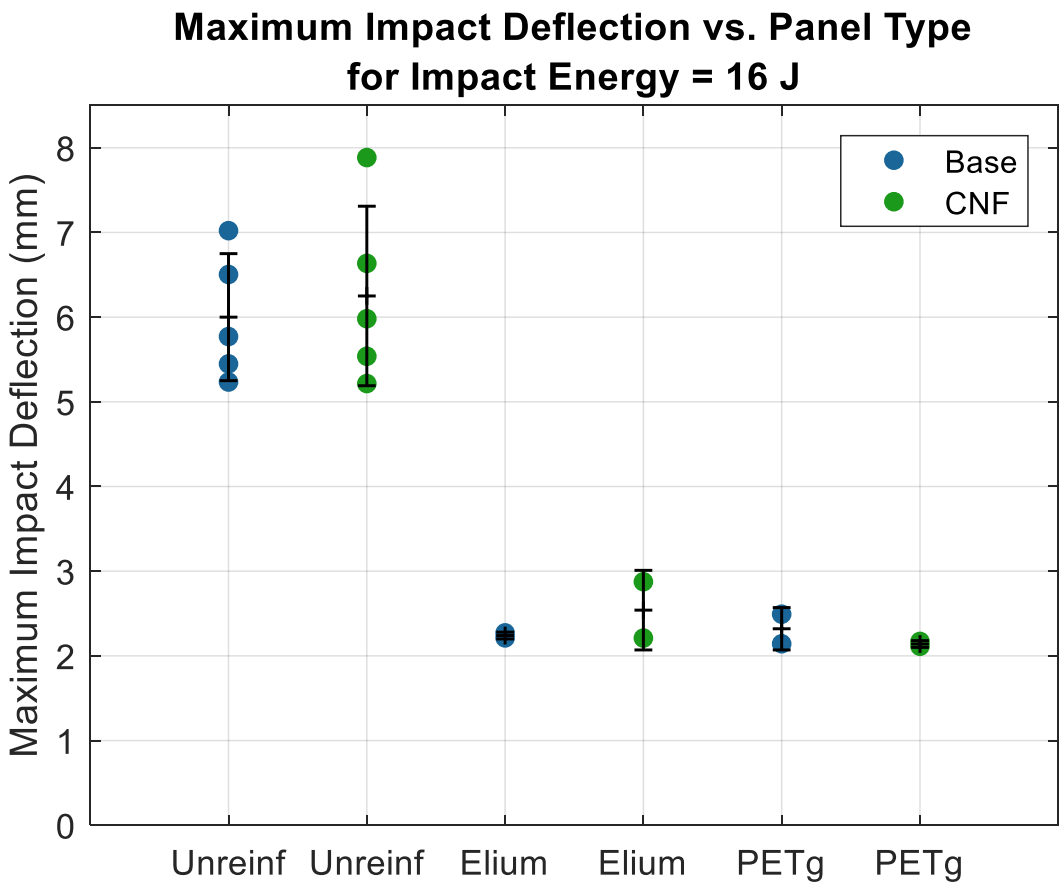

The thermoplastic composite reinforced UHPC panels were also impacted at energy values of 24, 32, and 40 J. Figure 5.15 shows the results for the maximum impact deflection of the different thermoplastic composite panels at the different impact energies. As expected there appeared to be a correlation between the maximum impact deflection and the impact energy. The only outliers from the apparent linear relationship was the Elium-reinforced CNF-modified UHPC panels at an impact energy of 40 J. They suffered delamination at an impact of 40 J, which resulted in a larger maximum deflection during impact. The delamination may have been caused by a fabrication error where the rear face of the panels had large dry spots requiring reinfusion.

Figure 5.15. Max impact deflection of the thermoplastic-reinforced panels for all impact energies

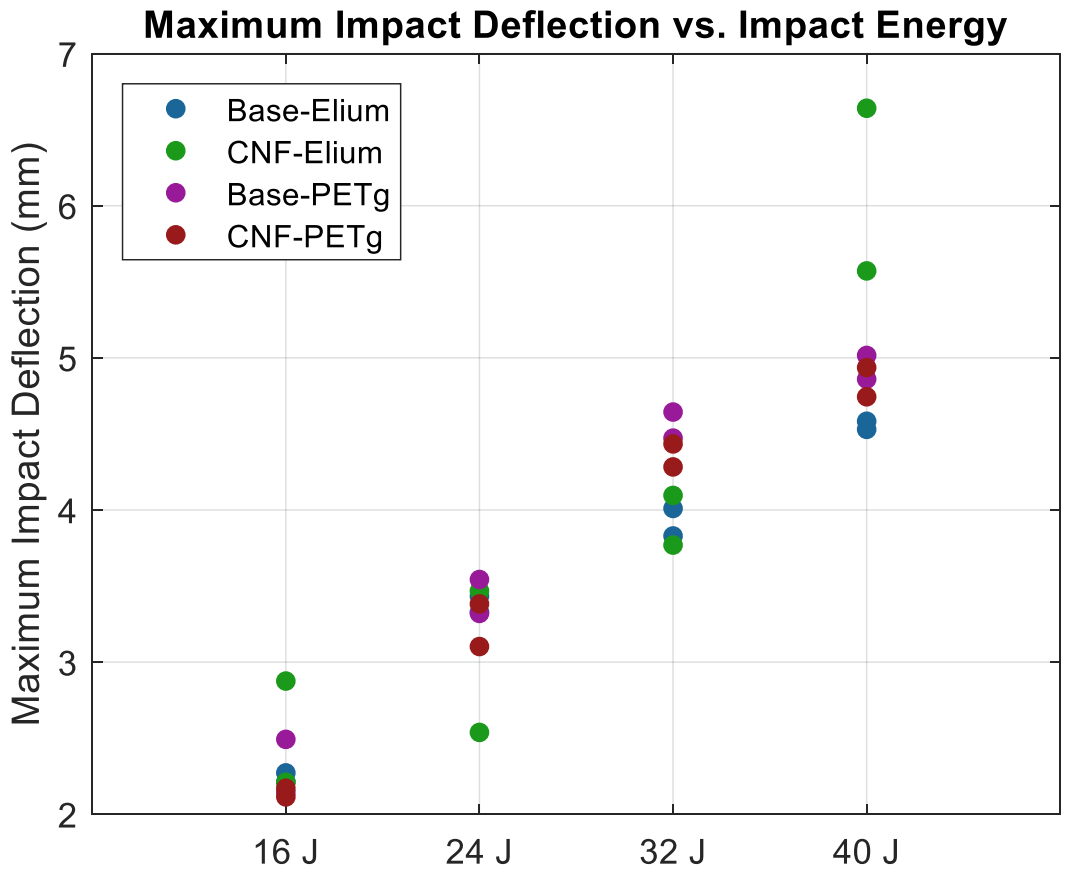

The residual deflection of the specimen was related to the maximum impact deflection, since the UHPC and thermoplastic composites were not elastic materials. Figure 5.16 represents the mean residual deflection of all specimen types at an impact energy of 16 J. The specimen types with a thermoplastic composite skin had a far lower residual deflection than the unreinforced UHPC panels. This was due to the brittle punching-shear failure of the UHPC. Without the skins to catch the displaced concrete there was no control of the residual displacement. There did not appear to be a significant difference between the base and CNF-modified UHPC unreinforced panels or the base and CNF-modified Elium-reinforced panels. The unreinforced panels and Elium-reinforced panels had a mean residual deflection of 2.81 mm

and 0.54 mm, respectively. When compared to the unreinforced UHPC panels the Elium reinforcement reduced the residual deflection by 81%. The PETg tape reinforced base and CNF-modified panels had a larger difference between their residual deflections. For the base UHPC panels reinforced with PETg tapes the mean residual deflection for the two specimens was 0.26 mm. When CNF was introduced to the UHPC reinforced with PETg tapes the residual deflection was reduced by 85% to 0.04 mm. This was a significant change due to the addition of CNF, but more testing is required to confirm the reduction in residual deflection was caused by the addition of CNF. When the mean residual deflection for the base and CNF-modified panels reinforced with PETg tapes were averaged the PETg tape reinforced specimens have a mean residual deflection of 0.15 mm. Therefore, the PETg tape reinforcement caused a 95% reduction in the residual deflection of the unreinforced panels. In this case the PETg tape reinforcement appeared to have better impact resistance than the Elium reinforcement.

Figure 5.16. Residual deflection from a 16 J impact for all specimen types

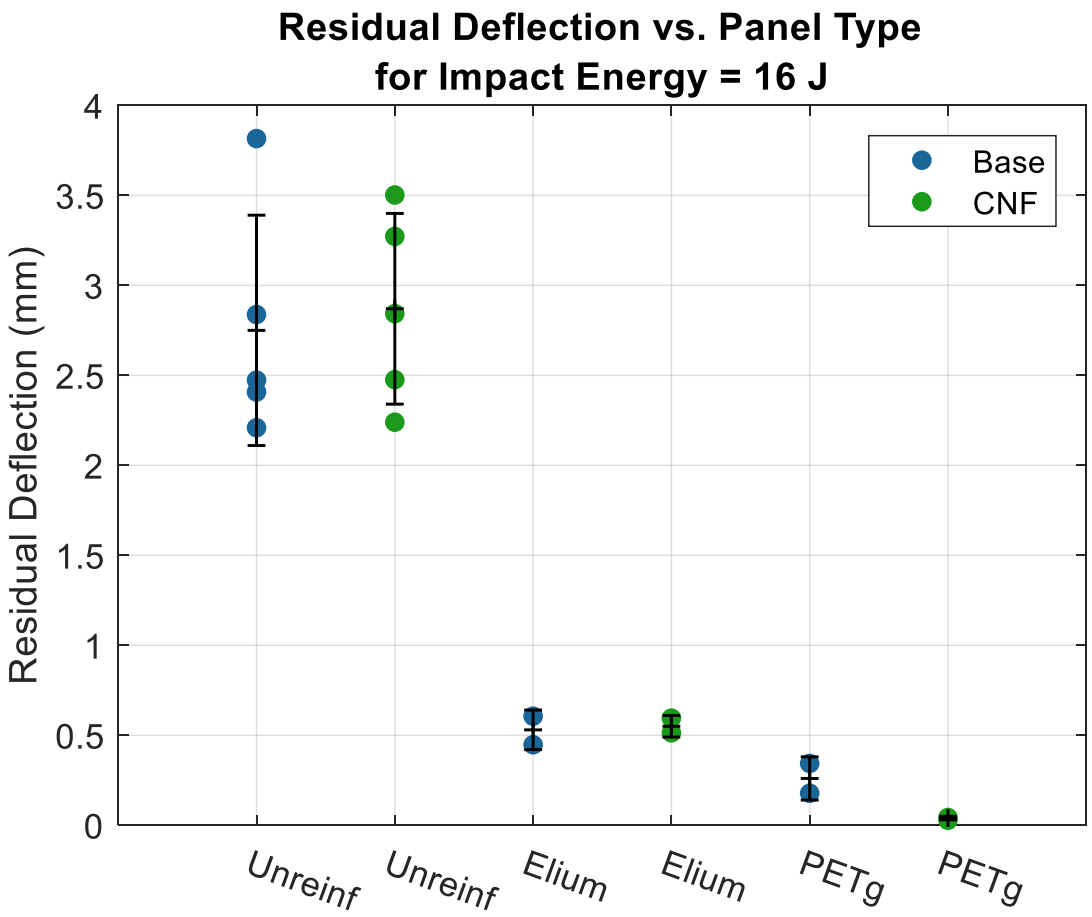

The residual deflection results for the thermoplastic composite reinforced panels at different impact energies were similar to the maximum impact deflection results. Figure 5.17 shows the residual deflection results of the different thermoplastic composite panels at the different impact energies. As previously stated these results were similar to the maximum impact deflection and there was a correlation between the residual deflection and the impact energy. This correlation was identical to the previous correlation where the residual deflection increased with the impact energy. Again, the outliers at the 40 J impact energy were caused by the delamination of the Elium-reinforced CNF-modified panels.

Figure 5.17. Residual deflection of the thermoplastic-reinforced panels for all impact energies

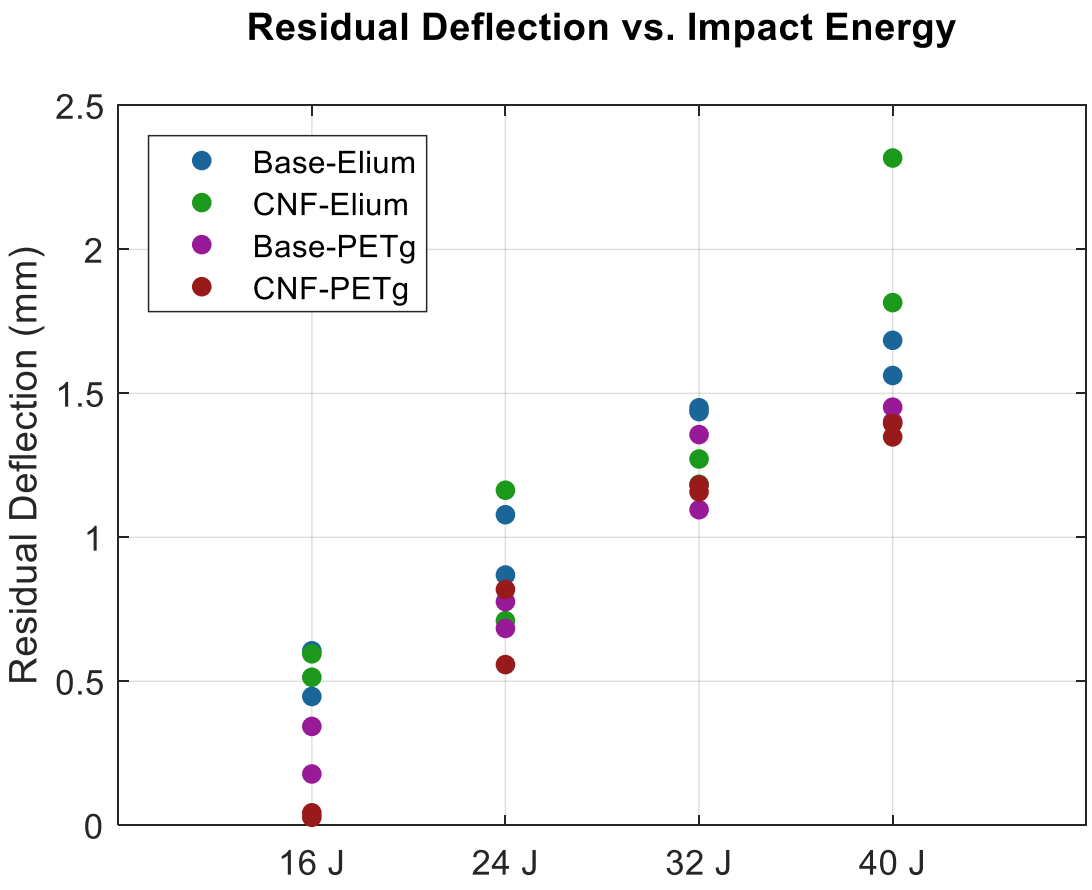

Compliance is defined as the inverse of the structural stiffness. The pre-impact stiffness and the post-impact stiffness was computed for each specimen as a measure of structural damage. Then the difference between the inverse of each stiffness was computed. Figure 5.18 represents a plot of the static data where the red lines indicate the estimated pre- and post-impact compliance. The residual deflection is also represented in this figure. The low velocity impact testing results for each individual specimen can be found in Appendix D.

Figure 5.18. Example plot of the static portion of a low velocity impact test

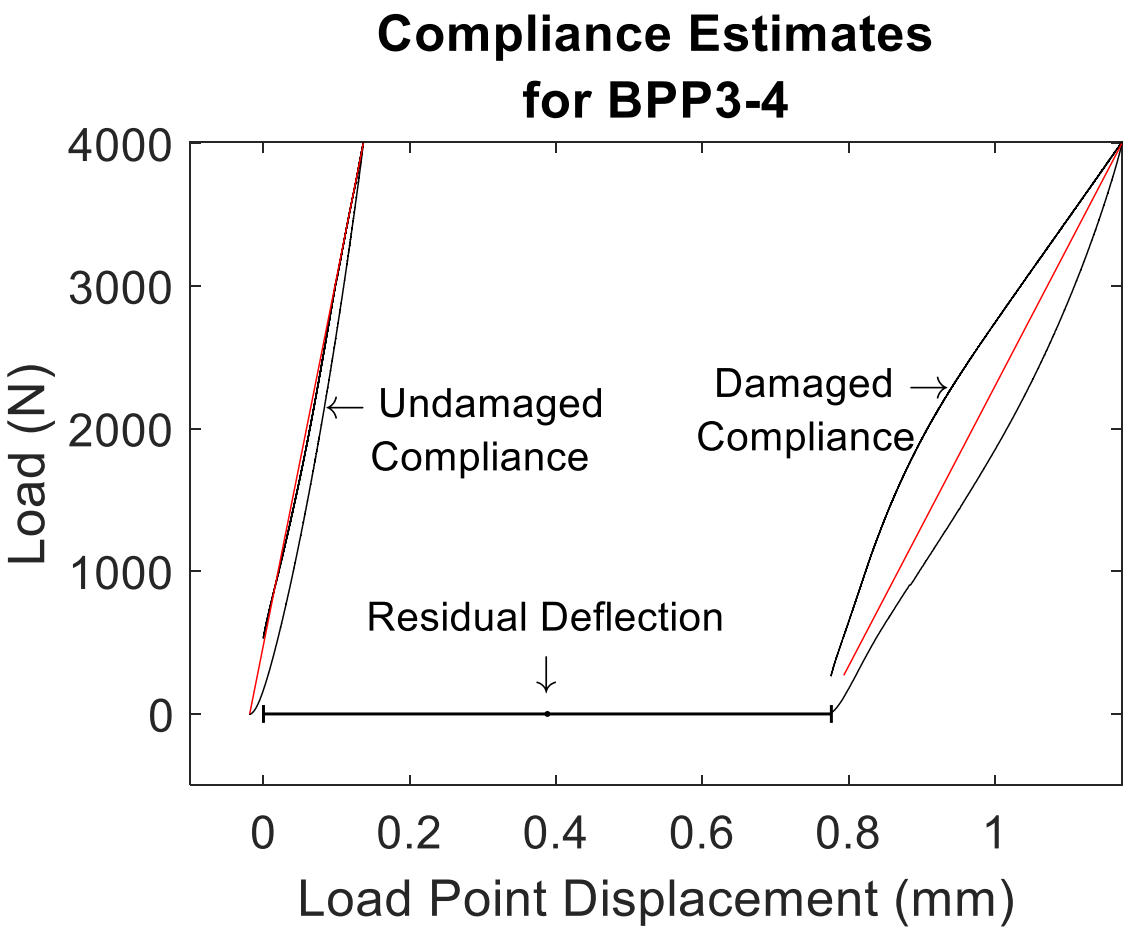

In Figure 5.19 each specimen's change in compliance for a 16 J impact is shown for the different panels types. The compliance changes of the unreinforced specimens showed significant scatter for both the base and CNF-modified UHPC. This scatter may be due to the high level of damage caused by the impacts. When the panels were reloaded to get the post-impact compliance the panels began to fail at different rates. One panel failed completely through brittle punching-shear. The fact that there was little residual strength remaining in the unreinforced panels could explain the scatter in the data. All the scatter made it difficult to determine if there were effects from the CNF. Therefore, the mean change in compliance for the unreinforced panels, base and CNF-modified, was 2.1 x 10^{-4} mm/N. The

thermoplastic composite reinforced panels suffered limited damage from the 16 J impact. The two reinforcement forms reduced the change in compliance by similar values when compared to the unreinforced panels. A reduction of 87% for the Elium panels and 91% for the PETg tape panels. There was a slight difference between the base and CNF-modified panels, but not a significant difference. The Elium-reinforced panels had a mean change in compliance of 2.8 x 10^{-5} mm/N and the PETg tape reinforced panels had a mean change in compliance of 1.9 x 10^{-5} mm/N. The PETg tape skins were twice as thick as the Elium skins, which could be a potential cause of its superior performance over the Elium under impact loading.

Figure 5.19. Compliance change from a 16 J impact for all specimen types

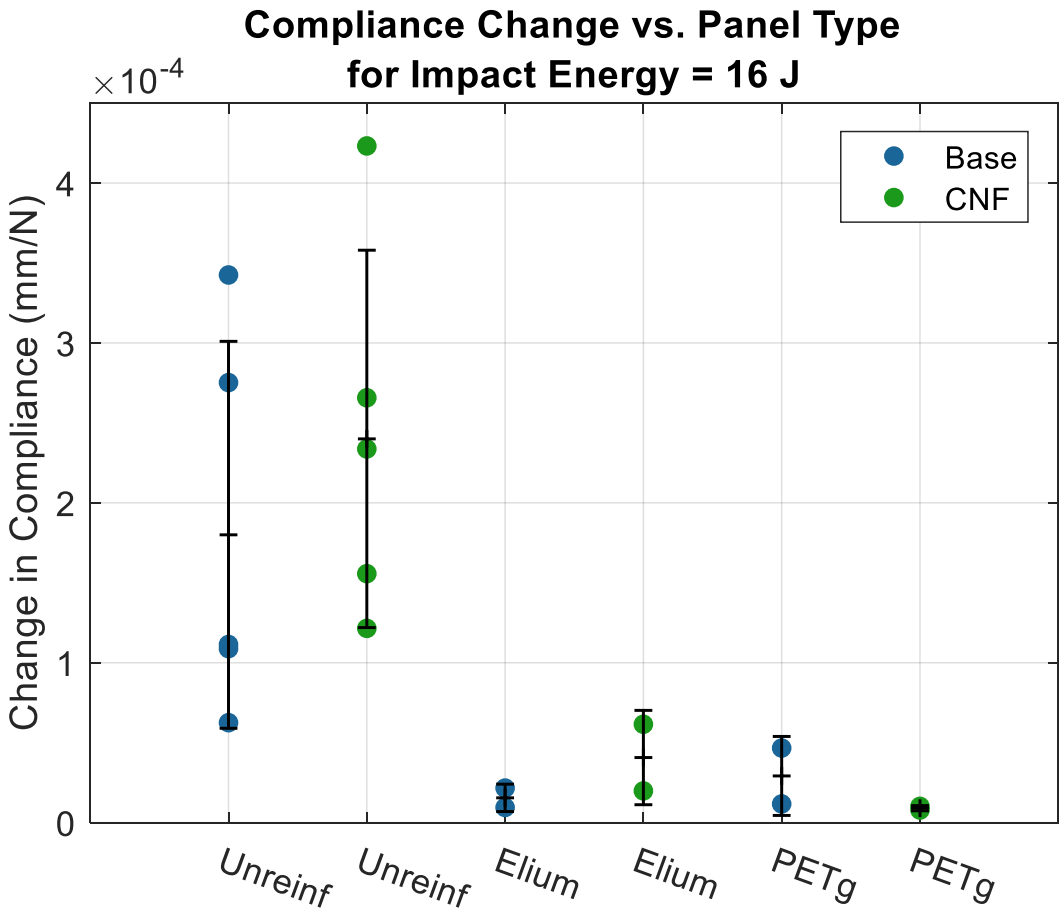

The thermoplastic composite reinforced panels were also tested at varying levels of impact energy since they incurred limited damage at 16 J. The results were not consistent for all of the specimen types. Figure 5.20 shows the change in compliance for the different thermoplastic composite UHPC panels at varying impact energies. The panels made without CNF had varying levels of damage as the impact energy increased. The base panels reinforced with Elium suffered the most damage at 24 J and 32 J, while its CNF counterpart's damage increased proportional to the impact energy. It should be noted that the large changes in compliance at 40 J for the CNF Elium-reinforced panels were due to delamination of the rear face thermoplastic. The PETg tape reinforced base panels had consistent values at 24, 32, and 40 J. This could be another indicator of increased impact resistance for PETg tape reinforced UHPC panels.

Figure 5.20. Compliance change of the thermoplastic-reinforced panels for all impact energies

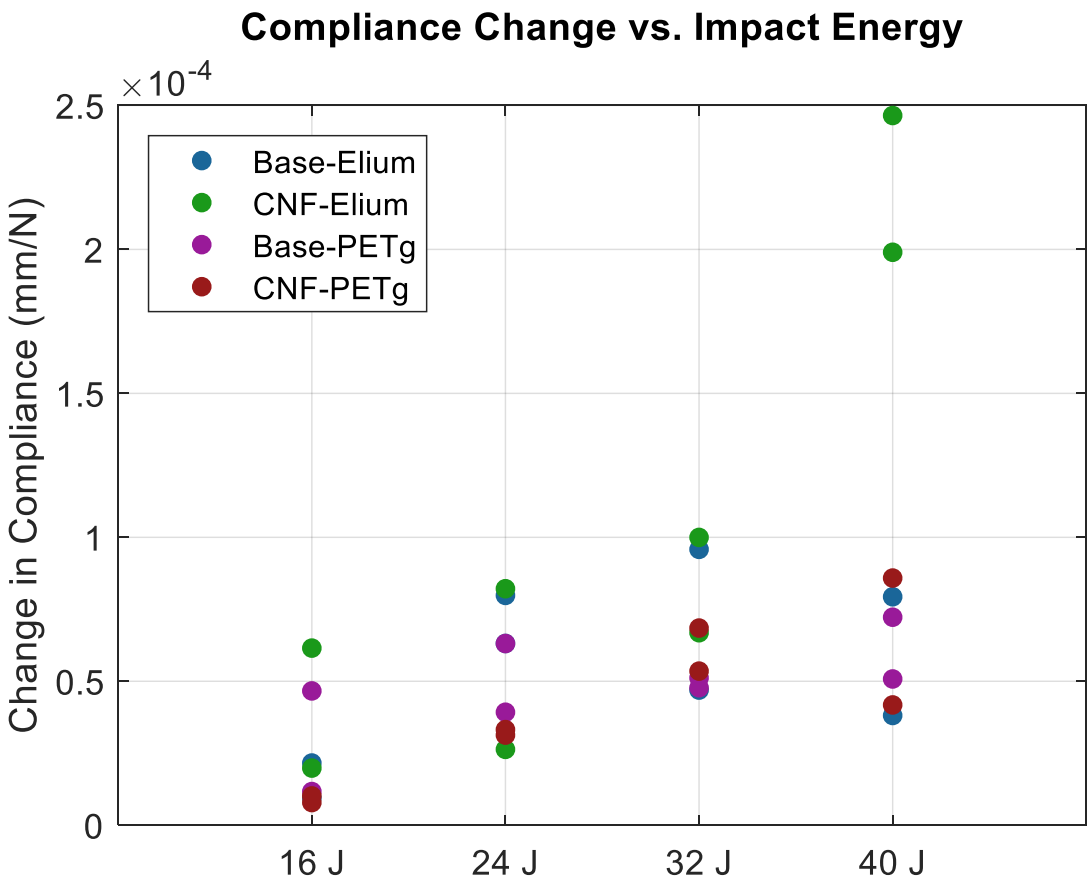

The failure modes of the specimens after impact were similar to the failure modes during quasi-static testing. In Figure 5.21 the start of a punching-shear failure can be seen on the unreinforced UHPC specimen. This failure mode was expected based on the literature. The Elium-reinforced specimen shown in Figure 5.22 is showing radial delamination. It was concluded from the quasi-static testing that this was most likely caused by displaced UHPC. As previously stated the CNF-modified UHPC panels reinforced with Elium delaminated when they were impacted with 40 J of energy. Figure 5.23 shows the reinfused section on the rear face of one of these panels. The dry spot from the initial infusion followed by the reinfusion of the panel was suspected to be the reason for the delamination. Typically, the

thermoplastic reinforced specimens only suffered radial delamination, but in the case of these two specimens a complete delamination occurred where the Elium composite separated from the UHPC. The separation of the Elium composite is also shown in Figure 5.23. No PETg tape reinforced specimens suffered complete delamination and it was more difficult to identify the radial delamination due to the color of the PETg. Based on the quasi-static testing it was assumed that some level of radial delamination occurs during the impact testing on the PETg tape reinforced specimens.

Figure 5.21. Failure mode of unreinforced UHPC specimens

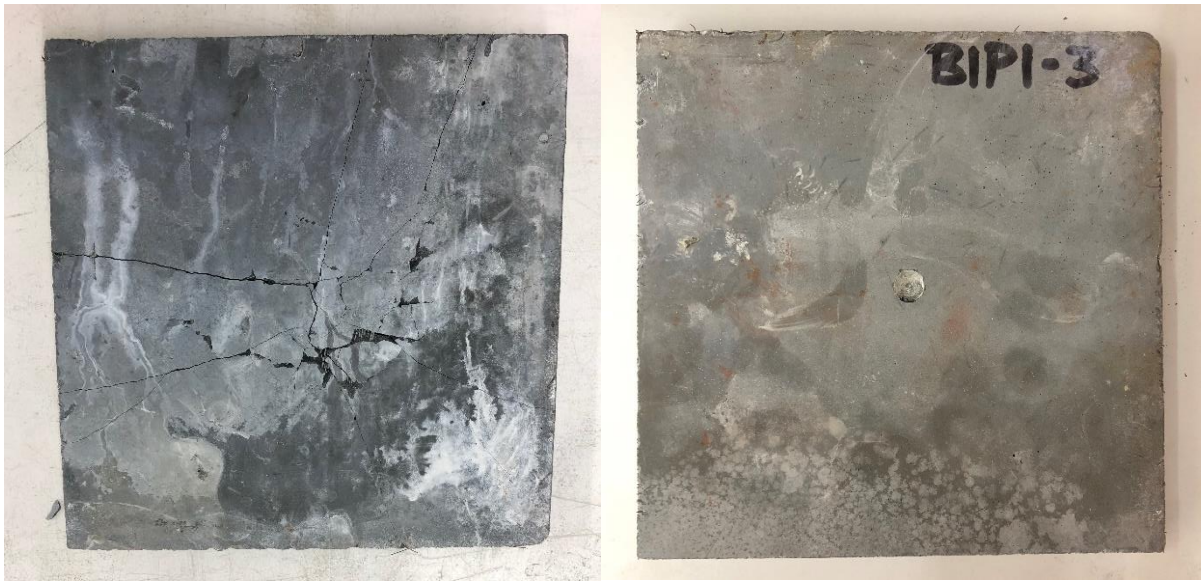

Figure 5.22. Radial delamination on the rear face of an Elium-reinforced specimen

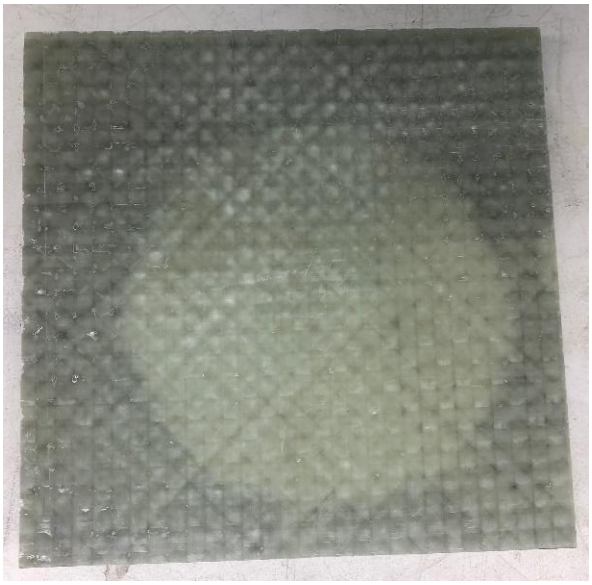

Figure 5.23. Delamination of an Elium-reinforced CNF-modified specimen impacted with 40 J

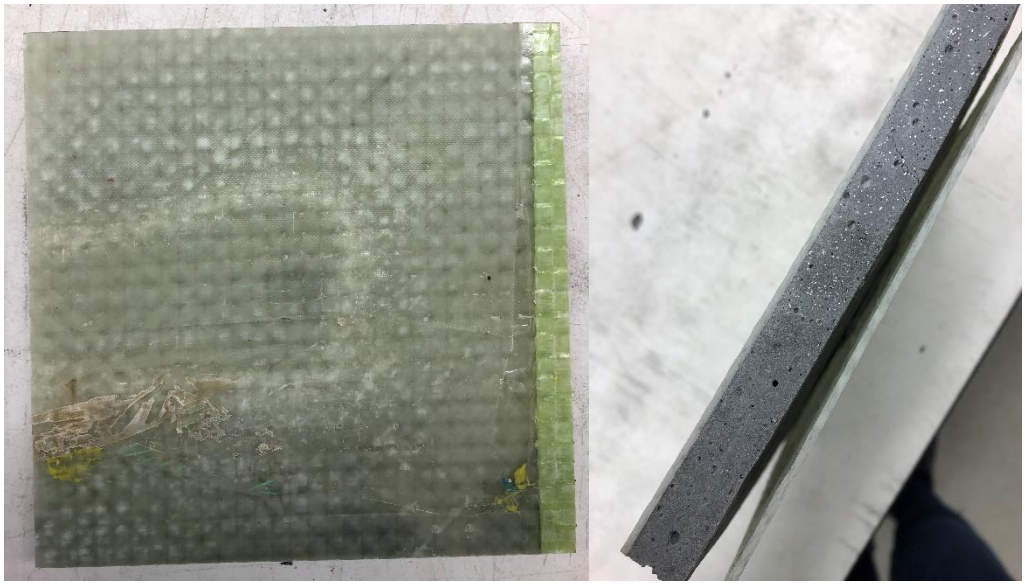

5.4 Conclusions and Recommendations

One concern that presented itself during the low velocity impact testing was the difference between the measured impact energy and the impact energy calculated from the CEAST drop-weight parameters.

The measured impact energy calculated from the load and displacement data provided by the CEAST was 3 to 6 J higher than the impact energy specified by the user. This indicated that the panels were potentially effected by inertial forces. As discussed previously there was a method discussed in the literature where accelerometers were attached to the specimen during the low velocity impact. This method used the results of the accelerometer to calculate a generalized inertial load which was removed from the tup load to determine the true bending load carried by the panel (Banthia et al. 1989; Ong et al. 1999). In the future this method should be integrated into the low velocity impact testing to account for any inertial effects. In this case all of the low velocity impact specimens were subject to what appears to be uniform inertial effects, therefore the inertial effects were still neglected.

It was concluded from the quasi-static and low velocity impact testing that the addition of thermoplastic composite skins to UHPC panels significantly increased the impact resistance of the UHPC. While there was an effect on the UHPC performance from the thermoplastic skins the same cannot be reported for the addition of CNF. The difference between the base and CNF-modified specimens was shown to be insignificant in almost every test. The results from the quasi-static and low velocity impact tests indicated a potential shift in the performance of the thermoplastic composite reinforced UHPC panels. The quasi-static tests showed the Elium reinforcement to have superior energy absorption, but when the loading rate was increased during the impact tests the PETg tape reinforced panels outperformed the Elium-reinforced panels. The PETg tape reinforcement had the advantage of being two times as thick as the Elium reinforcement. This was a potential reason for its superior performance during the low velocity impact tests. Since, this was a preliminary panel design more testing should be performed on both reinforcement types to determine an optimized design.

In order to optimize the panel design there are multiple factors to take into account. One important factor is the thermoplastic composite skins. Each form of reinforcement has its own properties that can

be adjusted to create an optimum reinforcement for impact resistance. The PETg tape reinforcement has the advantage of being a unidirectional reinforcement that can be stacked in different directions to tailor the properties of the final laminate. Many studies have been performed to determine the effect of stacking sequence on the impact resistance of FRP laminates (Cantwell and Morton 1991; Hongkarnjanakul et al. 2013; Strait et al. 1992). In this case the goal of the PETg tape reinforcement was to decrease the amount of energy transferred to the UHPC. Therefore, a study should be performed to determine a PETg tape layup with superior energy absorption capacity. This would be an ideal laminate for the front face of the UHPC, but due to the failure mechanism of rear face composite, brittle delamination, a second PETg tape layup should be designed. The goal of the rear face composite is to catch any concrete debris from the scabbing of the UHPC panel. It was observed that the rear face delamination was often caused by displaced UHPC. A PETg tape laminate with high ductility should be developed in order to prevent failure through brittle delamination.

The Elium reinforcement should also be optimized with the same performance goals in mind. A woven fabric was selected for use as the fiber reinforcement in the Elium composites, this could explain why the PETg tape reinforced panels performed slightly better under impact loading. Cantwell and Morton reported that woven fabrics should be used to avoid ply delamination in a laminate (Cantwell and Morton 1991). One way composite laminates absorb impact energy is through ply delamination, therefore the selection of a woven fabric might have had a negative effect on the performance of the front face reinforcement, where the goal was to maximize energy absorption. For future development of the Elium composite reinforced panels a unidirectional stitched fabric should be considered to replace the woven fabric. The unidirectional fabric could be oriented to increase the energy absorption capacity in the front face composite. Like the PETg tape reinforcement, a more ductile laminate should be

developed for the rear face in order to increase the ability of the composite to catch the displaced UHPC.

Once an optimized panel design has been developed some of the larger challenges like high velocity impact resistance and large scale panel fabrication can be tackled. The current prototypes described above should have high velocity impact testing performed, for example projectile testing. These results would determine if there is a significant difference in the thermoplastic composite reinforced panels' performance under low velocity impact versus high velocity impact. If a correlation between the two can be determine then low velocity impact testing can be used for the initial evaluation of new panel designs until an optimized design is developed. Another challenge that needs to be addressed before a complete evaluation of the prototypes' impact performance can be performed is large scale production of the thermoplastic composite reinforced panels. The biggest change required to begin large scale fabrication is upscaling the size of the UHPC panels. In order to produce UHPC at a larger scale more material, different equipment and more labor is required. The application of the thermoplastic composite skins at a larger scale would stay roughly the same. The automated tape layout placement machine used to produce the PETg multidirectional tailored blanks has many advantages for large scale fabrication. An assembly line could be developed where there PETg blank was produced, then transferred to the infrared oven and finally pressed to the UHPC. The University of Maine's Thermoplastics Lab at the Advanced Structures and Composites Center could be utilized for the large scale production of PETg tape reinforced UHPC panels. Upscaling the panel size would also provide advantages for dealing with the issue of leaks in vacuum infusion. If the UHPC panel edges were trimmed prior to the vacuum infusion the issue of protruding steel fibers at the edges would be eliminated. This would help prevent the occurrence of leaks and dry spots, which negatively affect the impact resistance of the final panels. One of the advantages of Elium is its ability to produce large scale parts through vacuum infusion. A

disadvantage of large scale production of Elium-reinforced panels would be the labor intensive nature of vacuum infusion. The first step in exploring large scale production of thermoplastic composite reinforced UHPC panels would be to try sizing up from a square foot panel to a square yard panel.

CHAPTER 6: SUMMARY AND RECOMMENDATIONS

Overall the work described in this thesis successfully improved the impact performance of UHPC. The greatest improvement was achieved through the application of the thermoplastic composite skins. The addition of the CNFs to the UHPC mix had little to no effect on the impact resistance of the UHPC. Due to the preliminary nature of the prototype design and testing it was difficult to determine whether the PETg tape or Elium reinforcement was the superior option. Based on the quasi-static three-point bending and the quasi-static panel testing, Elium outperformed the PETg tape reinforcement. But, when it came to the low velocity impact testing the PETg tape reinforcement was shown to have more impact resistance. This could be due to the fact that the PETg tape reinforcement was twice as thick as the Elium reinforcement. PETg tape reinforcement also has a fabrication method well suited for automated production, which is an advantage over the labor intensive vacuum infusion procedures of the Elium reinforcement.

More work must be performed in order to optimize the thermoplastic composite reinforced UHPC panel design for impact resistance. There are many factors that affect the impact resistance of the thermoplastic composite reinforced UHPC panels such as fiber reinforcement orientation in the thermoplastic composite, the thermoplastic-UHPC bond and the rigidity of the thermoplastic composite. In order to optimize these factors a number of studies should be performed. First the UHPC-thermoplastic bond should be optimized. To do this a standardized test method needs to be developed to evaluate the fracture properties of the UHPC-thermoplastic interface. Many of these test methods require specialized specimens and test fixtures, but once this test method is developed it could be used to evaluate the different factors affecting the bond. Major factors that need to be evaluated are the difference between the thermoplastic composite types (PETg vs. Elium) and the UHPC surface preparation procedures used. A peel test has potential to a be a simple test method used to quantify the

thermoplastic-UHPC bond. The type of specimen required for a peel test could easily be fabricated using the current fabrication methods, stamp thermoforming and vacuum infusion, of the thermoplastic composite reinforced panels.

Literature shows a rougher surface will produce a better bond between concrete and FRP, therefore different methods to roughen the surface of the UHPC should be experimented with. By observation, the UHPC-thermoplastic bond of the existing panels appeared to perform better when small voids were present on the surface. The voids were filled with either the PETg from the neat resin layer during stamp thermoforming or Elium during the vacuum infusion. Once the thermoplastic cured it acted as an anchor for the thermoplastic composite. Finding a method to distribute these surface voids across the UHPC surface could potentially increase the UHPC-thermoplastic bond performance.

Once an ideal UHPC-thermoplastic interface is developed and proven, the rigidity and fiber reinforcement orientation of the thermoplastic composite can be evaluated. The rear face thermoplastic composite often suffered some form of delamination, which in some cases lead to a brittle delamination failure where the panel lost all of its load carrying capacity. Therefore, varying the rigidity of the front face composite versus the rear face should be tested. By using a composite with more ductility on the rear face more concrete displacement could occur before the composite suffered delamination. The goal of the front face composite was to absorb a large amount of energy, which reduces the amount of energy impacting the UHPC. Increasing the stiffness of the front face composite and maximizing its energy absorption capacity could have a positive impact on the performance of the thermoplastic composite reinforced panels. One way to achieve both of these goals is by testing different fiber reinforcement layups for the thermoplastic composites. In the literature there is extensive information regarding the effects of fiber orientation on the impact resistance of FRPs (Cantwell and Morton 1991; Hongkarnjanakul et al. 2013; Strait et al. 1992). A selection of different layups should be fabricated and

applied to UHPC panels for testing. This will help determine the ideal fiber reinforcement orientations for the front and rear face.

Once an optimized panel design has been developed some of the larger challenges like high velocity impact resistance and large scale panel fabrication can be tackled. High velocity impact testing should be performed on the current design of the thermoplastic composite reinforced panels. If a correlation between the results presented above and the high velocity impact results can be determined, then low velocity impact testing can be used for the initial evaluation of new panel designs until an optimized design is developed. Another challenge that needs to be addressed in the development process is the large scale production of the thermoplastic composite reinforced panels. The biggest change required to begin large scale fabrication is upscaling the size of the UHPC cores. This will require more material, different equipment and more labor. The stamp thermoforming of the thermoplastic composite skins at a larger scale would stay roughly the same. The University of Maine's Thermoplastics Lab at the Advanced Structures and Composites Center could be utilized to develop an assembly line for the large scale production of PETg tape reinforced UHPC panels. Upscaling the panel size would also provide advantages for dealing with the issue of leaks in vacuum infusion. Minimizing the occurrence of leaks would help prevent the development of dry spots, which negatively affected the impact resistance of the final panels. The next step in exploring large scale production of thermoplastic composite reinforced UHPC panels would increasing the size of the panels from one square foot to one square yard.

REFERENCES

Abdel-Kader, M., and Fouda, A. (2014). "Effect of reinforcement on the response of concrete panels to impact of hard projectiles." *International Journal of Impact Engineering*, 63, 1–17.

Abrate, S. (1997). "Localized Impact on Sandwich Structures With Laminated Facings." *Applied Mechanics Reviews*, 50(2), 69–82.

Agrawal, S., Singh, K. K., and Sarkar, P. K. (2014). "Impact damage on fibre-reinforced polymer matrix composite – A review." *Journal of Composite Materials*, 48(3), 317–332.

Akil Hazizan, M., and Cantwell, W. J. (2002). "The low velocity impact response of foam-based sandwich structures." *Composites Part B: Engineering*, 33(3), 193–204.

Almansa, E. M., and Cánovas, M. F. (1999). "Behaviour of normal and steel fiber-reinforced concrete under impact of small projectiles." *Cement and Concrete Research*, 29(11), 1807–1814.

Anderson, T., and Madenci, E. (2000). "Experimental investigation of low-velocity impact characteristics of sandwich composites." *Composite Structures*, 50(3), 239–247.

Aram, M. R., Czaderski, C., and Motavalli, M. (2008). "Debonding failure modes of flexural FRP-strengthened RC beams." *Composites Part B: Engineering*, 39(5), 826–841.

Arduini, M., and Nanni, A. (1997). "Parametric Study of Beams with Externally Bonded FRP Reinforcement." *ACI Structural Journal*, 94(5).

Arduini, M., Tommaso, A. D., and Nanni, A. (1997). "Brittle Failure in FRP Plate and Sheet Bonded Beams." *ACI Structural Journal*, 8.

Attari, N., Amziane, S., and Chemrouk, M. (2012). "Flexural strengthening of concrete beams using CFRP, GFRP and hybrid FRP sheets." *Construction and Building Materials*, 37, 746+.

Au, C., and Büyüköztürk, O. (2006). "Debonding of FRP plated concrete: A tri-layer fracture treatment." *Engineering Fracture Mechanics*, 73(3), 348–365.

Banthia, N., Mindess, S., Bentur, A., and Pigeon, M. (1989). "Impact testing of concrete using a drop-weight impact machine." *Experimental Mechanics*, 29(1), 63–69.

Bhalerao, N., Wayal, A. S., Patil, P. G., and Bharimalla, A. K. (2015). "A REVIEW ON EFFECT OF NANO CELLULOSE ON CONCRETE." *International Journal of Civil and Structural Engineering Research*, 3(1), 251–254.

Bindiganavile, V., and Banthia, N. (2005). "Impact response of the fiber-matrix bond in concrete." *Canadian Journal of Civil Engineering*, 32(5), 924–933.

Bindiganavile, V., Banthia, N., and Aarup, B. (2002). "Impact Response of Ultra-High-Strength Fiber-Reinforced Cement Composite." *Materials Journal*, 99(6), 543–548.

Buyukozturk, O., Gunes, O., and Karaca, E. (2004). “Progress on understanding debonding problems in reinforced concrete and steel members strengthened using FRP composites.” *Construction and Building Materials*, 18(1), 9–19.

Buyukozturk Oral, and Hearing Brian. (1998). “Failure Behavior of Precracked Concrete Beams Retrofitted with FRP.” *Journal of Composites for Construction*, 2(3), 138–144.

Cantwell, W. J. (2007). “Geometrical effects in the low velocity impact response of GFRP.” *Composites Science and Technology*, 67(9), 1900–1908.

Cantwell, W. J., and Morton, J. (1989). “Geometrical effects in the low velocity impact response of CFRP.” *Composite Structures*, 12(1), 39–59.

Cantwell, W. J., and Morton, J. (1991). “The impact resistance of composite materials — a review.” *Composites*, 22(5), 347–362.

Caprino, G., and Teti, R. (1994). “Impact and post-impact behavior of foam core sandwich structures.” *Composite Structures*, 29(1), 47–55.

Chajes, M. J., Thomson, T. A., Januszka, T. F., and Finch, W. W. (1994). “Flexural strengthening of concrete beams using externally bonded composite materials.” *Construction and Building Materials*, 8(3), 191–201.

Chamis, C., Hanson, M., and Serafini, T. (1972). “Impact Resistance of Unidirectional Fiber Composites.” *Composite Materials: Testing and Design (Second Conference)*, H. Corten, ed., ASTM International, 100 Barr Harbor Drive, PO Box C700, West Conshohocken, PA 19428-2959, 324-324–26.

Curson, A. D., Leach, D. C., and Moore, D. R. (1990). “Impact Failure Mechanisms in Carbon Fiber/PEEK Composites.” *Journal of Thermoplastic Composite Materials*, 3(1), 24–31.

Dancygier, A. N. (1997). “Effect of reinforcement ratio on the resistance of reinforced concrete to hard projectile impact.” *Nuclear Engineering and Design*, 172(1), 233–245.

Dancygier, A. N., Yankelevsky, D. Z., and Jaegermann, C. (2007). “Response of high performance concrete plates to impact of non-deforming projectiles.” *International Journal of Impact Engineering*, 34(11), 1768–1779.

Dan-Jumbo, E., Leewood, A., and Sun, C. (1989). “Impact Damage Characteristics of Bismaleimides and Thermoplastic Composite Laminates.” *Composite Materials: Fatigue and Fracture, Second Volume*, P. Lagace, ed., ASTM International, 100 Barr Harbor Drive, PO Box C700, West Conshohocken, PA 19428-2959, 356-356–17.

Davood, M., and Ehsan, M. (2010). “Grooving as Alternative Method of Surface Preparation to Postpone Debonding of FRP Laminates in Concrete Beams.” *Journal of Composites for Construction*, 14(6), 804–811.

Dear, J. P., Lee, H., and Brown, S. A. (2005). “Impact damage processes in composite sheet and sandwich honeycomb materials.” *International Journal of Impact Engineering*, Fifth International Symposium on Impact Engineering, 32(1), 130–154.

Elber, W. (1983). *Failure mechanics in low-velocity impacts on thin composite plates*.

Evci, C., and Gülgeç, M. (2012). “An experimental investigation on the impact response of composite materials.” *International Journal of Impact Engineering*, 43, 40–51.

Farnam, Y., Mohammadi, S., and Shekarchi, M. (2010). “Experimental and numerical investigations of low velocity impact behavior of high-performance fiber-reinforced cement based composite.” *International Journal of Impact Engineering*, 37(2), 220–229.

Ferraris, C. F., and Martys, N. S. (2003). “Relating Fresh Concrete Viscosity Measurements from Different Rheometers.” *Journal of research of the National Institute of Standards and Technology*, 108(3), 229.

Galecki, G., Maerz, N., Nanni, A., and Myers, J. (2001). *Limitations to the Use of Waterjets in Concrete Substrate Preparation*.

Gunes, O., Buyukozturk, O., and Karaca, E. (2009). “A fracture-based model for FRP debonding in strengthened beams.” *Engineering Fracture Mechanics*, 76(12), 1897–1909.

Habel, K., and Gauvreau, P. (2008). “Response of ultra-high performance fiber reinforced concrete (UHPFRC) to impact and static loading.” *Cement and Concrete Composites*, 30(10), 938–946.

Harding, J. (2011). “Impact Damage in Composite Materials.” *Science and Engineering of Composite Materials*, 1(2), 41–68.

Hong, S., and Liu, D. (1989). “On the relationship between impact energy and delamination area.” *Experimental Mechanics*, 29(2), 115–120.

Hongkarnjanakul, N., Bouvet, C., and Rivallant, S. (2013). “Validation of low velocity impact modelling on different stacking sequences of CFRP laminates and influence of fibre failure.” *Composite Structures*, 106, 549–559.

Husman, G., Whitney, J., and Halpin, J. (1975). “Residual Strength Characterization of Laminated Composites Subjected to Impact Loading.” *Foreign Object Impact Damage to Composites*, L. Greszczuk, ed., ASTM International, 100 Barr Harbor Drive, PO Box C700, West Conshohocken, PA 19428-2959, 92-92–22.

Jiao, L., Su, M., Chen, L., Wang, Y., Zhu, H., and Dai, H. (2016). “Natural Cellulose Nanofibers As Sustainable Enhancers in Construction Cement.” *PLOS ONE*, 11(12), e0168422.

Leissa, A. W. (1969). *Vibration of Plates*. Technical Report. DTIC Document.

Leung Christopher K. Y. (2001). “Delamination Failure in Concrete Beams Retrofitted with a Bonded Plate.” *Journal of Materials in Civil Engineering*, 13(2), 106–113.

Liu, D. (1988). “Impact-Induced Delamination—A View of Bending Stiffness Mismatching.” *Journal of Composite Materials*, 22(7), 674–692.

Liu I. S. T., Oehlers D. J., and Seracino R. (2007). “Study of Intermediate Crack Debonding in Adhesively Plated Beams.” *Journal of Composites for Construction*, 11(2), 175–183.

Lopes, C. S., Seresta, O., Coquet, Y., Gürdal, Z., Camanho, P. P., and Thuis, B. (2009). “Low-velocity impact damage on dispersed stacking sequence laminates. Part I: Experiments.” *Composites Science and Technology*, 69(7), 926–936.

Máca, P., Sovják, R., and Konvalinka, P. (2014). “Mix design of UHPFRC and its response to projectile impact.” *International Journal of Impact Engineering*, 63(Supplement C), 158–163.

Mall, S., Law, G. E., and Katouzian, M. (1987). “Loading Rate Effect on Interlaminar Fracture Toughness of a Thermoplastic Composite.” *Journal of Composite Materials*, 21(6), 569–579.

McGowan, D. M., and Ambur, D. R. (1999). “Structural Response of Composite Sandwich Panels Impacted With and Without Compression Loading.” *Journal of Aircraft*, 36(3), 596–602.

Nemes, J. A., and Simmonds, K. E. (1992). “Low-Velocity Impact Response of Foam-Core Sandwich Composites.” *Journal of Composite Materials*, 26(4), 500–519.

Nguyen Dai Minh, Chan Toong Khuan, and Cheong Hee Kiat. (2001). “Brittle Failure and Bond Development Length of CFRP-Concrete Beams.” *Journal of Composites for Construction*, 5(1), 12–17.

Ni, C. Y., Hou, R., Xia, H. Y., Zhang, Q. C., Wang, W. B., Cheng, Z. H., and Lu, T. J. (2015). “Perforation resistance of corrugated metallic sandwich plates filled with reactive powder concrete: Experiment and simulation.” *Composite Structures*, 127, 426–435.

Oehlers, D. J. (2006). “FRP Plates Adhesively Bonded to Reinforced Concrete Beams: Generic Debonding Mechanisms.” *Advances in Structural Engineering*, 9(6), 737–750.

Ong, K. C. ., Basheerkhan, M., and Paramasivam, P. (1999). “Resistance of fibre concrete slabs to low velocity projectile impact.” *Cement and Concrete Composites*, 21(5), 391–401.

Pan, J., and Wu, Y.-F. (2014). “Analytical modeling of bond behavior between FRP plate and concrete.” *Composites Part B: Engineering*, 61, 17–25.

Peng, Y., Smith, R., and Landis, E. (2017). “Milestones 15: Final materials level characterization of CNF modified concrete.”

Qiao, P., and Chen, Y. (2008). “Cohesive fracture simulation and failure modes of FRP–concrete bonded interfaces.” *Theoretical and Applied Fracture Mechanics*, 49(2), 213–225.

Ranade, R., Li, V. C., Heard, W. F., and Williams, B. A. (2017). “Impact resistance of high strength-high ductility concrete.” *Cement and Concrete Research*, 98(Supplement C), 24–35.

Remennikov, A. M., and Kong, S. Y. (2012). “Numerical simulation and validation of impact response of axially-restrained steel–concrete–steel sandwich panels.” *Composite Structures*, 94(12), 3546–3555.

Reyes Villanueva, G., and Cantwell, W. J. (2004). “The high velocity impact response of composite and FML-reinforced sandwich structures.” *Composites Science and Technology*, 64(1), 35–54.

Richardson, M. O. W., and Wisheart, M. J. (1996). “Review of low-velocity impact properties of composite materials.” *Composites Part A: Applied Science and Manufacturing*, 27(12), 1123–1131.

Ross, C. A., and Sierakowski, R. L. (1973). “Studies on the impact resistance of composite plates.” *Composites*, 4(4), 157–161.

ROTEM, A. (1988). “Residual flexural strength of FRP composite specimens subjected to transverse impact loading.” *SAMPE Journal*, 3, 19–25.

Saadatmanesh Hamid, and Ehsani Mohammad R. (1991). “RC Beams Strengthened with GFRP Plates. I: Experimental Study.” *Journal of Structural Engineering*, 117(11), 3417–3433.

Sarva, S., Nemat-Nasser, S., McGee, J., and Isaacs, J. (2007). “The effect of thin membrane restraint on the ballistic performance of armor grade ceramic tiles.” *International Journal of Impact Engineering*, 34(2), 277–302.

Saxton, H. J., Ireland, D. R., and Server, W. L. (1974). “Analysis and Control of Inertial Effects During Instrumented Impact Testing.” *Instrumented Impact Testing, ASTM STP 563*, American Society for Testing and Materials, 50–73.

Sayed-Ahmed, E. Y., Bakay, R., and Shrive, N. G. (2009). “Bond Strength of FRP Laminates to Concrete: State-of-the-Art Review.” 18.

Scarponi, C., Briotti, G., Barboni, R., Marcone, A., and Iannone, M. (1996). “Impact Testing on Composites Laminates and Sandwich Panels.” *Journal of Composite Materials*, 30(17), 1873–1911.

Schubel, P. M., Luo, J.-J., and Daniel, I. M. (2005). “Low velocity impact behavior of composite sandwich panels.” *Special Issue Honouring Jack Vinson on his 75th Birthday*, 36(10), 1389–1396.

Schubel, P. M., Luo, J.-J., and Daniel, I. M. (2007). “Impact and post impact behavior of composite sandwich panels.” *Composites Part A: Applied Science and Manufacturing*, 38(3), 1051–1057.

Stevanović, M., Kostić, M., Stecenko, T., and Briški, D. (1987). “IMPACT BEHAVIOUR OF CFRP COMPOSITES OF DIFFERENT STACKING GEOMETRY A2 - Herriot, J.” *Composites Evaluation*, Butterworth-Heinemann, 78–83.

Strait, L. H., Karasek, M. L., and Amateau, M. F. (1992). “Effects of Stacking Sequence on the Impact Resistance of Carbon Fiber Reinforced Thermoplastic Toughened Epoxy Laminates.” *Journal of Composite Materials*, 26(12), 1725–1740.

Su, K. (1989). “Delamination Resistance of Stitched Thermoplastic Matrix Composite Laminates.” *Advances in Thermoplastic Matrix Composite Materials*, G. Newaz, ed., ASTM International, 100 Barr Harbor Drive, PO Box C700, West Conshohocken, PA 19428-2959, 279-279–22.

Tai, Y. S. (2009). “Flat ended projectile penetrating ultra-high strength concrete plate target.” *Theoretical and Applied Fracture Mechanics*, 51(2), 117–128.

Takeda, N., Sierakowski, R. L., and Malvern, L. E. (1981). “Transverse cracks in glass/epoxy cross-ply laminates impacted by projectiles.” *Journal of Materials Science*, 16(7), 2008–2011.

Takeda, N., Sierakowski, R. L., Ross, C. A., and Malvern, L. E. (1982). “Delamination-crack propagation in ballistically impacted glass/epoxy composite laminates.” *Experimental Mechanics*, 22(1), 19–25.

Teng, J. G., Yuan, H., and Chen, J. F. (2006). “FRP-to-concrete interfaces between two adjacent cracks: Theoretical model for debonding failure.” *International Journal of Solids and Structures*, 43(18), 5750–5778.

Toutanji, H., and Ortiz, G. (2001). “The effect of surface preparation on the bond interface between FRP sheets and concrete members.” *Composite Structures*, 53(4), 457–462.

Verma, M., Prem, P. R., Rajasankar, J., and Bharatkumar, B. H. (2016). “On low-energy impact response of ultra-high performance concrete (UHPC) panels.” *Materials & Design*, 92(Supplement C), 853–865.

Wang, J. (2006). “Cohesive zone model of intermediate crack-induced debonding of FRP-plated concrete beam.” *International Journal of Solids and Structures*, 43(21), 6630–6648.

Wang, R., Gao, X., Huang, H., and Han, G. (2017). “Influence of rheological properties of cement mortar on steel fiber distribution in UHPC.” *Construction and Building Materials*, 144(Supplement C), 65–73.

Wen, H. M., Reddy, T. Y., Reid, S. R., and Soden, P. D. (1998). “Indentation, Penetration and Perforation of Composite Laminate and Sandwich Panels under Quasi-Static and Projectile Loading.” *Key Engineering Materials*, <https://www.scientific.net/KEM.141-143.501> (Oct. 25, 2018).

Wright, H. D., Oduyemi, T. O. S., and Evans, H. R. (1991). “The experimental behaviour of double skin composite elements.” *Journal of Constructional Steel Research*, 19(2), 97–110.

Wu, H., Fang, Q., Chen, X. W., Gong, Z. M., and Liu, J. Z. (2015). “Projectile penetration of ultra-high performance cement based composites at 510–1320m/s.” *Construction and Building Materials*, 74(Supplement C), 188–200.

Yoo, D.-Y., and Banthia, N. (2017a). “Mechanical and structural behaviors of ultra-high-performance fiber-reinforced concrete subjected to impact and blast.” *Construction and Building Materials*, 149(Supplement C), 416–431.

Yoo, D.-Y., and Banthia, N. (2017b). “Size-dependent impact resistance of ultra-high-performance fiber-reinforced concrete beams.” *Construction and Building Materials*, 142, 363–375.

Yoo, D.-Y., Banthia, N., Kang, S.-T., and Yoon, Y.-S. (2016). “Effect of fiber orientation on the rate-dependent flexural behavior of ultra-high-performance fiber-reinforced concrete.” *Composite Structures*, 157, 62–70.

Yoo, D.-Y., Banthia, N., and Yoon, Y.-S. (2017). “Impact Resistance of Reinforced Ultra-High-Performance Concrete Beams with Different Steel Fibers.” *Structural Journal*, 114(1), 113–124.

Yu, R., Spiesz, P., and Brouwers, H. J. H. (2014). “Static properties and impact resistance of a green Ultra-High Performance Hybrid Fibre Reinforced Concrete (UHPHFRC): Experiments and modeling.” *Construction and Building Materials*, 68, 158–171.

Zhang, M. H., Shim, V. P. W., Lu, G., and Chew, C. W. (2005). “Resistance of high-strength concrete to projectile impact.” *International Journal of Impact Engineering*, 31(7), 825–841.

Zhang, M.-H., Sharif, and Lu. (2007). *Impact resistance of high-strength fibre-reinforced concrete*.

Zhou, G., Hill, M., and Hookham, N. (2007). “Investigation of Parameters Governing the Damage and Energy Absorption Characteristics of Honeycomb Sandwich Panels.” *Journal of Sandwich Structures & Materials*, 9(4), 309–342.

Zhou, J., Hassan, M. Z., Guan, Z., and Cantwell, W. J. (2012). “The low velocity impact response of foam-based sandwich panels.” *Composites Science and Technology*, 72(14), 1781–1790.

APPENDIX A: THREE-POINT BENDING DATA

This appendix contains the data from the three-point bending tests. The data is separated by specimen type which is defined by the UHPC type, base or CNF-modified, and the reinforcement type, unreinforced, Elium-reinforced or PETg tape reinforced. Each table provides the peak load, energy dissipation, peak displacement, failure mode, and the delaminated area for each individual specimen.

Unreinforced Base UHPC Specimens

Table A.1 Data for Unreinforced Base UHPC Beam Specimens

Specimen ID	Peak Load (N)	Energy Dissipation (N·mm)	Peak Displacement (mm)	Failure Mode
B1B1-1	505	240	0.20	Flexure
B1B1-2	469	278	0.16	Flexure
B1B1-3	619	404	1.06	Flexure
B1B1-4	718	384	1.03	Flexure
B1B1-5	650	352	1.03	Flexure
B2B1-1	531	274	0.16	Flexure
B2B1-2	500	321	0.21	Flexure
B2B1-3	570	366	1.04	Flexure
B2B1-4	543	342	1.02	Flexure
B2B1-5	597	407	1.03	Flexure

Unreinforced CNF-Modified UHPC Specimens

Table A.2 Data for Unreinforced CNF-Modified UHPC Beam Specimens

Specimen ID	Peak Load (N)	Energy Dissipation (N·mm)	Peak Displacement (mm)	Failure Mode
C1B1-1	370	237	0.24	Flexure
C1B1-2	402	215	0.20	Flexure
C1B1-3	417	284	0.93	Flexure
C1B1-4	574	322	1.08	Flexure
C1B1-5	427	278	0.90	Flexure
C3B1-1	396	222	0.15	Flexure
C3B1-2	464	249	0.16	Flexure
C3B1-3	391	242	0.14	Flexure
C3B1-4	508	353	1.03	Flexure
C3B1-5	487	258	0.22	Flexure

Elium-Reinforced Base UHPC Specimens

Table A.3 Data for Elium-Reinforced Base UHPC Beam Specimens

Specimen ID	Peak Load (N)	Energy Dissipation (N·mm)	Peak Displacement (mm)	Delaminated Area (mm^2)	Failure Mode
CEB1-1	1480	675	0.81	1530	Flexural/ Delamination
CEB1-2	2120	1670	1.16	2900	Flexural/ Delamination
CEB1-3	2080	1760	1.40	2510	Flexural/ Delamination
CEB1-4	2170	1600	1.15	2410	Flexural/ Delamination
CEB1-5	2040	1510	1.25	2510	Flexural/ Delamination
CEB1-6	2150	1340	1.11	1730	Flexural/ Delamination
CEB1-7	2200	1560	1.38	359	Flexural/ Delamination
CEB1-8	2060	1250	1.08	2110	Flexural/ Delamination
CEB1-9	2060	1230	0.93	95	Shear
CEB1-10	1910	1160	1.05	36	Shear
CEB2-1	1520	669	0.70	1300	Flexural/ Delamination
CEB2-2	1600	696	0.74	1300	Flexural/ Delamination
CEB2-3	2200	1400	1.06	1910	Flexural/ Delamination
CEB2-4	1660	866	0.92	1790	Flexural/ Delamination
CEB2-5	1830	885	1.04	0	Shear
CEB2-6	1820	1140	0.95	0	Shear
CEB2-7	1390	624	0.62	0	Shear
CEB2-8	1700	806	0.78	0	Shear

Elium-Reinforced CNF-Modified UHPC Specimens

Table A.4 Data for Elium-Reinforced CNF-Modified UHPC Beam Specimens

Specimen ID	Peak Load (N)	Energy Dissipation (N·mm)	Peak Displacement (mm)	Delaminated Area (mm^2)	Failure Mode
BEB1-1	1900	1380	1.33	2680	Flexural/ Delamination
BEB1-2	1890	798	1.10	0	Shear
BEB1-3	1750	991	1.17	2230	Flexural/ Delamination
BEB1-4	1610	947	0.98	2590	Flexural/ Delamination
BEB1-5	1470	738	0.84	2140	Flexural/ Delamination
BEB1-6	1720	894	0.93	2240	Flexural/ Delamination
BEB1-7	1630	703	0.68	2320	Flexural/ Delamination
BEB1-8	1760	963	0.82	2160	Flexural/ Delamination
BEB1-9	1560	709	0.69	1970	Flexural/ Delamination
BEB1-10	1690	819	0.80	2430	Flexural/ Delamination
BEB2-1	1660	908	0.98	1980	Flexural/ Delamination
BEB2-2	1590	1210	1.20	2530	Flexural/ Delamination
BEB2-3	1750	1240	1.11	2390	Flexural/ Delamination
BEB2-4	1540	855	1.15	2120	Flexural/ Delamination
BEB2-5	1800	1180	1.05	2290	Flexural/ Delamination
BEB2-6	1770	1110	1.08	2480	Flexural/ Delamination
BEB2-7	1970	1450	1.32	2500	Flexural/ Delamination
BEB2-8	1690	931	1.05	2330	Flexural/ Delamination
BEB2-9	1990	1400	1.11	0	Shear
BEB2-10	2440	1820	1.27	1800	Flexural/ Delamination

PETg Tape Reinforced Base UHPC Specimens

Table A.5 Data for PETg Tape Reinforced Base UHPC Beam Specimens

Specimen ID	Peak Load (N)	Energy Dissipation (N·mm)	Peak Displacement (mm)	Delaminated Area (mm^2)	Failure Mode
BPB1-1	2110	1610	1.19	0	Shear
BPB1-2	1540	789	0.91	621	Shear/ Delamination
BPB1-3	1390	837	1.00	2070	Flexural/ Delamination
BPB1-4	1390	595	0.71	1530	Flexural/ Delamination
BPB1-5	1570	672	0.81	0	Shear
BPB1-6	2020	1390	1.21	1330	Flexural/ Delamination
BPB1-7	1860	1240	1.08	956	Shear/ Delamination
BPB1-8	1490	873	0.97	2300	Shear/ Delamination
BPB1-9	1590	1230	0.74	0	Shear
BPB1-10	1660	1020	0.96	2070	Flexural/ Delamination
BPB2-1	817	133	0.29	1170	Flexural/ Delamination
BPB2-2	1250	326	0.49	494	Flexural/ Delamination
BPB2-3	2040	1540	1.00	1420	Shear/ Delamination
BPB2-4	2400	1560	1.07	1450	Flexural/ Delamination
BPB2-5	2200	1390	1.02	1940	Flexural/ Delamination
BPB2-6	1860	999	0.84	1450	Shear/ Delamination
BPB2-7	1660	652	0.70	466	Shear/ Delamination
BPB2-8	1010	211	0.38	541	Shear/ Delamination
BPB2-9	861	378	0.29	922	Flexural/ Delamination
BPB2-10	1340	369	0.50	834	Flexural/ Delamination

PETg Tape Reinforced CNF-Modified UHPC Specimens

Table A.6 Data for PETg Tape Reinforced CNF-Modified UHPC Beam Specimens

Specimen ID	Peak Load (N)	Energy Dissipation (N·mm)	Peak Displacement (mm)	Delaminated Area (mm^2)	Failure Mode
CPB2-1	1640	606	0.70	1600	Flexural/ Delamination
CPB2-2	1660	692	0.66	244	Shear
CPB2-3	1880	1530	1.18	2640	Flexural/ Delamination
CPB2-4	2120	1380	1.03	2480	Flexural/ Delamination
CPB2-5	1610	760	0.74	1370	Flexural/ Delamination
CPB2-6	1540	820	0.70	1920	Flexural/ Delamination
CPB2-7	1500	598	0.66	2100	Flexural/ Delamination
CPB2-8	1280	495	0.63	2020	Flexural/ Delamination
CPB2-9	1510	768	0.78	1970	Flexural/ Delamination
CPB2-10	1790	1190	0.95	2640	Flexural/ Delamination
CPB1-1	2190	1850	1.38	229	Shear
CPB1-2	1510	846	0.84	2030	Flexural/ Delamination
CPB1-3	1230	356	0.51	1880	Flexural/ Delamination
CPB1-4	1150	366	0.55	1700	Flexural/ Delamination
CPB1-5	1690	810	0.78	1790	Flexural/ Delamination
CPB1-6	2340	2020	1.36	2430	Flexural/ Delamination
CPB1-7	1840	1080	0.93	1840	Flexural/ Delamination
CPB1-8	1970	1360	0.93	1380	Flexural/ Delamination
CPB1-9	1810	1030	0.92	1650	Flexural/ Delamination
CPB1-10	1730	942	0.87	1530	Flexural/ Delamination

APPENDIX B: QUASI-STATIC TESTING DATA

This appendix contains the data from the quasi-static tests. The data is separated by specimen type which is defined by the UHPC type, base or CNF-modified, and the reinforcement type, unreinforced, Elium-reinforced or PETg tape reinforced. Each table provides the peak load, energy dissipation, and maximum displacement for each individual specimen.

Unreinforced Base UHPC Specimens

Table B.1 Data for Unreinforced Base UHPC Quasi-Static Specimens

Specimen ID	Peak Load (N)	Energy Dissipation (N·mm)	Maximum Displacement (mm)
B1P1-1	4460	15200	4.01
B1P1-2	4040	12200	4.01
B1P2-1	4320	13700	3.94
B1P2-2	3320	10600	3.80
B2P1-1	4640	15100	3.95

Unreinforced CNF-Modified UHPC Specimens

Table B.2 Data for Unreinforced CNF-Modified UHPC Quasi-Static Specimens

Specimen ID	Peak Load (N)	Energy Dissipation (N·mm)	Maximum Displacement (mm)
C1P1-2	5090	15200	3.89
C1P1-3	4340	13100	3.85
C2P1-2	3610	9290	3.58
C2P1-4	4320	10600	3.99
C3P1-2	3630	10500	3.99

Elium-Reinforced Base UHPC Specimens

Table B.3 Data for Elium-Reinforced Base UHPC Quasi-Static Specimens

Specimen ID	Peak Load (N)	Energy Dissipation (N·mm)	Maximum Displacement (mm)
BEP1-1	9470	21500	3.03
BEP1-2	11900	29400	3.50
BEP2-1	10600	29800	3.81
BEP2-2	11900	31800	4.58
BEP3-1	12600	29500	3.72
BEP3-2	11100	26400	3.40
BEP4-1	12000	28700	3.72
BEP4-2	10100	27300	3.82

Elium-Reinforced CNF-Modified UHPC Specimens

Table B.4 Data for Elium-Reinforced CNF-Modified UHPC Quasi-Static Specimens

Specimen ID	Peak Load (N)	Energy Dissipation (N·mm)	Maximum Displacement (mm)
CEP1-1	9260	25900	4.19
CEP1-2	10000	26300	3.73
CEP2-1	9250	23600	3.77
CEP2-2	9510	20600	3.28
CEP3-1	10400	27500	3.77
CEP3-2	10900	26000	3.72
CEP4-1	10500	28000	3.77
CEP4-2	10800	21500	3.11

PETg Tape Reinforced Base UHPC Specimens

Table B.5 Data for PETg Tape Reinforced Base UHPC Quasi-Static Specimens

Specimen ID	Peak Load (N)	Energy Dissipation (N·mm)	Maximum Displacement (mm)
BPP1-1	10200	17600	2.80
BPP1-2	12600	16900	2.91
BPP2-1	10700	17100	2.84
BPP2-2	10700	18000	2.83
BPP3-1	10300	17300	2.85
BPP3-2	9800	17100	3.44
BPP4-1	11200	18200	2.84
BPP4-2	12200	18100	2.73

PETg Tape Reinforced CNF-Modified UHPC Specimens

Table B.6 Data for PETg Tape Reinforced CNF-Modified UHPC Quasi-Static Specimens

Specimen ID	Peak Load (N)	Energy Dissipation (N·mm)	Maximum Displacement (mm)
CPP1-1	12900	15800	2.66
CPP1-2	13100	20700	2.61
CPP2-1	11300	19000	2.86
CPP2-2	12300	19600	2.78
CPP3-1	12900	17400	2.58
CPP3-2	12900	18400	2.66
CPP4-1	11300	18800	2.81
CPP4-2	11800	18400	2.86

APPENDIX C: FORCE VERSUS TIME DATA FROM LOW VELOCITY IMPACT TESTS

This appendix contains the low velocity impact force-time records. For conciseness, the thermoplastic composite reinforced specimen data is condensed by specimen type. The specimen type is defined by the UHPC type, either base or CNF-modified, and the reinforcement type, either Elium-reinforced or PETg tape reinforced. The unreinforced specimens were all impacted with 16 J of energy, while the thermoplastic composite reinforced specimens were impacted with either 16 J, 24 J, 32 J or 40 J of energy.

Unreinforced Base UHPC Specimens

Figure C.1. Force-Time record for the low velocity impact of specimen B1P1-3

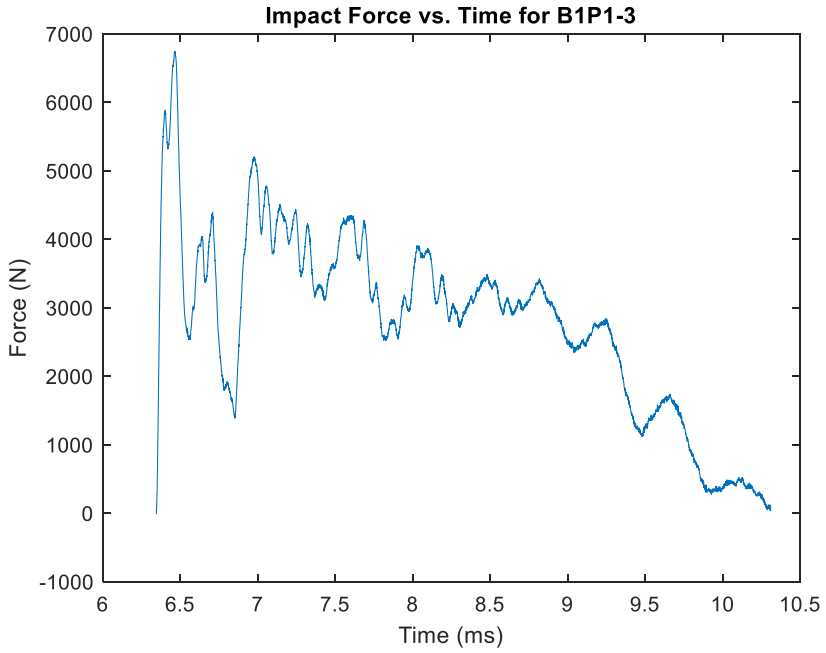

Figure C.2. Force-Time record for the low velocity impact of specimen B1P1-4

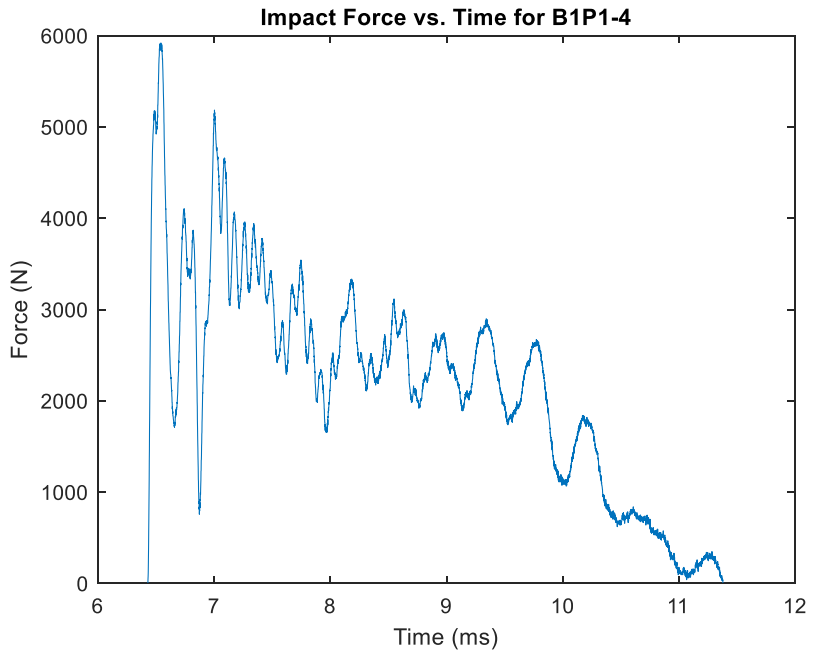

Figure C.3. Force-Time record for the low velocity impact of specimen B1P2-3

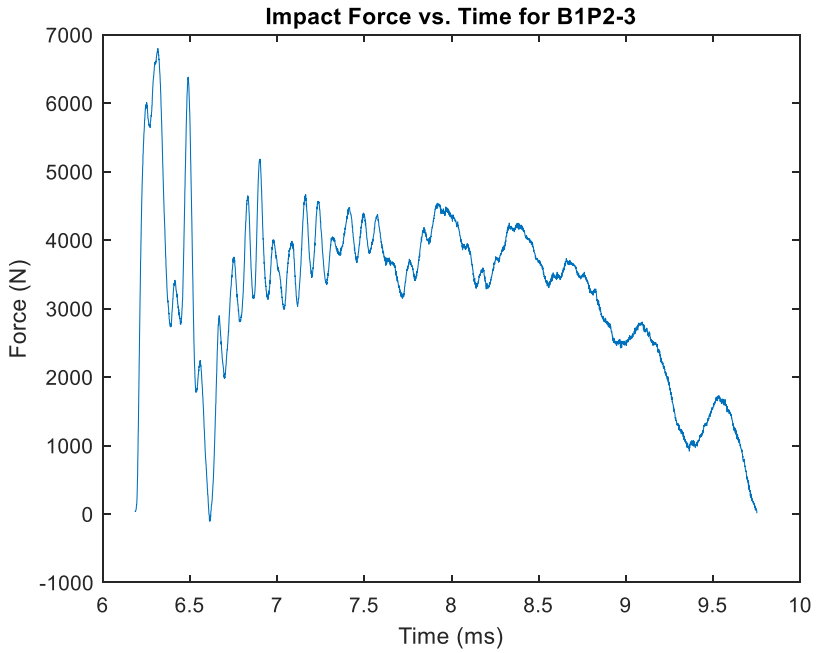

Figure C.4. Force-Time record for the low velocity impact of specimen B2P1-2

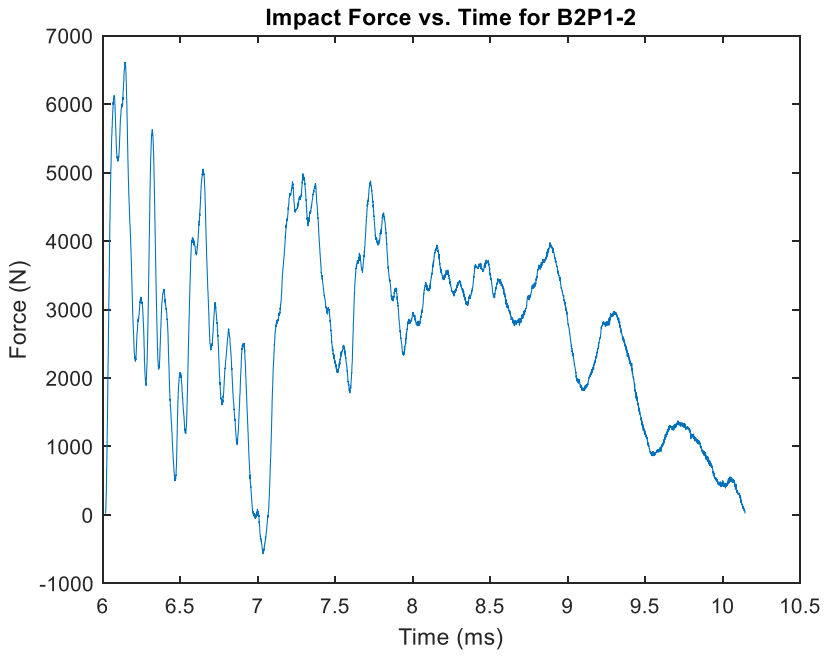

Figure C.5. Force-Time record for the low velocity impact of specimen B2P1-3

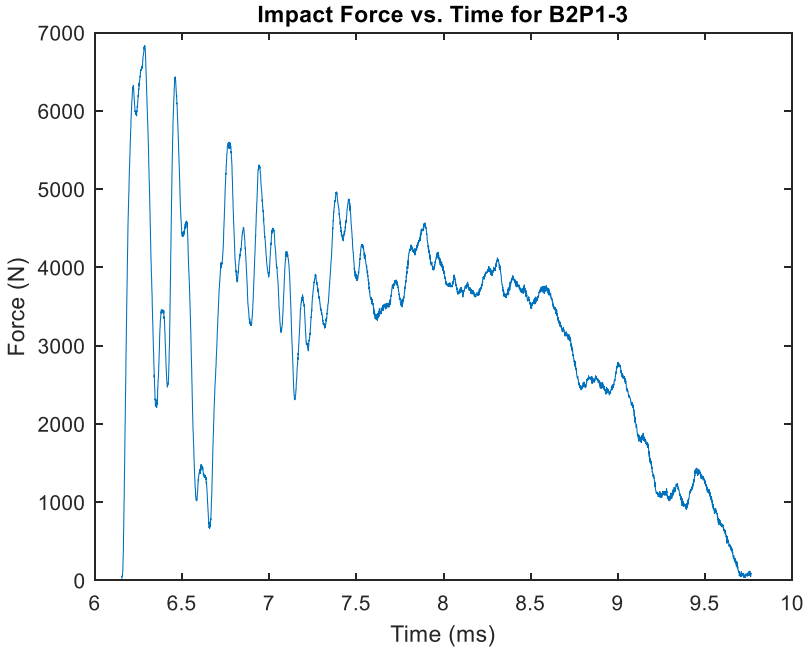

Unreinforced CNF-Modified UHPC Specimens

Figure C.6. Force-Time record for the low velocity impact of specimen C1P1-1

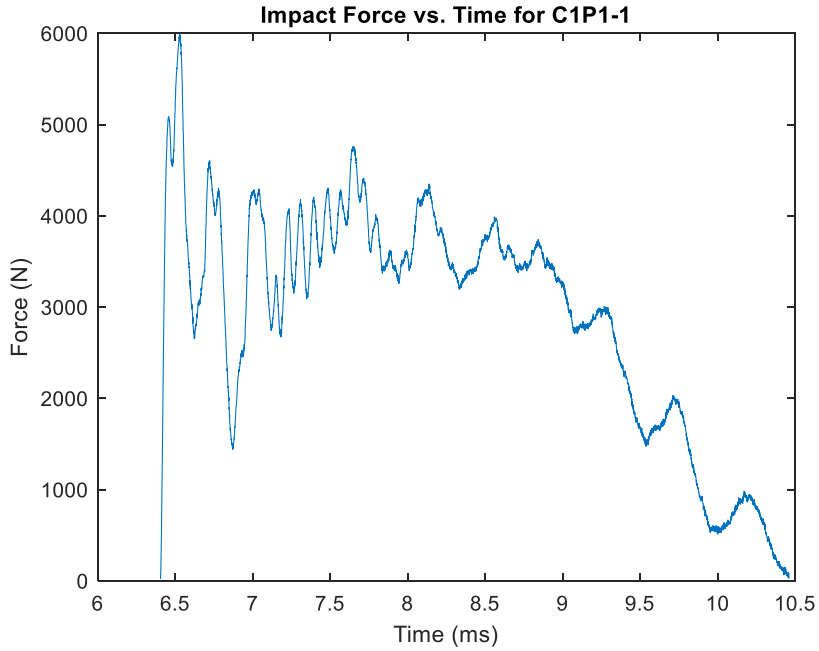

Figure C.7. Force-Time record for the low velocity impact of specimen C2P1-1

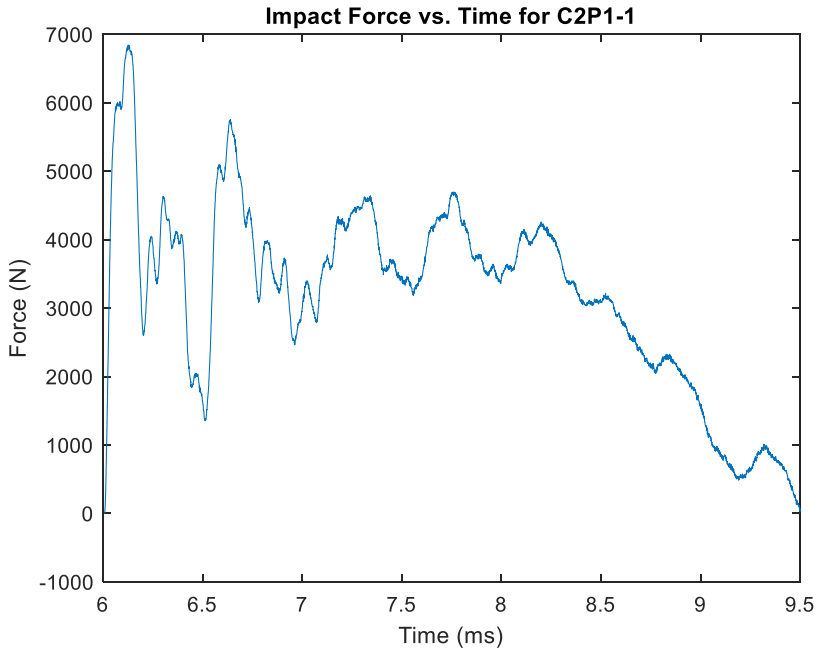

Figure C.8. Force-Time record for the low velocity impact of specimen C2P1-3

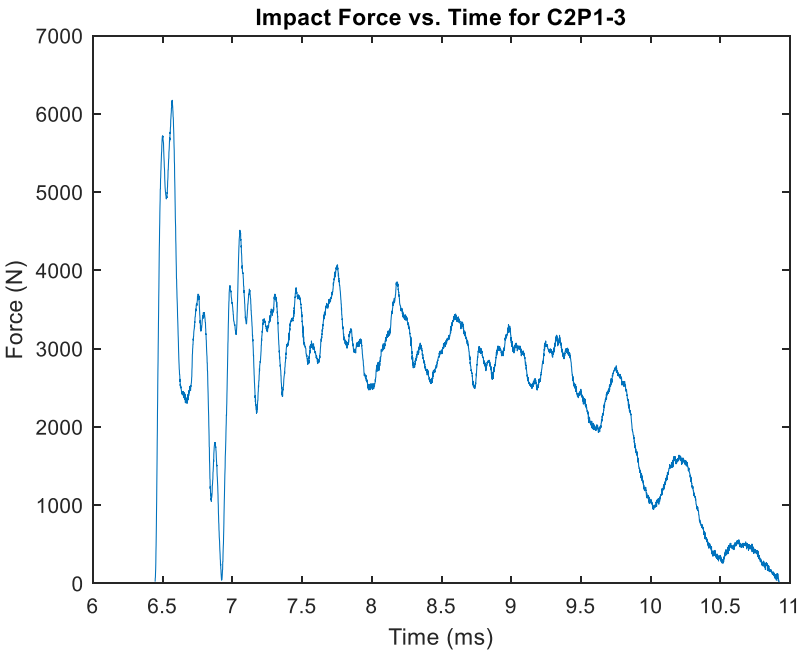

Figure C.9. Force-Time record for the low velocity impact of specimen C3P1-1

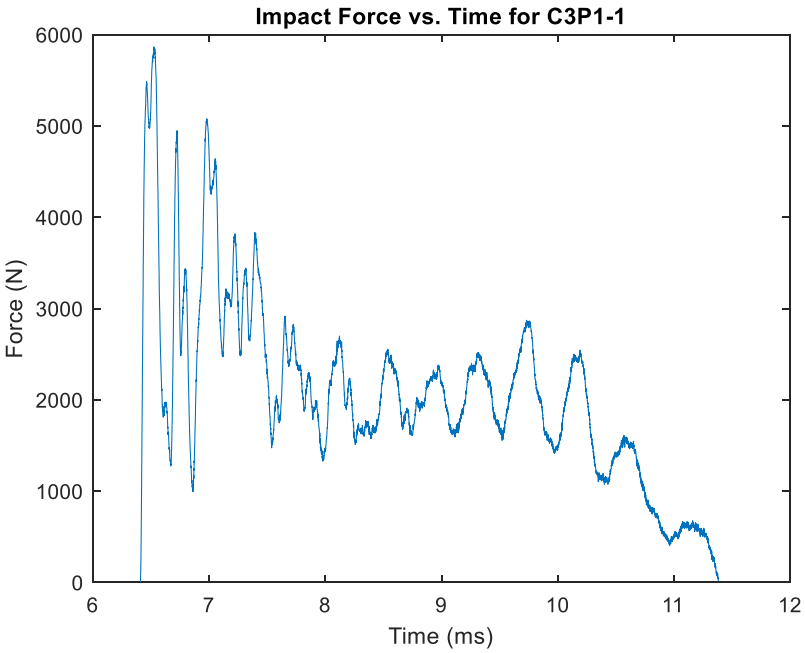

Figure C.10. Force-Time record for the low velocity impact of specimen C3P1-3

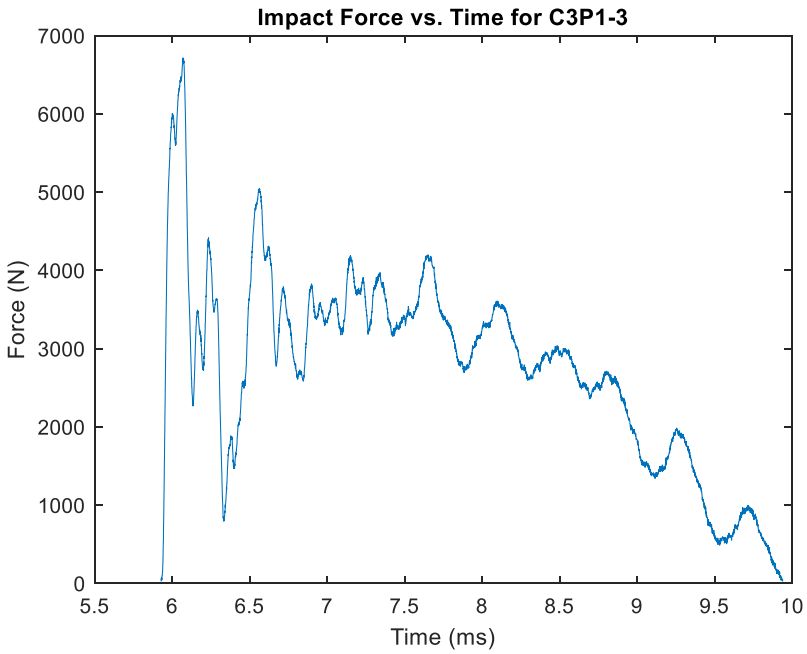

Elium-Reinforced Base UHPC Specimens

Figure C.11. Force-Time records of the Elium-reinforced base UHPC panels

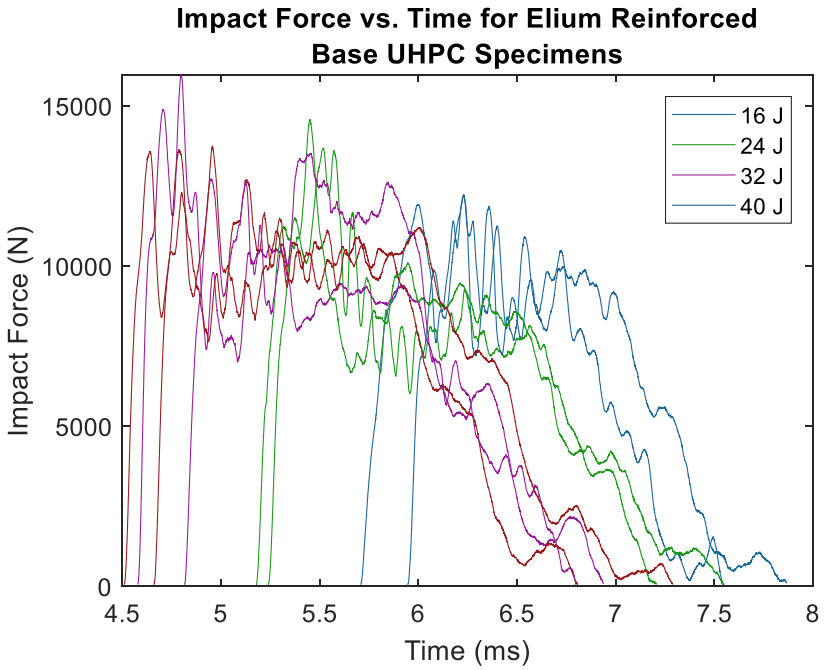

Elium-Reinforced CNF-Modified UHPC Specimens

Figure C.12. Force-Time records of the Elium-reinforced CNF-modified UHPC panels

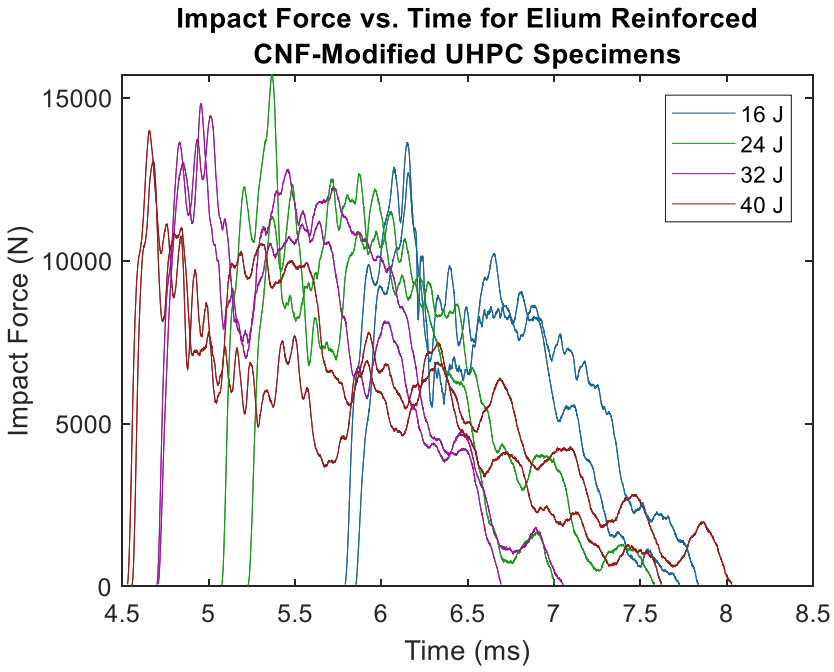

PETg Tape Reinforced Base UHPC Specimens

Figure C.13. Force-Time records of the PETg-reinforced base UHPC panels

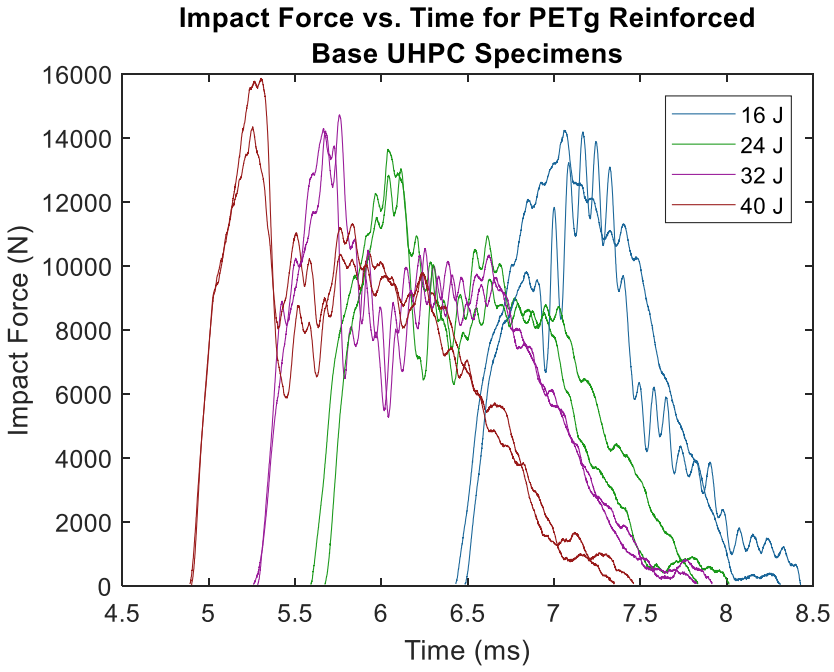

PETg Tape Reinforced CNF-Modified Specimens

Figure C.14. Force-Time records of the PETg-reinforced CNF-modified UHPC panels

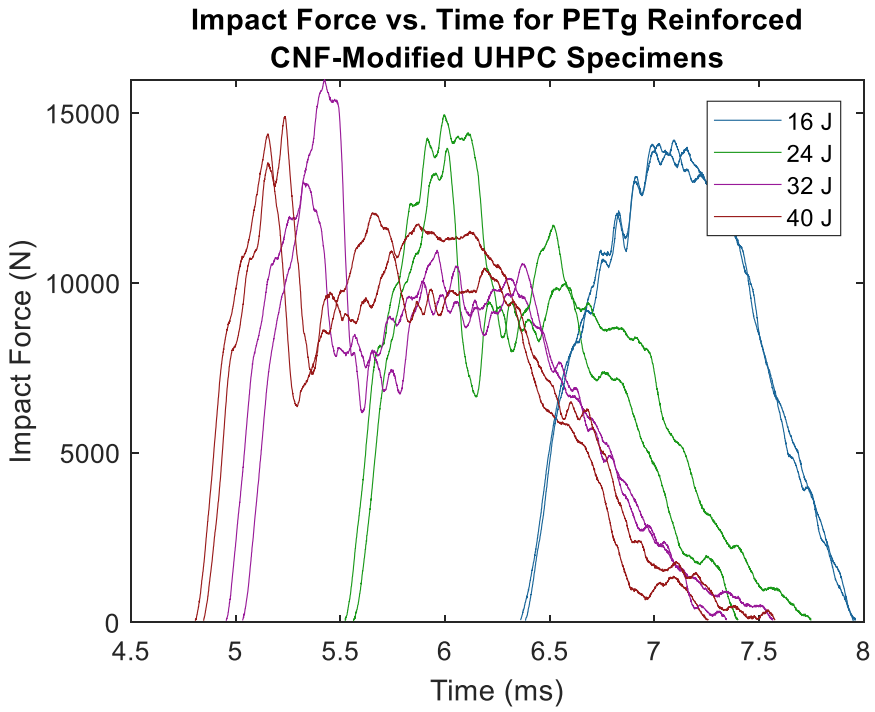

APPENDIX D: LOW VELOCITY IMPACT TESTING DATA

This appendix contains the data from the low velocity impact testing. The data is separated by specimen type which is defined by the UHPC type, base or CNF-modified, and the reinforcement type, unreinforced, Elium-reinforced or PETg tape reinforced. Each table provides the impact energy, peak impact load, maximum displacement during impact, change in compliance, and residual deflection for each individual specimen.

Unreinforced Base UHPC Specimens

Table D.1 Data for Unreinforced Base UHPC Impact Specimens

Specimen ID	Impact Energy (J)	Peak Impact Load (N)	Maximum Impact Displacement (mm)	Residual Displacement (mm)	Change in Compliance (mm/N)
B1P1-3	16	6740	5.77	2.84	2.75E-04
B1P1-4	16	5920	7.02	3.82	3.43E-04
B1P2-3	16	6800	5.45	2.47	1.09E-04
B2P1-3	16	6835	5.23	2.41	1.11E-04
B2P1-2	16	6610	6.50	2.21	6.25E-05

Unreinforced CNF-Modified UHPC Specimens

Table D.2 Data for Unreinforced CNF-Modified UHPC Impact Specimens

Specimen ID	Impact Energy (J)	Peak Impact Load (N)	Maximum Impact Displacement (mm)	Residual Displacement (mm)	Change in Compliance (mm/N)
C1P1-1	16	5990	5.54	2.24	2.66E-04
C2P1-1	16	6840	5.22	2.48	1.22E-04
C2P1-3	16	6170	6.63	3.50	1.56E-04
C3P1-1	16	5870	7.88	3.27	4.23E-04
C3P1-3	16	6710	5.98	2.84	2.34E-04

Elium-Reinforced Base UHPC Specimens

Table D.3 Data for Elium-Reinforced Base UHPC Impact Specimens

Specimen ID	Impact Energy (J)	Peak Impact Load (N)	Maximum Impact Displacement (mm)	Residual Displacement (mm)	Change in Compliance (mm/N)
BEP1-3	16	12200	2.27	0.61	9.49E-06
BEP1-4	24	13700	3.43	0.87	7.98E-05
BEP2-3	32	16000	4.01	1.44	9.58E-05
BEP2-4	16	12200	2.21	0.45	2.16E-05
BEP3-3	40	13600	4.58	1.68	3.81E-05
BEP3-4	24	14600	3.33	1.08	6.31E-05
BEP4-3	32	13500	3.83	1.45	4.69E-05
BEP4-4	40	13800	4.53	1.56	7.93E-05

Elium-Reinforced CNF-Modified UHPC Specimens

Table D.4 Data for Elium-Reinforced CNF-Modified UHPC Impact Specimens

Specimen ID	Impact Energy (J)	Peak Impact Load (N)	Maximum Impact Displacement (mm)	Residual Displacement (mm)	Change in Compliance (mm/N)
CEP1-3	24	12300	3.47	1.16	8.22E-05
CEP1-4	16	13600	2.21	0.51	1.99E-05
CEP2-3	32	14800	3.77	1.18	6.69E-05
CEP2-4	40	14000	6.64	2.32	2.47E-04
CEP3-3	24	12700	2.54	0.71	2.63E-05
CEP3-4	16	15700	2.87	0.60	6.15E-05
CEP4-3	32	14400	4.10	1.27	1.00E-04
CEP4-4	40	13000	5.57	1.82	1.99E-04

PETg Tape Reinforced Base UHPC Specimens

Table D.5 Data for PETg Tape Reinforced Base UHPC Impact Specimens

Specimen ID	Impact Energy (J)	Peak Impact Load (N)	Maximum Impact Displacement (mm)	Residual Displacement (mm)	Change in Compliance (mm/N)
BPP1-3	16	14200	2.14	0.18	1.17E-05
BPP1-4	24	13700	3.32	0.68	3.93E-05
BPP2-3	32	14300	4.47	1.36	5.12E-05
BPP2-4	40	14400	4.86	1.40	7.23E-05
BPP3-3	16	14200	2.49	0.34	4.67E-05
BPP3-4	24	13000	3.54	0.78	6.31E-05
BPP4-3	32	14700	4.64	1.10	4.78E-05
BPP4-4	40	15900	5.02	1.45	5.08E-05

PETg Tape Reinforced CNF-Modified UHPC Specimens

Table D.6 Data for PETg Tape Reinforced CNF-Modified UHPC Impact Specimens

Specimen ID	Impact Energy (J)	Peak Impact Load (N)	Maximum Impact Displacement (mm)	Residual Displacement (mm)	Change in Compliance (mm/N)
CPP1-3	16	14200	2.17	0.03	1.02E-05
CPP1-4	24	14900	3.10	0.56	3.32E-05
CPP2-3	32	13000	4.43	1.16	6.85E-05
CPP2-4	40	14400	4.74	1.35	4.18E-05
CPP3-3	16	14100	2.11	0.04	7.87E-06
CPP3-4	24	14000	3.38	0.82	3.13E-05
CPP4-3	32	16000	4.28	1.18	5.35E-05
CPP4-4	40	14900	4.94	1.40	8.58E-05

BIOGRAPHY OF THE AUTHOR

Reagan Smith Gillis was born in Bangor, ME and grew up in Holden, ME. She graduated from John Bapst High School in 2013. During high school she discovered her love for math and science, which led her to enroll in the University of Maine's Civil Engineering program. Through her undergraduate studies she learned more about the Civil Engineering profession and became intrigued by how much knowledge there was to gain in the different sub disciplines. An undergraduate internship at CES, Inc. peaked her interest in Structural Engineering and she then made the decision to pursue graduate school because of the complex issues associated with structural engineering. In May 2017 she graduated from the University of Maine with a B.S. in Civil & Environmental Engineering and a minor in Mathematics. She is a member of Tau Beta Pi, the engineering honor society, Chi Epsilon, the civil engineering honor society, and the American Concrete Institute (ACI). As a graduate student in the Civil Engineering Department at the University of Maine she has worked with Eric Landis and the U.S. Army Engineer Research and Development Center (ERDC) investigating the material properties of ultra-high performance concrete. She is a candidate for the Master of Science degree in Civil Engineering from the University of Maine in December 2018.